Inference of computational models of tendon networks via sparse experimentation

by

Manish Umesh Kurse

A Dissertation Presented to the
FACULTY OF THE USC GRADUATE SCHOOL
UNIVERSITY OF SOUTHERN CALIFORNIA
In Partial Fulfillment of the
Requirements for the Degree
DOCTOR OF PHILOSOPHY
(BIOMEDICAL ENGINEERING)

June 2012

Dedication

To my parents.

Acknowledgements

Little did I know when I started my Ph.D. that this journey I was about to undertake would teach me invaluable life lessons that would change my view of the world. I have several people to thank for these lessons, whose roads crossed mine during these years.

Firstly, I would like to thank Dr. Francisco Valero-Cuevas for being a fantastic adviser and mentor to me the last five and a half years. He has guided me, supported me and helped me get an education that goes well beyond engineering. I have learnt from him the importance of good presentation of ideas and how to communicate to a diverse audience. By bringing together a team of very smart individuals from different academic and cultural backgrounds, he gave me an opportunity to enrich myself, expand my thinking and along the way make some great friends.

In spite of a three hour time zone difference and a busy schedule, Dr. Hod Lipson was always available to meet with me for our teleconference meetings. Some of his ideas form the core of my dissertation research. Working in his lab during Dec '09-Jan '10 at Cornell University, though short, was a great experience and had significant impact on my Ph.D.

I would like to thank Dr. Gerald Loeb and Dr. Eva Kanso for being on my dissertation committee and for their honest comments and inputs which helped me question, rethink

and reshape my approach to the problem I was trying to solve. I would like to thank Dr. Terence Sanger for being on my dissertation guidance committee.

Dr. Jason Kutch taught me to question, think and innovate. I learned that with good planning and sincere hard work any idea can be taken from concept to reality. I owe it to him for training me in the art of experimentation.

Every Ph.D. has its ups and downs and I've had my fair share over the last few years. Sudarshan has been a fantastic friend who has been by my side throughout this journey to share the joys and frustrations of Ph.D. research. We started and finished our journeys at USC around the same time and having him around definitely made the journey easier and more fun. I have always admired his knowledge and view of the world that has greatly influenced my own thinking.

Josh Inouye has been a great friend and a source of inspiration. His efficient working style, getting things done attitude and discipline has motivated me to work harder and be more productive. I have had good discussions with him about my research and his feedback has always been very valuable.

Kornelius has been a good friend and a co-traveller in my journey from almost the very beginning. Along with Sudarshan, we saw the growth of the lab from the very scratch. Its been great working with him over the years.

Thanks to Brendan for helping me with computer hardware, graphics related issues and making good videos. He has been a good friend, my tennis buddy and introduced me to some great fiction.

Several people have been an integral part of the cadaver experiments: Heiko Hoffmann, forming the 'cadaver dream team' with Jason and me; the hand surgeons: Dr. Vincent

Hentz, Dr. Caroline Leclercq, Dr. Isabella Fassola and Dr. Nina Lightdale; and the Brain-Body Dynamics Lab members and alumni : Dr. Marta Mora Aguilar, Emily Lawrence, Srideep Musuvathy, John Rocamora and Hannah Ko. Thanks to Alex, Evangelos, for their inputs to my research at various points in my PhD.

Mischalgrace Diasanta has been a great graduate student adviser and a fun collaborator during my Biomedical Engineering Senator year.

Harsha, Kapish, Heeral, Tapan, Anish and Devanshi have become very close friends with whom I have shared fun times over many dinners and card game nights. It is thanks to them and the Veggie Hiker group that I fell in love with Los Angeles.

I would like to thank my dear parents who have been extremely supportive throughout my education. I have shared with them my successes and my disappointments at every stage in my life and they have always been encouraging and positive. Without their love and support, I would not have been able to come this far. I also thank my grandmother for her best wishes, love and affection.

Table of Contents

List Of Tables

List Of Figures

Abstract

This dissertation presents novel computational methods to infer accurate functional models of musculoskeletal systems from minimal experimental data focussing on the tendon networks of the human fingers as an example. State of the art biomechanical modeling consists of assuming a fixed structure to the system being modeled and measurement or regression of specific parameter values. However, the assumed structure may not be the best representation of the system and hence lead to a functionally less-accurate model. The objective here is to simultaneously infer both the structure and the parameter values directly from experimental input-output data. We present novel methods to infer computational models of two kinds– analytical models capturing input-output behavior without specifically modeling the mechanics of the system, and physics-based models that explicitly capture the mechanics of interactions of the constitutive elements. Using experimental data from a tendon-driven robotic system and synthetic data from simulated musculoskeletal systems, a novel method based on symbolic regression using genetic programming that simultaneously infers the form and parameter values of mathematical expressions is presented and shown to outperform polynomial regression, the state of the art method used in musculoskeletal modeling. This method is then implemented

on experimental data collected from a cadaveric index finger to obtain accurate analytical functions for the tendon excursions of the seven tendons of the finger. Whether the goal is to obtain accurate subject-specific models or to obtain generalizable models, the functions obtained using this novel technique are more accurate than both polynomial regressions and Landsmeer-based models, both of which have been used in the literature. Experimental control of a cadaveric index finger to produce simple finger movements gives some insight on how a muscle-like spring based control can be more advantageous than using simple force or position control. Two different kinds of equilibria is demonstrated in the human cadaveric index finger, for the first time to our knowledge, and their relationship to the null space of the moment arm matrix is studied. An experimental validation, of some common models of the index finger in their ability to predict fingertip output is presented and it is shown that the fingertip force is sensitive to moment arm values. A novel non-linear finite element method based solver is developed that can be used to model the interactions of elastic tendon networks on arbitrarily shaped bones. This solver which is validated using experimental data is then used to model the extensor mechanism draped on the finger bones and a local sensitivity analysis is performed to see how the fingertip force output is affected by changes to the properties of the network. It is concluded that fingertip force output is most sensitive to topology and the resting lengths of the bands of the extensor mechanism. Finally, a novel inference algorithm that is based on the co-evolution of models and tests is used to infer the parameters and topology of a 3 dimensional model of the extensor mechanism directly from cadaveric data with minimal number of experimental data points through intelligent testing. It is

shown that the inferred models are more accurate in predicting fingertip force magnitude

and direction compared to a model popularly used in the literature.

Chapter 1

Introduction

1.1 Background

Computational models are useful tools to understand the behavior of musculoskeletal systems and have been extensively used by the biomechanics community for some time now. They help us understand how movement and force are produced by the human body, to test theories of motor control and to determine the states of a system that cannot be measured experimentally. They are useful to simulate changes on injury or disease and to predict outcomes of surgeries. Chapter 2 has details on the uses of musculoskeletal models and how they can be built. Most often, these models are built based on anatomical observations, assumptions about the structure of the system and measurement of some individual parameters through experimental studies. Many times anatomical observations may be inaccurate or not capture the mechanical/functional behavior of the system. Also experimentally measuring all properties of the system is not always feasible. Hence there can be large discrepancies between the data and the model. Most cases these models

are not validated with experimental data. This dissertation focuses on the concept of inference of musculoskeletal models directly from experimental data with few assumptions about the structure and parameter values. The hypothesis is that models inferred from experimental data would more accurately capture the functional behavior of the system than these existing models based on assumptions about the anatomy. Inference of such models requires a combination of tools from carefully measured experimental data consisting of system inputs and outputs to a modeling environment where these musculoskeletal systems can be represented, to inference algorithms that can estimate the structure and parameters of these models directly from experimental data. With advances in the field of electromechanical actuation, computational mechanics, machine learning, artificial intelligence and optimization, we are at a unique position to combine these different tools to develop informative models of these complex systems. This dissertation demonstrates new inference methods to learn models of musculoskeletal systems from experimental data using the tendon networks of the fingers as an example.

1.2   Modeling the human tendon networks

Finger joint motion and fingertip force production are critical to the activities of daily living. These are produced by the coordinated actuation of multiple finger muscles through the intricate network of interconnections constituting the extensor mechanism. How these different finger muscles coordinate to produce finger motion and force is still an unanswered question. While it is important to understand the neural control of the muscles actuating the fingers, it is also critical to understand the role of passive biomechanical

tissue that transfers forces from the muscles to the finger joints. In fact, developing and testing theories of neural control heavily depend on a good representation of the 'plant'.

1.2.1 Anatomy

Tendons in most parts of the body connect a single muscle to a single point of attachment on the bone. In the hand, tendons form complex networks of interconnections that connect multiple muscles to multiple points of attachment on the bones. These networks exist within a single finger (i.e. the extensor mechanism, Fig. 1.1a) as well as across multiple fingers (i.e. the *junctura tendinae*, Fig. 1.1b). The finger musculature is able to coordinate finger movement and finger force production by transmitting forces through this intricate network of collagenous fibers.

Fig. 1.2 shows the main components of the extensor mechanism of the fingers. It consists of bands of collagenous fibers that transfer forces from three main sets of inputs to two tendon slips, the central and terminal slip, that actuate the joints. In the case of the index finger, these three inputs come from four muscles : the extensor indicis, extensor digitorum communis, first palmar interosseous and the lumbrical.

1.2.2 Functional significance of the extensor mechanism

Clinicians, anatomists, biomechanists and neurophysiologists have been interested in understanding the role of the tendon networks in human manipulation for several decades now (Haines 1951, Landsmeer 1949, Schieber & Santello 2004, Valero-Cuevas 2005, Brand & Hollister 1999). Most studies so far have been qualitative analyses of the functional significance of the extensor mechanism based on testing of cadaveric specimens
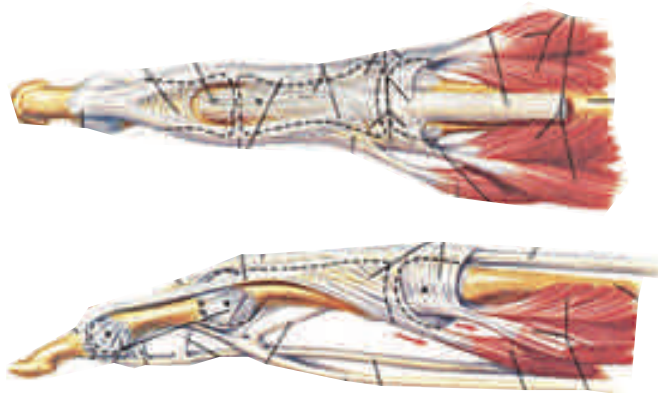
3
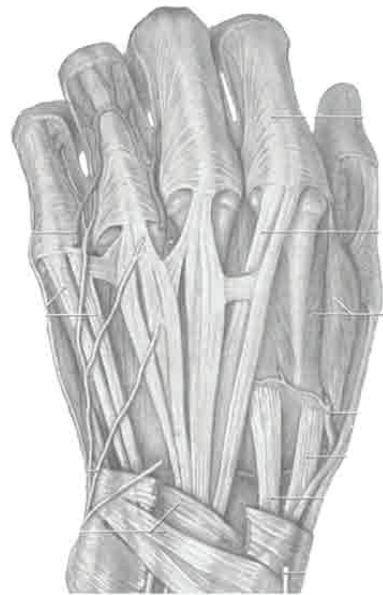
(a) Extensor mechanism of the finger

(b) *Juncturae tendinae* across fingers

Figure 1.1: Tendon networks of the hand
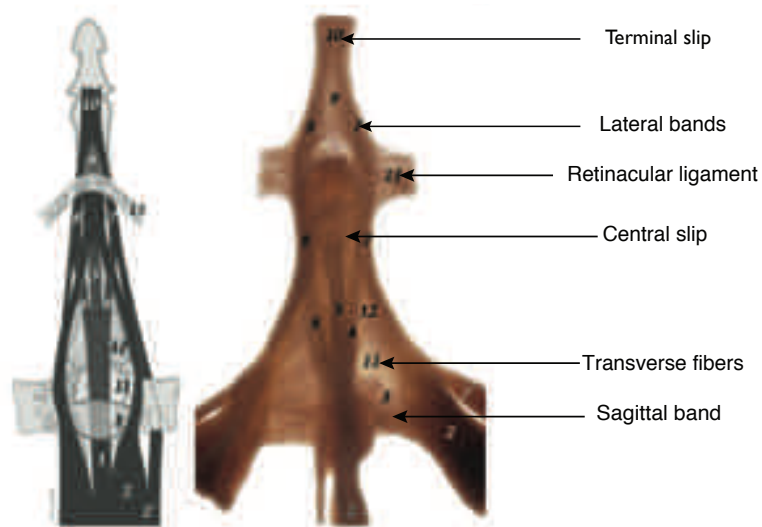
Terminal slip

Lateral bands

Retinacular ligament

Central slip

Transverse fibers

Sagittal band

Figure 1.2: (Clavero et al. 2003)

4

(Smith 1974, Landsmeer 1949, Harris Jr & Rutledge Jr 1972, Littler 1967). These studies have shown that the extensor mechanism produces anatomical coupling of interphalangeal joint rotations (Landsmeer 1963, Harris Jr & Rutledge Jr 1972) and its absence causes the interphalangeal joints to flex sequentially and not in unison (Brand & Hollister 1999). There have been simplistic 2D planar models of the extensor mechanism that have also tried to demonstrate this effect (Spoor & Landsmeer 1976, Leijnse, Bonte, Landsmeer, Kalker, Van der Meulen & Snijders 1992, Leijnse 1996, Kamper, George Hornby & Rymer 2002). The contribution of the extensor mechanism versus neural factors towards interphalangeal coupling is still not clear (Darling, Cole & Miller 1994, Kuo, Lee, Jindrich & Dennerlein 2006).

Several studies have focussed on understanding the geometric and tensile properties of the different components of the extensor mechanism(Landsmeer 1949, Haines 1951, Garcia-Elias, An, Berglund, Linscheid, Cooney Iii & Chao 1991, Garcia-Elias, An, Berglund, Linscheid, Cooney & Chao 1991). It has been shown that the relative orientation of the different bands of the extensor mechanism vary significantly with finger posture, thus changing the effective moment arm of the extensor mechanism about the interphalangeal joints (Garcia-Elias, An, Berglund, Linscheid, Cooney Iii & Chao 1991). The force distribution through the different bands of the extensor mechanism also changes significantly with finger posture; the lateral bands transmitting majority of the force in the extended posture and the central and terminal bands transferring majority of the force in the flexed posture (Sarrafian, Kazarian, Topouzian, Sarrafian & Siegelman 1970, Micks & Reswick 1981).

The clinical significance of understanding the function of the extensor mechanism cannot be overstated (Bunnell 1945, Brand & Hollister 1999, Zancolli 1979). Even slight damage to these networks leads to finger deformities and loss of function (Stark, Boyes & Wilson 1962, Littler 1967, Rockwell, Butler & Byrne 2000). Two of the most common finger deformities caused due to damage of the extensor mechanism are the boutonniere deformity (Fig. 1.3a) and the mallet finger (Fig. 1.3b).The boutonniere deformity occurs due to rupture of the central slip of the extensor mechanism and the mallet finger deformity due to rupture of the terminal slip. Also other finger deformities like the swan neck deformity caused due to inflammation of the proximal interphalangeal (PIP) joint during rheumatoid arthritis results in force imbalance in the extensor mechanism leading to loss of function. How the different components of the extensor mechanism contribute to force transmission and how forces redistribute upon damage has still not been understood.

(a) Boutonniere deformity   (b) Mallet finger
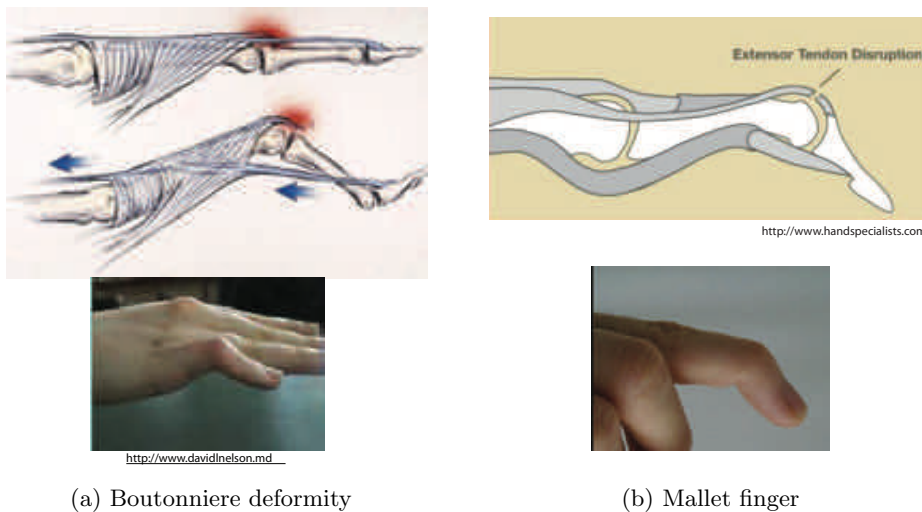
Figure 1.3: Finger deformities caused by damage to the extensor mechanism.

1.3 Previous Work

The Winslow's rhombus representation originally described by Winslow and reproduced in drawing by Zancolli (Zancolli 1979) has been the generally accepted representation for the extensor mechanism, though there have been alternative descriptions that have been suggested in the literature(Garcia-Elias, An, Berglund, Linscheid, Cooney Iii & Chao 1991, Garcia-Elias, An, Berglund, Linscheid, Cooney & Chao 1991). This model (the Winslow's rhombus) was based on qualitative anatomical observations in cadaveric tissue and no quantitative proof exists even today if this is a good functional representation of the real structure. Hence there is need to either validate this model in its ability to reproduce experimental data or suggest alternative, more accurate, functional models. The reason why Winslow's model representation has not been validated so far is largely because of the computational complexity involved in modeling a deformable elastic network wrapped on a set of irregular bones and also because obtaining extensive experimental data from cadaveric specimens is very difficult.

The work of An and Chao on modeling hand function was one of the early computational studies to employ the Winslow's rhombus representation to model the extensor mechanism (An, Chao, Cooney & Linscheid 1979, An, Chao, Cooney & Linscheid 1985, Chao & An 1978a). These studies assumed a fixed distribution of tendon tensions among the different bands of the extensor mechanism for all postures. This model was later used in other studies as well (Li, Zatsiorsky & Latash 2001, Harding, Brandt & Hillberry 1993, Dennerlein, Diao, Mote Jr & Rempel 1998, Weightman & Amis 1982). But earlier studies had shown that the geometry of the bands as well as the force distribution

through them, change significantly with posture (Garcia-Elias, An, Berglund, Linscheid, Cooney Iii & Chao 1991, Sarrafian et al. 1970, Micks & Reswick 1981). Hence a 3D 'floating net' model was suggested by Valero-Cuevas et al. where the tension distribution in the different bands would vary with posture (Valero-Cuevas, Zajac & Burgar 1998). They found that only when they allowed the distribution of tensions to change with posture that the finger model could accurately predict the measured maximal isometric forces and the coordination patterns that produced them. Two dimensional planar models of the finger have also used a simplified Winslow's rhombus representation (Leijnse et al. 1992, Leijnse 1996, Spoor 1983). But two dimensional models combine the lumbrical and interossei tendons as one tendon, do not include ad-abduction of the finger and they cannot capture all the interdependencies of the different bands of the extensor mechanism.

Recently, Sueda et al. have developed a dynamic simulator of hand motion that models the tendon networks in three dimensions (Sueda, Kaufman & Pai 2008). Tendinous connections are represented as cubic splines and their interactions with bones are modeled by line and surface constraints. This model, developed mainly for the graphics community, aims to produce physically realistic simulations of hand motion and has not been validated for its functional accuracy in modeling finger motion and force data. The predecessor to the computational simulator that we have developed here, is the one developed by Valero-Cuevas and Lipson that is based on the relaxation algorithm (Valero-Cuevas & Lipson 2004, Valero-Cuevas, Anand, Saxena & Lipson 2007, Valero-Cuevas, Yi, Brown, McNamara, Paul & Lipson 2007, Lipson 2006). This simulator uses simple cylinders to models bones and is computationally slow.

Other finger dynamic models use analytical functional representations for the different components of the tendon networks (Brook, Mizrahi, Shoham & Dayan 1995, Buchner, Hines & Hemami 1988, Sancho-Bru, Perez-Gonzalez, Vergara-Monedero & Giurintano 2001). These analytical expressions, derived by Landsmeer based on geometry, map joint angles to tendon excursions (Landsmeer 1961). While these functional models may be convenient for dynamic modeling and for purposes of control, they do not capture the physics of interaction of the different components of the extensor mechanism. Also these models have not been validated with experimental data. Most full body musculoskeletal modeling software like SIMM (Motion Analysis Corporation) (Delp & Loan 1995), AnyBody (AnyBody Technology) (Damsgaard, Rasmussen, Christensen, Surma & de Zee 2006) and MSMS (Davoodi, Urata, Hauschild, Khachani & Loeb 2007) do not model the tendon networks of the hand. We have described the steps involved in computational modeling of biomechanical systems and provided an overview of current methods in our recently published review article (Valero-Cuevas, Hoffmann, Kurse, Kutch & Theodorou 2009).

The estimation-exploration algorithm is an active machine learning technique based on coevolution that has been used successfully for the inference of the topologies and parameter values of several complex nonlinear systems through minimum experimentation(Bongard & Lipson 2005a, Bongard & Lipson 2005b, Bongard & Lipson 2004a, Bongard & Lipson 2004b, Lipson, Bongard, Zykov & Malone 2006).

The same algorithm has also been successfully employed for the inference of the structure of the extensor mechanism in two dimensions with simulated data generated by a hidden target network as well as data from synthetic networks and cadaveric tissue
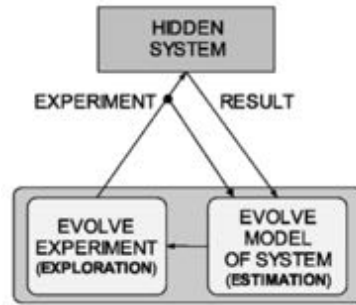
Figure 1.4: General representation of the Estimation-Exploration Algorithm (Bongard & Lipson 2005a)

(Valero-Cuevas, Anand, Saxena & Lipson 2007). This is briefly described in section 1.3.1.

1.3.1 Prior work in the lab leading to current work

- Importance in motor control : It was shown using cadaveric experimental data and in computer simulations that the extensor mechanism could be performing a complex transformation from muscle forces to finger joint torques. Hence, understanding the function of these passive structures is critical for the development of theories of motor control (Valero-Cuevas, Yi, Brown, McNamara, Paul & Lipson 2007).

- Importance of topology: Using a three-dimensional computational model of the extensor mechanism draped on bones, it was shown that the output of the finger critically depends on the assumed topology of the network(Valero-Cuevas, Anand, Saxena & Lipson 2007, Valero-Cuevas, Yi, Brown, McNamara, Paul & Lipson 2007).

Hence computational models of the hand being developed to understand finger function would require accurate representations of the extensor mechanism topology.

- Inference of network topologies from simulated data in 2D : The topologies of hidden, two dimensional, elastic networks were inferred from simulated data (Valero-Cuevas, Anand, Saxena & Lipson 2007). It was shown that the estimation-exploration algorithm required fewer experimental tests and converged to more accurate functional representations of the hidden elastic networks in comparison to random testing.

- Inference of planar two dimensional networks from experimental data : The topologies of planar, synthetic, elastic networks were inferred from experimental data generated by sequential loading of these networks. This demonstrated that the estimation-exploration algorithm could be successfully employed in the inference of complex network topologies even with noisy experimental data (*Manuscript in review*).

- Inference of the topology of the extensor mechanism in two dimensions : The topology of the extensor mechanism in two dimensions was successfully inferred using the estimation-exploration algorithm from experimental data collected by differential loading of cadaveric tissue. This was further proof that the estimation-exploration algorithm can be successfully used for the inference of topology and parameters of complex biological systems (*Manuscript in review*)..

1.4 Significance of Research

This dissertation presents novel methods for the development of computational models of musculoskeletal systems, specifically focussing on the tendinous networks of the human fingers. It combines experimental studies of human cadaveric specimens with mathematical analyses, solid mechanics and novel inference algorithms to develop computational models of two kinds : analytical functional models and physics-based models. The methods of computational modeling presented here make contributions to the areas of motor control, clinical research, evolutionary understanding of biomechanical systems and in the development of robotics and prosthetics.

Understanding motor control of human movement and force require accurate mathematical representations of the 'plant'. The inference of compact, analytical functions modeling tendon routing in musculoskeletal systems and the specific models for the index finger presented here enable the development of dynamical models to test theories of motor control. Cadaveric control of the index finger to produce simple finger movements as well as the observation of two forms of equilibria in specific postures and tendon tension combinations contributes to our understanding of finger movement control. While there have been several simplified representations of the tendon networks of the fingers, none of the existing representations actually model the physics of interactions of these networks with the bones. The finite element solver presented here would allow clinicians and researchers to mathematically understand how the different components of these networks help transform forces generated by the muscles to end point fingertip force. Simulation of injury and damage to these networks could help predict changes in force transformation

and help surgeons plan repair and surgery to restore function in the fingers. Simulating different network topologies, node positions and elastic properties of the extensor mechanism throws light on the significance and uniqueness of the existing structure from an evolutionary perspective. The estimation exploration algorithm implemented here to optimize models of the extensor mechanism with minimal experimentation is a step towards development of subject-specific musculoskeletal models through intelligent testing. The ultimate goal would be to infer accurate subject-specific models of musculoskeletal systems in human subjects by performing only those tests that provide most information about the system being modeled.

1.5   Dissertation outline

1.5.1   Chapter 2

This chapter reviews musculoskeletal modeling literature and demonstrates the steps involved in constructing a musculoskeletal model using the example of the human arm. This formed a part of the section on musculoskeletal modeling that I wrote in the review paper (Valero-Cuevas et al. 2009) published in the IEEE Reviews in Biomedical Engineering. Dr. Francisco J. Valero-Cuevas is a co-author of this section.

1.5.2   Chapter 3

This chapter presents a novel method based on symbolic regression using genetic programming to simultaneously infer both the form and parameter values of analytical functions describing tendon excursions and moment arms in musculoskeletal systems. Using (i)

experimental data from a physical tendon-driven robotic system with arbitrarily routed multiarticular tendons and (ii) synthetic data from musculoskeletal models, it is shown that these analytical functions outperforms polynomial regressions in the amount of training data, ability to extrapolate, robustness to noise, and representation containing fewer parameters – all critical to realistic and efficient computational modeling of complex musculoskeletal systems. This is a paper that was published in the IEEE Transactions on Biomedical Engineering (Kurse, Lipson & Valero-Cuevas 2012). Dr. Hod Lipson and Dr. Francisco J. Valero-Cuevas are co-authors.

1.5.3   Chapter 4

This chapter presents the application of the above method to infer analytical functions for the tendon excursions in a human index finger from cadaveric experimental data. It demonstrates that these inferred models are more accurate and have fewer parameters compared to both polynomial regressions and models based on geometry, whether the goal is to obtain subject-specific models or models that generalize across subjects. Dr. Hod Lipson and Dr. Francisco J. Valero-Cuevas are co-authors.

1.5.4   Chapter 5

This chapter presents the use of the tendon actuation system to control a human index finger to produce slow tapping motion. It also demonstrates a specific kind of equilibrium (what we term neutral equilibrium) in specific finger postures and combinations of tendon tensions which are shown to lie in the null space of the finger's moment arm matrix in those postures. Dr. Jason Kutch and Dr. Francisco J. Valero-Cuevas are co-authors.

1.5.5 Chapter 6

Three existing models of the human index finger are evaluated with experimental data. It is shown that fingertip output is sensitive to moment arm values and these existing models diverge from experimental data necessitating more accurate representations. This was presented at the American Society of Biomechanics conference 2011 at Long Beach. Dr. Hod Lipson and Dr. Francisco J. Valero-Cuevas are co-authors.

1.5.6 Chapter 7

A novel nonlinear finite element method based tendon network simulator is presented, validated with experimental data and used to study the sensitivity of the fingertip force output to the topology and parameters of the finger's extensor mechanism. Dr. Hod Lipson and Dr. Francisco J. Valero-Cuevas are co-authors.

1.5.7 Chapter 8

Three dimensional models of the finger's extensor mechanism topology and parameter values are inferred directly from experimental data collected from a cadaveric index finger through intelligent testing using the estimation-exploration algorithm. Dr. Hod Lipson and Dr. Francisco J. Valero-Cuevas are co-authors.

1.5.8 Chapter 9

Chapter 9 discusses some of the challenges faced in the inference of computational models of the tendon networks from experimental data.

1.5.9 Chapter 10

Chapter 10 discusses conclusions and future work.

Chapter 2

Fundamentals of Biomechanical Modeling

Computational models of the musculoskeletal system (i.e., the physics of the world and skeletal anatomy, and the physiological mechanisms that produce muscle force) are a necessary foundation when building models of neuromuscular function. Musculoskeletal models have been widely used to characterize human movement and understand how muscles can be coordinated to produce function. While experimental data are the most reliable source of information about a system, computer models can give access to parameters that cannot be measured experimentally and give insight on how these internal variables change during the performance of the task. Such models can be used to simulate neuromuscular abnormalities, identify injury mechanisms and plan rehabilitation (Neptune 2000, McLean, Su & van den Bogert 2003, Fregly 2008). They can be used by surgeons to simulate tendon transfer (Herrmann & Delp 1999, Magermans, Chadwick, Veeger, Rozing & Van der Helm 2004, Valero-Cuevas & Hentz 2002) and joint replacement surgeries (Piazza & Delp 2001), to analyze the energetics of human movement (Kuo 2002), athletic performance (Hull & Jorge 1985), design prosthetics and biomedical implants (Huiskes & Chao 1983), and functional electric stimulation controllers (Schutte,

Rodgers, Zajac, Glaser, Center & Alto 1993, Davoodi, Brown & Loeb 2003, Davoodi & Loeb 2003).

Naturally, the type, complexity and physiological accuracy of the models vary depending on the purpose of the study. Extremely simple models that are not physiologically realistic can and do give insight into biological function (e.g., (Garcia, Chatterjee, Ruina & Coleman 1998)). On the other hand, more complex models that describe the physiology closely might be necessary to explain some other phenomenon of interest (Van der Helm 1994). Most models used in understanding neuromuscular function lie in-between, with a combination of physiological reality and modeling simplicity. While several papers (Pandy 2001, Zajac 2002, Zajac, Neptune & Kautz 2002, Buchanan, Lloyd, Manal & Besier 2004, Hatze 2005, Thelen, Anderson & Delp 2003, Piazza 2006, Fernandez & Pandy 2006) and books (Winter 1990, Winters 2000, Yamaguchi 2005) discuss the importance of musculoskeletal models and how to build them, we will give a brief overview of the necessary steps and discuss some commonly performed analyses and limitations using these models. We will illustrate the procedure for building a musculoskeletal model by considering the example of the human arm consisting of the forearm and upper arm linked at the elbow joint as shown in Fig. 2.1.

2.1   Computational environments

The motivation and advantage of graphical/computational packages like SIMM (Motion Analysis Corporation), AnyBody (AnyBody Technology), MSMS, etc. (Delp & Loan 1995, Davoodi et al. 2003, Damsgaard et al. 2006) is to build graphical representations
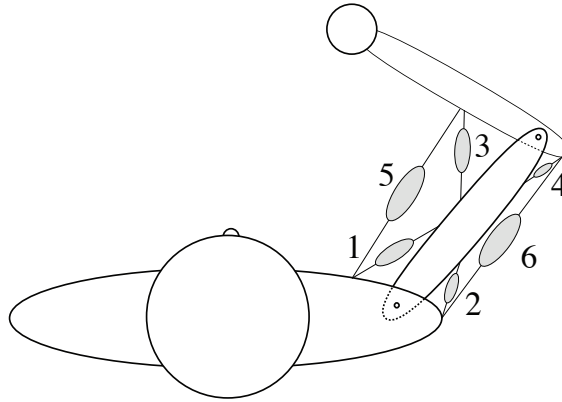
Figure 2.1: Simple model of the human arm consisting of two planar joints and six muscles.

of musculoskeletal systems, and translate them into code that is readable by multibody dynamics computational packages like SDFast (PTC), Autolev (Online Dynamics Inc.), ADAMS (MSC Software Corp.), MATLAB (Mathworks Inc.), etc. or use their own dynamics solvers. These packages allow users to define musculoskeletal models, calculate moment arms and musculotendon lengths, etc.

This engineering approach dates back to the use of computer aided design tools and finite element analysis packages to study bone structure and function in the 60's, which grew to include rigid body dynamics simulators in the mid 80's like ADAMS and Autolev. Before the advent of these programming environments (as in the case of computer aided design), engineers had to generate their own equations of motion or Newtonian analysis by hand, and write their own code to solve the system for the purpose of interest. Available packages for musculoskeletal modeling have now empowered researchers without training in engineering mechanics to assemble and simulate complex nonlinear dynamical systems. The risk, however, is that the lack of engineering intuition about how

complex dynamical systems behave can lead the user to accept results that one otherwise would not. In addition, to our knowledge, multibody dynamics computational packages have not been cross-validated against each other, or a common standard, to the extent that finite elements analysis code has (Anderson, Ellis & Weiss 2007) and the simulation of nonlinear dynamical systems remains an area of study with improved integrators and collision algorithms developed every year. An exercise the user can do is to simulate the same planar double or triple pendulum (i.e., a limb) in different multi-body dynamics computational packages and compare results after a few seconds of simulation. The differences are attributable to the nuances of the computational algorithms used, which are often beyond the view and control of the user. Whether these shortcomings in dynamical simulators affect the results of the investigation can only be answered by the user and reviewers on a case-by case basis, and experts can also disagree on computational results in the mainstream of research like gait analysis (Neptune, Kautz & Zajac 2001, Neptune, Zajac & Kautz 2004, Kuo & Maxwell Donelan 2009).

2.2 Dimensionality and redundancy

The first decision to be made when assembling a musculoskeletal model is to define dimensionality of the musculoskeletal model (i.e., number of kinematic degrees-of-freedom and the number of muscles acting on them). If the number of muscles exceeds the minimal number required to control a set of kinematic degrees-of-freedom, the musculoskeletal model will be redundant for some sub-maximal tasks. The validity and utility of the model to the research question will be affected by the approach taken to address muscle

redundancy. Most musculoskeletal models have a lower dimensionality than the actual system they are simulating because it simplifies the mathematical implementation and analysis, or because a low-dimensional model is thought sufficient to simulate the task being analyzed. Kinematic dimensionality is often reduced to limit motion to a plane when simulating arm motion at the level of the shoulder (Abend, Bizzi & Morasso 1982, Mussa-Ivaldi, Hogan & Bizzi 1985, Shadmehr & Mussa-Ivaldi 1994), when simulating fingers flexing and extending (Dennerlein, Diao, Mote Jr & Rempel 1998) or when simulating leg movements during gait (Olney, Griffin, Monga & McBride 1991). Similarly, the number of independently controlled muscles is often reduced (An et al. 1985) for simplicity, or even made equal to the number of kinematic degrees-of-freedom to avoid muscle redundancy (Harding et al. 1993). While reducing the dimensionality of a model can be valid in many occasions, one needs to be careful to ensure it is capable of replicating the function being studied. For example, an inappropriate kinematic model can lead to erroneous predictions (Valero-Cuevas, Towles & Hentz 2000, Jinha, Ait-Haddou, Binding & Herzog 2006), or reducing a set of muscles too severely may not be sufficiently realistic for clinical purposes.

A subtle but equally important risk is that of assembling a kinematic model with a given number of degrees of freedom, but then not considering the full kinematic output. For example, a three-joint planar linkage system to simulate a leg or a finger has three kinematic degrees of freedom at the input, and also three kinematic degrees of freedom at the output: the x and y location of the endpoint *plus the orientation of the third link.* As a rule, the number of rotational degrees-of-freedom (i.e., joint angles) maps into as many kinematic degrees-of-freedom at the endpoint (Murray, Li & Sastry 1994). Thus,

for example, studying muscle coordination to study endpoint location without considering the orientation of the terminal link can lead to variable results. As we have described in the literature (Valero-Cuevas et al. 1998, Valero-Cuevas 2009), the geometric model and Jacobian of the linkage system need to account for all input and output kinematic degrees-of-freedom to properly represent the mapping from muscle actions to limb kinematics and kinetics.

2.3 Skeletal mechanics

In neuromuscular function studies, skeletal segments are generally modeled as rigid links connected to one another by mechanical pin joints with orthogonal axes of rotation. These assumptions are tenable in most cases, but their validity may depend on the purpose of the model. Some joints like the thumb carpometacarpal joint, the ankle and shoulder joints are complex and their rotational axes are not necessarily perpendicular (Hollister, Buford, Myers, Giurintano & Novick 1992, Inman 1944, Van Langelaan 1983), or necessarily consistent across subjects (Hollister et al. 1992, Santos & Valero-Cuevas 2006, Cerveri, De Momi, Marchente, Lopomo, Baud-Bovy, Barros & Ferrigno 2008). Assuming simplified models may fail to capture the real kinematics of these systems (Valero-Cuevas, Johanson & Towles 2003). While passive moments due to ligaments and other soft tissues of the joint are often neglected, at times they are modeled as exponential functions of joint angles (Yoon & Mansour 1982, Hatze 1997) at the extremes of range of motion to passively prevent hyper-rotation. In other cases, passive moments *well within* the range of motion could be particularly important in the case of systems like the fingers (Esteki

& Mansour 1996, Sancho-Bru et al. 2001) where skin, fat and hydrostatic pressure tend to resist flexion.

Modeling of contact mechanics could be important for joints like the knee and the ankle where there is significant loading on the articulating surfaces of the bones, and where muscle force predictions could be affected by contact pressure. Joint mechanics are also of interest for the design of prostheses, where the knee or hip could be simulated as contact surfaces rolling and sliding with respect to each other (Bartel, Bicknell & Wright 1986, Rawlinson & Bartel 2002, Rawlinson, Furman, Li, Wright & Bartel 2006). Several studies estimate contact pressures using quasi-static models with deformable contact theory (e.g., (Wismans, Veldpaus, Janssen, Huson & Struben 1980, Blankevoort, Kuiper, Huiskes & Grootenboer 1991, Pandy, Sasaki & Kim 1997, Pandy & Sasaki 1998)). But these models fail to predict muscle forces during dynamic loading. Multibody dynamic models with rigid contact fail to predict contact pressures (Piazza & Delp 2001).

For the illustrative example carried throughout this review we will use the simple two-joint, six-muscle planar limb shown in Fig. 2.1. We model the upper arm and the forearm as two rigid cylindrical links connected to each other by a pin joint representing the elbow and shoulder joints as hinges. We will neglect moment due to passive structures and assume frictionless joints. We will not consider any contact mechanics at the joints. This model will simulate the movement and force production of the hand (i.e., a fist with a frozen wrist) in a two-dimensional plane perpendicular to the torso as is commonly done in studies of upper extremity function (Abend et al. 1982, Mussa-Ivaldi et al. 1985, Shadmehr & Mussa-Ivaldi 1994).

2.4 Musculotendon routing

Next, we need to select the routing of the musculotendon unit consisting of a muscle and its tendon in series (Zajac, Biosci, Physiol, Biol, Physiol, Lond, Physiol, Soc, Acta & Biochem 1989, Zajac 1992). The reason we speak in general about musculotendons (and not simply tendons) is that in many cases it is the belly of the muscle that wraps around the joint (e.g., *gluteus maximus* over the hip, *medial deltoid* over the shoulder). In other cases, however, it is only the tendon that crosses any joints as in the case of the patellar tendon of the knee or the flexors of the wrist. In addition, the properties of long tendons affect the overall behavior of muscle like by stretching out the force-length curve of the muscle fibers (Zajac et al. 1989). Most studies assume correctly that musculotendons insert into bones at single points or multiple discrete points (if the actual muscle attaches over a long or broad area of bone). Musculotendon routing defines the direction of travel of the force exerted by a muscle when it contracts. This defines the moment arm r of a muscle about a particular joint, and determines both the excursion δs the musculotendon will undergo as the joint rotates an angle $\delta\theta$ defined by the equation, $\delta s = r * \delta\theta$, as well as the joint torque τ at that joint due to the muscle force f_m transmitted by the tendon $\tau = r * f_m$ where r is the minimal perpendicular distance of the musculotendon from the joint center for the planar (scalar) case (Zajac 1992). For the three dimensional case the torque is calculated by the cross product of the moment arm with the vector of muscle force $\boldsymbol{\tau} = \mathbf{r} \times \mathbf{f_m}$.

In today's models, musculotendon paths are modeled and visualized either by straight lines joining the points of attachment of the muscle; straight lines connecting "via points"

attached to specific points on the bone which are added or removed depending on joint configuration (Garner & Pandy 2000) or as cubic splines with sliding and surface constraints (Sueda et al. 2008). Several advances also allow representing muscles as volumetric entities with data extracted from imaging studies (Blemker & Delp 2005, Blemker, Asakawa, Gold & Delp 2007), and defining tendon paths as wrapping in a piecewise linear way around ellipses defining joint locations (Delp & Loan 1995, Davoodi et al. 2003). The path of the musculotendon in these cases is defined based on knowledge of the anatomy. Sometimes, it may not be necessary to model the musculotendon paths but obtaining a mathematical expression for the moment arm (r) could suffice. The moment arm is often a function of joint angle and can be obtained by recording incremental tendon excursions (δs) and corresponding joint angle changes ($\delta \theta$) in cadaveric specimens (Eg. (Otis, Jiang, Wickiewicz, Peterson, Warren & Santner 1994, An, Ueba, Chao, Cooney & Linscheid 1983)).

For the arm model example (Fig. 2.1), we will model musculotendon paths as straight lines connecting their points of insertion. We will attach single-joint flexors and extensors at the shoulder (*pectoralis* and *deltoid*) and elbow (*biceps long head* and *triceps lateral head*) and double-joint muscles across both joints (*biceps short head* and *triceps long head*). Muscle origins and points of insertion are estimated from the anatomy. In our model of the arm in Fig. 2.1, we shall model musculotendons as simple linear springs. We then assign values to model parameters like segment inertia, elastic properties of the musculotendons, etc. At this point the model is complete and ready for dynamical analysis.

2.5   Musculotendon models

The most commonly used computational model of musculotendon force is the one based on the Hill-type model of muscle(Zajac et al. 1989), largely because of its computational efficiency, scalability, and because it is included in simulation packages like SIMM (Motion Analysis Corporation). In Hill-type models, the entire muscle is considered to behave like a large sarcomere with its length and strength scaled-up, respectively, to the fiber length and physiological cross sectional area of the muscle of interest. This model consists of a parallel elastic element representing passive muscle stiffness, a parallel dashpot representing muscle viscosity and a parallel contractile element representing activation-contraction dynamics; all in series with a series elastic element representing the tendon. The force generated by a muscle depends on muscle activation, physiological cross sectional area of the muscle, pennation angle and force-length and force-velocity curves for that muscle. These parameter values are generally based on animal or cadaveric work (Lieber, Jacobson, Fazeli, Abrams & Botte 1992). Five parameters define the properties of this musculotendon model. Four of these are specific to the muscle: the optimal muscle fiber length, the peak isometric force (found by multiplying maximal muscle stress by physiological cross-sectional area), the maximal muscle shortening velocity, and the pennation angle. The fifth is the slack length of the tendon (tendon cross sectional area is assumed to scale with its muscle's physiological cross sectional area (An, Linscheid & Brand 1991)). Model activation-contraction dynamics is adjusted to match the properties of slow or fast muscle fiber types by changing the activation and deactivation time constants of a first order differential equation (Zajac et al. 1989). This Hill-type model

has undergone several modifications but remains a first-order approximation to muscle as a large sarcomere with limited ability to simulate the full spectrum of muscles, or of fiber types found within a same muscle, or the properties of muscle that arise from it being composed of populations of motor units such as signal dependent noise, etc. Several researchers have developed alternative models for muscle contraction, which were used in specific studies (Zahalak & Ma 1990, Karniel & Inbar 1997, Gonzalez, Hutchins, Barr & Abraham 1996, Soechting & Flanders 1997).

The alternative approach has been to model muscles as populations of motor units. While this is much more computationally expensive, it is done with the purpose of being more physiologically realistic and enabling explorations of other features of muscle function. A well known model is that proposed by Fuglevand and colleagues (Fuglevand, Winter & Patla 1993), which has been used extensively to investigate muscle physiology, electromyography and force variability. However, the computational overhead of this model has largely limited it to studies of single muscles, and is not usually part of neuromuscular models of limbs. In order to develop a population-based model that could be used easily by researchers, Loeb and colleagues developed the Virtual Muscle software package (Cheng, Brown & Loeb 2000). It integrates motor recruitment models from the literature and extensive experimentation with musculotendon contractile properties into a software package that can be easily included in multibody dynamic models run in MATLAB (The Mathworks, Natick, MA).

2.6 Forward and inverse simulations

In "forward" models, the behavior of the neuromuscular system is calculated in the natural order of events: from neural or muscle command to limb forces and movements. In "inverse" models, the behavior is assumed or measured and the model is used to infer and predict the time histories of neural, muscle or torque commands that produced it. The same biomechanical model governed by Newtonian mechanics is used in either approach, but it is used differently in each analysis (Yamaguchi 2005, Winter 1990).

2.6.1 Forward models

The inputs to a forward musculoskeletal model are usually in the form of muscle activations (or torque commands if the model is torque driven) and the outputs are the forces and/or movements generated by the musculoskeletal system. The system dynamics is represented using the following equation,

$$M(q)\ddot{q} + C(q, \dot{q}) + G(q) = R(q)F_M + F_{\text{ext}}(q, \dot{q}) \tag{2.1}$$

where M is the system mass matrix, $\ddot{q}$ the vector of joint accelerations, q the vector of joint angles, C the vector of Coriolis and centrifugal forces, G the gravitational torque, R the instantaneous moment arm matrix, F_M the vector of muscle forces and F_{ext}, the vector of external torques due to ground reaction forces and other environmental forces. This system of ordinary differential equations is numerically integrated to obtain the time course of all the states (joint angles q and joint angle velocities $\dot{q}$) of the system.

The input muscle activations could be derived from measurements of muscle activity (electromyogram) or from an optimization algorithm that minimizes some cost function, for example the error in joint angle trajectory for all joints and energy consumed (Hatze 1977). Forward dynamics has also been used in determining internal forces that cannot be experimentally measured like in the ligaments during activity or contact loads in the joints. It gives insight on energy utilization, stability and muscle activity during function for example in walking simulations (Neptune, McGowan & Kautz 2009). It gives the user access to all the parameters of the system and to simulate effects when these are changed. This makes it a useful tool to study pathological motion and for rehabilitation. (Piazza 2006) provides a review on many of the applications of forward dynamics modeling.

2.6.2 Inverse models

Inverse dynamics consists of determining joint torque and muscle forces from experimentally measured movements and external forces. Since the number of muscles crossing a joint is higher than the degrees-of-freedom at the joint, multiple sets of muscle forces could give rise to the same joint torques. This is the load-sharing problem in biomechanics (Chao & An 1978b). A single combination is chosen by introducing constraints such that the number of unknown variables is reduced and/or based on some optimization criterion, like minimizing the sum of muscle forces or muscle activations. Several optimization criteria have been used in the literature (Patriarco, Mann, Simon & Mansour 1981, Anderson & Pandy 2001, Prilutsky & Zatsiorsky 2002). Muscle forces determined by this analysis are often corroborated by electromyogram recordings from specific muscles (Kaufman,

An, Litchy & Chao 1991, Happee & Van der Helm 1995). Since inverse dynamics consists of using the outputs of the real system as inputs to a mathematical model whose dynamics don't exactly match with the real system, the predicted behavior of the model does not necessarily match with the measured behavior of the real system. This is an important problem in inverse dynamics and is discussed in more detail in (Hatze 2002).

Both forward and inverse models are useful and can be complementary and the choice is largely driven by the goals of the study. The main challenge with both these analyses is experimental validation because many of the variables determined using either approach cannot be measured directly. The reader is directed to articles and textbooks that describe these methods in detail (Delp & Loan 1995, Delp, Anderson, Arnold, Loan, Habib, John, Guendelman & Thelen 2007, Winter 1990, Davoodi et al. 2003, An, Chao & Kaufman 1991, Andriacchi, Natarajan & Hurwitz 1991).

Chapter 3

Extrapolatable analytical functions for tendon excursions and moment arms from sparse datasets

3.1 Abstract

Computationally efficient modeling of complex neuromuscular systems for dynamics and control simulations often requires accurate analytical expressions for moment arms over the entire range of motion. Conventionally, polynomial expressions are regressed from experimental data. But these polynomial regressions can fail to extrapolate, may require large datasets to train, are not robust to noise, and often have numerous free parameters. We present a novel method that simultaneously estimates both the form and parameter values of arbitrary analytical expressions for tendon excursions and moment arms over the entire range of motion from sparse datasets. This symbolic regression method based on genetic programming has been shown to find the appropriate form of mathematical expressions that capture the physics of mechanical systems. We demonstrate this method by applying it to (i) experimental data from a physical tendon-driven robotic system with arbitrarily routed multiarticular tendons and (ii) synthetic data from musculoskeletal

models. We show it outperforms polynomial regressions in the amount of training data, ability to extrapolate, robustness to noise, and representation containing fewer parameters – all critical to realistic and efficient computational modeling of complex musculoskeletal systems.

3.2 Introduction

Computational modeling of complex musculoskeletal systems is sensitive to accurate representation of tendon routing, insertion points, and moment arm values (Hoy, Zajac & Gordon 1990, Valero-Cuevas et al. 2009). The most commonly used technique to obtain moment arm variations over the range of motion of a joint is the tendon and joint displacement method (An, Takahashi, Harrigan & Chao 1984). Implementation of this method generally involves fitting explicit analytical expressions for tendon excursions as functions of joint angles. Tendon excursions arise from changes in length of a musculotendon either due to active contraction or passive stretching. Hence they are directly related to muscle length changes and the maximal force a muscle can generate, as determined by the force-length properties (Zajac et al. 1989). Moment arms over the range of motion can then be obtained by taking partial derivatives of these tendon excursion expressions with respect to the corresponding joint angle changes. This standard approach has been used extensively in the literature to understand the contribution of different muscles towards the production of joint torque and limb motion (Eg. (An et al. 1983, Spoor, Van Leeuwen, Meskers, Titulaer & Huson 1990, Herzog & Read 1993, Liu, Hughes, Smutz, Niebur & Nan-An 1997)). It has also been used to validate musculoskeletal models representing

bone geometry and musculotendon pathways (Murray, Delp & Buchanan 1995, Buford Jr, Ivey Jr, Malone, Patterson, Pearce, Nguyen & Stewart 1997). Simulation of musculoskeletal dynamics for the development and testing of theories of motor control also specifically require analytical expressions for tendon excursions and moment arms as functions of joint angles (Scott 2004, Valero-Cuevas et al. 2009). Very often, dynamic equations of the system (which include the moment arm functions) need to be evaluated *iteratively* (perhaps tens of thousands of times) to solve for an optimal control law for each cost function and task goal (Theodorou, Todorov & Valero-Cuevas 2011). Such algorithms require accurate, computationally-efficient analytical expressions for moment arms for the entire range of motion.

Analytical expressions for moment arms and tendon excursions are of two kinds: (i) Idealized geometric models, or (ii) Empirical models. The coefficients of the analytical expressions in both these approaches are regressed from experimental data. These data consist of joint angles and tendon excursion measurements, often obtained from cadaveric specimens (An et al. 1983, An et al. 1984, Spoor et al. 1990, Visser, Hoogkamer, Bobbert & Huijing 1990, Pigeon, Yahia & Feldman 1996, Liu et al. 1997). In the first case, idealized geometric models, tendon routings are approximated by simple geometric shapes and the mathematical forms of the expressions are derived using trigonometry (Eg. (Landsmeer 1961, Stern Jr 1971, Van Zuylen, Van Velzen & van der Gon 1988)). While this might be sufficient to obtain approximate values of moment arms and tendon excursions in some simple cases, it may not necessarily be accurate for all muscles and is heavily dependent on assumptions about the anatomy. It is likely not appropriate for

the complex routing of many tendons around joints, as well as non-uniform bone geometry, deformity, surgical modification and injury. Therefore, most studies in biomechanics use the second approach: empirical models. These almost always consist of polynomial expressions (including splines, which are piecewise polynomials stitched together) mapping joint angles to tendon excursions, and are regressed from experimental measurements, such as using cadaveric specimens (Spoor et al. 1990, Visser et al. 1990, Pigeon et al. 1996, Liu et al. 1997, Menegaldo, de Toledo Fleury & Weber 2004, Franko, Winters, Tirrell, Hentzen & Lieber 2011). But these polynomial regressions have several inherent mathematical pitfalls; they can fail to extrapolate, may require large datasets to train, are not robust to noise, and often have numerous free parameters (Green & Silverman 1994). Hence they may not be the best choice to model multi-degrees of freedom biomechanical systems where (i) obtaining a rich dataset from the entire range of motion can be difficult (Clewley, Guckenheimer & Valero-Cuevas 2008), (ii) data are generally sparse and contain noise from measurement errors and skin deformations (Cappozzo, Catani, Leardini, Benedetti & Della Croce 1996, Holden, Orsini, Siegel, Kepple, Gerber & Stanhope 1997), and (iii) are susceptible to common errors in the estimation of axes of joint rotation and accurate joint angles (Woltring, Huiskes & de Lange 1983). In addition, polynomial functions are inherently a type of mathematical expression that is likely not reflective of the geometry and physics of tendon routing which even in the ideal case often contain trigonometric functions (Landsmeer 1961).

Here we present a novel method to find analytical functions for tendon excursions and moment arms as functions of joint angles that does not assume a specific mathematical form *apriori*. Rather, it simultaneously estimates directly from experimental

data both appropriate mathematical forms of the analytical expressions for moment arms and tendon excursions, and their best-fit parameter values. Previously we have called attention to the need for biomechanical modeling to go beyond parameter estimation and engage in the search for appropriate model forms (Valero-Cuevas, Anand, Saxena & Lipson 2007). Here we show an example of how to perform this simultaneous search of mathematical form, i.e. the structure consisting of mathematical building blocks; and parameter values, i.e. the coefficients and other constants accompanying each building block of the mathematical expression, using a software package called Eureqa (http://creativemachines.cornell.edu/eureqa). Eureqa implements symbolic regression using genetic programming (Schmidt & Lipson 2009). While symbolic regression and genetic programming have been used for over 15 years (Koza 1992) in the field of machine learning, Eureqa is a recent improvement that ensures faster convergence and more accurate solutions (Schmidt & Lipson 2005, Schmidt & Lipson 2006). Unlike other machine learning techniques that use a 'black box' approach to model input-output relationships, Eureqa has been shown to obtain computationally efficient, analytical expressions that can capture the physics of the system being modeled. In this chapter, we compare polynomial regression (the state-of-the-art used by the musculoskeletal modeling community to represent these systems) to our method. We apply the traditional polynomial regression approach and our novel machine learning method to both experimental data from a multi-articular tendon-driven robotic system, and computer-generated synthetic data from many simulated musculoskeletal systems with experimentally realistic noise added.
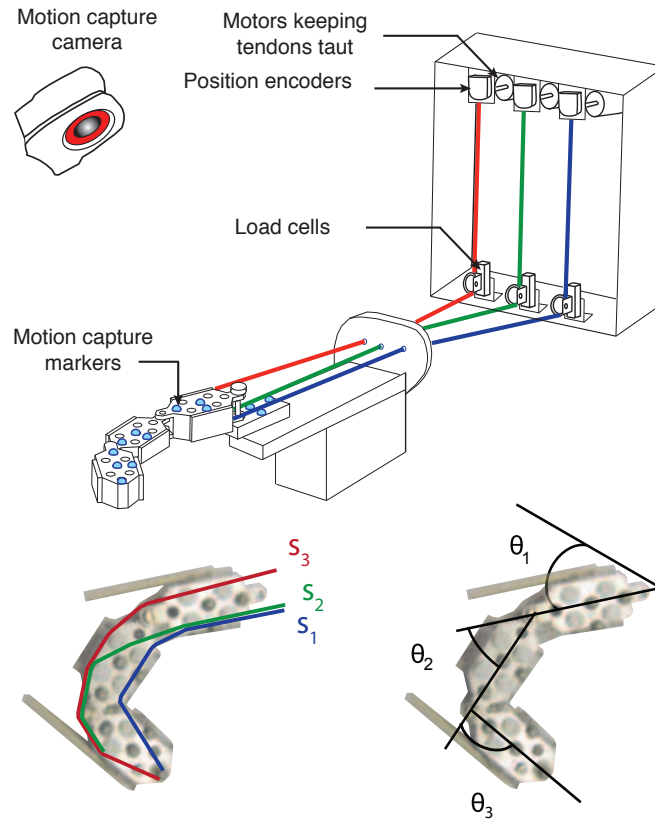
Figure 3.1: A three-joint planar robotic system with three arbitrarily routed tendons was moved manually to span a range of joint angles. The tendon excursions were recorded and joint angles calculated from motion capture data.

3.3 Methods

3.3.1 Symbolic regression using genetic programming

Symbolic regression is a machine learning technique that searches the space of mathematical operators, functions and parameter values to obtain analytical expressions that model available data based on a fitness criterion (Koza 1992). Evolutionary algorithms are generally used to guide this search in what is an infinite dimensional space. Here we use a software package called Eureqa that performs symbolic regression using genetic programming to infer implicit and explicit analytical functions to model input-output data (Schmidt & Lipson 2009). In our case, Eureqa searches for explicit analytical expressions of the form $s = f(\theta)$ mapping joint angles, θ to each tendon's excursion s (Fig. 3.1). The three joint angles and the excursion of the tendon of interest at any time step constitute a *data point*. Many such data points from the entire time series of the experiment form a *dataset*. We use sum of deviations of inferred analytical function predictions for the tendon excursions from true measurements (coming from experimental testing or computer simulation) over an entire dataset as the fitness criterion, i.e. the *fitness-error* to be minimized. In addition to this, Eureqa also penalizes the *equation-complexity*, defined as the sum of the number of parameters and terms in the analytical expressions being inferred. The search space consists of analytical expressions formed by parameter values and combinations of mathematical operations performed on the input variables (θ). In our case, we restricted the mathematical operations to addition, subtraction, multiplication, division, sine, cosine, tangent and square root. Polynomial expressions

are automatically generated by repeated multiplication of the input variables. In addition, Eureqa uses the concept of coevolution of fitness predictors, described in detail in (Schmidt & Lipson 2005), for faster and improved convergence of solutions. Instead of using the entire time history of the training dataset to calculate the fitness of evolving analytical expressions, it finds and uses a small set of data points (called fitness predictors) that can best distinguish between analytical expressions of otherwise equal fitness. Fitness predictors are chosen in every generation of evolution in parallel with the search for analytical expressions modeling the experimental data.

Unlike conventional optimization that would minimize fitness-error in a 'single line search' and find either the global minimum or one of the local minima of the fitness landscape, Eureqa uses multi-objective optimization to produce a family of multiple 'optimal' analytical expressions (15-20 expressions) that map joint angles to the tendon excursions. Each analytical expression has different levels of fitness-error and equation-complexity (defined above). This family of analytical expressions constitutes a Pareto front of fitness-error vs. equation-complexity. In this multi-objective optimization, the tradeoffs between the fitness criteria are made explicit to the user. The advantage of this approach is that it provides multiple analytical expressions that may be more or less sparse, accurate, computationally efficient, or revealing of the physics of the problem – either of which may be given more weight as 'optimal' by the user as desired. We chose to define as the optimal solution the one analytical expression that had the lowest extrapolation error (root mean squared error when tested with data points outside the range of training datasets). However, the reader is free to weigh other aspects more heavily. Our choice was driven by the need for analytical functions to have the ability

to extrapolate as it ensures that they are capturing the physics of the system; and not simply overfitting to the training data points. Each search in Eureqa starts with an initial set of multiple, random analytical functions, and terms are added/subtracted in discrete steps as the search progresses. Eureqa provides the support to run a search very easily on parallel computers that are connected in a network without requiring any special network architecture or hardware. On average, we ran each search in parallel for 12 hours on 20 computers (Dual Dualcore AMD Opteron 2.0 GHz) at the USC High-Performance Computing and Communications (www.usc.edu/hpcc) computer cluster. As is necessary in most machine learning problems without closed-form solutions, a stopping/convergence criterion needs to be defined. We defined the search to have converged if the fitness of the solution with the lowest fitness error remained unchanged for more than two hours. We repeated the entire search five times to test for consistency of results. The family of 'optimal' solutions was not necessarily of identical form in every repeat but of different representations of functions that modeled the data best with consistent RMS errors.

3.3.2 Comparison against polynomial regression

The state-of-the-art technique is to regress tendon excursions as polynomial functions of joint angles (Eg. (Spoor et al. 1990, Visser et al. 1990, Pigeon et al. 1996, Liu et al. 1997, Menegaldo et al. 2004)). We regressed the coefficients of multivariable linear, quadratic, cubic and quartic polynomials (all cross terms considered) using MATLAB © (Version R2009b, MathWorks, Natwick, MA). Polynomials of order greater than four overfit to the training data and performed worse than polynomial regressions of lower orders, and hence were not considered in this chapter. This is also the case with spline

functions, which are piecewise polynomials stitched together (Murray et al. 1995). Moreover, to evaluate dynamic equations of the system, for example to solve for an optimal controller, simple analytical functions modeling the behavior of the system throughout the range of motion are required. Splines or other piecewise surface fits would not be not suitable for this purpose and hence were not considered in this chapter. We compared the performance of analytical expressions from the multivariable linear, quadratic, cubic and quartic regressions against those from symbolic regression by testing with a cross-validation dataset (data points not selected for training, but within the range of training) and an extrapolation dataset (data points outside the range of training). We used root mean squared (RMS) error between the true tendon excursions (experimentally measured or simulated) and the analytical function predictions (coming from symbolic or polynomial regressions), normalized by the range of movement for that tendon and expressed as a percentage, as the fitness error criterion for the comparison. RMS errors were determined for cross-validation and extrapolation datasets.

3.3.3 Experimental data from a tendon-driven robotic system

We used a planar robotic finger with three links, three joints and three tendons to produce the motion capture data (Fig. 3.1). The three tendons were routed such that the first tendon flexed all joints (similar in action to the *flexor digitorum profundus* in the human finger), the second tendon, extended one joint and flexed the remaining two joints (similar to an intrinsic tendon) and the third tendon, extended all joints (similar to the *extensor digitorum communis*). We moved the robotic finger manually to span the full three-dimensional joint configuration space of flexion-extension in a human finger. Servo

40

dc motors maintained a constant tension of 1.5 N in every tendon to prevent tendons from going slack. As we moved the robotic finger, optical encoders measured tendon excursions at a sampling frequency of 10Hz. A 6-camera optical motion capture system, manufactured by Vicon (Lake Forest, CA), tracked reflective markers adhered to each segment of the robotic finger at a frequency of 30 Hz. The mean calibration residual error of the marker position reconstruction was less than 0.2 mm. We processed the 3D coordinates of the markers generated by the Vicon Nexus software to obtain joint angle changes for the entire duration of movement and then downsampled them to 10 Hz. We then partitioned the datasets to test for robustness of the inferred analytical expressions to (1) size of the training dataset and (2) range of extrapolation.

3.3.3.1 Reducing the size of the training dataset

We divided the experimental data into training, cross-validation and extrapolation datasets (training and cross-validation datasets coming from the same range of data and the extrapolation dataset consisting of data points outside the range of training). Then, we created nine independent training datasets by systematically reducing the number of training data points keeping the range fixed (n, $n/2$, $n/3$, etc. in Fig. 3.3). We performed symbolic and polynomial regressions using these nine different training datasets and tested the resulting analytical expressions with the fixed cross-validation and extrapolation datasets. This was repeated five times for each training dataset, for each tendon (S_1, S_2 and S_3), by re-sampling the training data points with replacement (Eureqa picked multiple random initial analytical functions at the beginning of each search). This was done to ensure that the observed results were consistent and not simply due to chance.

41

3.3.3.2 Increasing the range of extrapolation

We compared the regressions against one another in their ability to extrapolate, by performing regressions on training datasets and then testing with data points from six different ranges of extrapolation (25%, 50%, etc. in Fig. 3.4). We expressed each extrapolation range as percentage by volume of the training dataset (in joint angle space) where 0% means no extrapolation and 150% extrapolation refers to the situation where the volume of extrapolation is 150 % of the volume of the training dataset range (in joint angle space).[1] This was also repeated five times by re-sampling of training data points with replacement for each tendon (S_1, S_2 and S_3).

3.3.4 Computer-generated synthetic data

For validation purposes, we also tested our inference algorithm using synthetic (i.e., computer-generated) data because in this case, we would have access to the ground truth, and also be able to corrupt the datasets with noise in a systematic manner. Landsmeer's models I, II and III (Landsmeer 1961) are well-accepted analytical expressions mapping joint angles to tendon excursions describing three different kinds of tendon routings for limbs and fingers (An et al. 1983, Chao 1989, Brook et al. 1995). Landsmeer obtained these expressions using trigonometry assuming simplified geometry for anatomical systems (Landsmeer 1961). We generated synthetic datasets consisting of joint angles and tendon excursions from the 27 possible combinations (with repetition, 3x3x3) of the three

---

[1]For example consider a one-joint one-tendon system where the complete range of motion is 0-100 degrees. If we use 0-80 degrees as the range of training dataset for the regressions and test with joint angles between 80-100 degrees, it would be considered 25% extrapolation since we are extrapolating to a range that is 25% larger than the training range.

Landsmeer
model I
$s = 1.8\theta$

Landsmeer
model II
$s = 3.6sin(0.5\theta)$

Landsmeer
model III

$s = 0.6\theta + 3.2(1 - \dfrac{\theta/2}{tan(\theta/2)})$
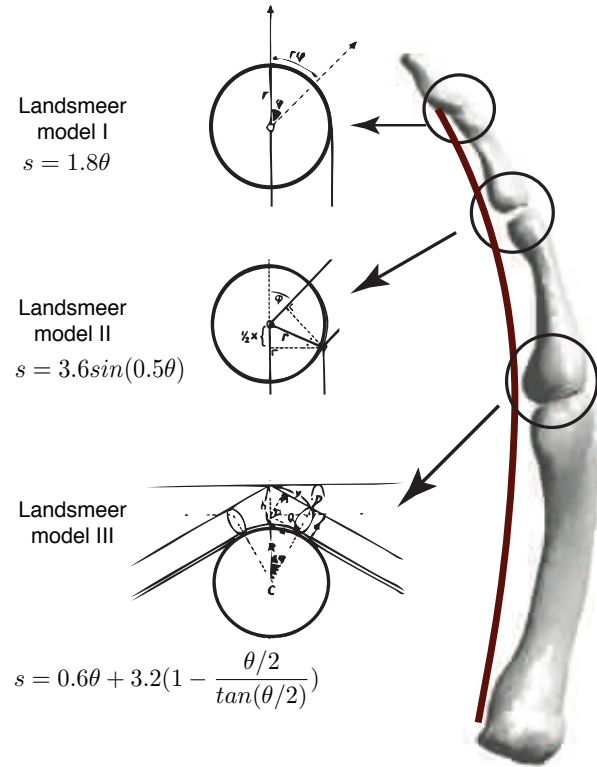
Figure 3.2: Synthetic data consisting of tendon excursions and joint angles were generated using models formed by combinations of Landsmeer's models I,II and III ([I I I],[I I II],...[III III III]).

Regression	Expressions
Symbolic	$13.7sin(\theta_1 - 0.78) + 12.3\theta_2 + 8.48\theta_3 + 4.02\theta_3 sin(\theta_3) + 14.5$
Linear	$9.26\theta_1 + 12.6\theta_2 + 11.8\theta_3 + 7.26$
Quadratic	$3.77\theta_1^2 + 0.89\theta_2^2 + 2.2\theta_3^2 - 0.338\theta_1\theta_2 - 0.457\theta_2\theta_3 - 0.142\theta_3\theta_1 + 8.35\theta_1 + 11.2\theta_2 + 9.7\theta_3 + 5.24$
Cubic	$-1.89\theta_1^3 - 2.05\theta_2^3 - 1.56\theta_3^3 - 0.438\theta_1^2\theta_2 + 0.258\theta_1\theta_2^2 - 0.0127\theta_1^2\theta_3 + 0.281\theta_3^2\theta_1 - 0.163\theta_2^2\theta_3 + 0.287\theta_3^2\theta_2 + 0.494\theta_3\theta_2\theta_1 + 4.8\theta_1^2 + 5.63\theta_2^2 + 5.02\theta_3^2 - 0.571\theta_2\theta_3 - 0.949\theta_1\theta_3 - 0.367\theta_1\theta_2 + 10.3\theta_1 + 8.88\theta_2 + 8.78\theta_3 + 4.83$
Quartic	$-1.26\theta_1^4 + 0.26\theta_2^4 - 0.0831\theta_3^4 + 0.208\theta_1^3\theta_2 - 0.635\theta_2^3\theta_1 + 0.756\theta_2^3\theta_3 - 0.222\theta_3^3\theta_2 - 0.26\theta_3^3\theta_1 - 0.159\theta_1^3\theta_3 - 0.0594\theta_1^2\theta_2^2 + 0.0947\theta_3^2\theta_1^2 - 0.824\theta_2^2\theta_3^2 + 0.0728\theta_3\theta_2^2\theta_1 - 0.112\theta_3^2\theta_2\theta_1 - 0.135\theta_3\theta_2\theta_1^2 - 1.08\theta_1^3 - 3.0\theta_2^3 - 0.903\theta_3^3 + 1.44\theta_2^2\theta_1 + 0.0506\theta_2\theta_1^2 + 0.109\theta_3\theta_1^2 + 0.516\theta_3\theta_2\theta_1 + 1.95\theta_3^2\theta_2 + 0.881\theta_3^2\theta_1 - 0.677\theta_3\theta_2^2 + 6.05\theta_1^2 + 6.64\theta_2^2 + 3.71\theta_3^2 - 1.26\theta_2\theta_1 - 1.54\theta_3\theta_2 - 1.11\theta_3\theta_1 + 9.72\theta_1 + 8.52\theta_2 + 9.44\theta_3 + 4.7$

Table 3.1: Examples of analytical expressions obtained using symbolic and the different polynomial regressions for one of the tendons of the robotic system.

Landsmeer models (Fig. 3.2). We then tested how well symbolic (i.e., Eureqa) and polynomial regressions could infer these hidden target expressions from input-output datasets. This allowed us to test whether or not the results obtained using the tendon-driven robotic finger also generalized to arbitrary combinations of anatomical tendon routing. We are not, however, suggesting that these Landsmeer's models are particularly accurate or realistic representations of real musculoskeletal systems.

We then compared the robustness of symbolic and polynomial regressions to (1) noise in the data and also (2) the number of free parameters in the analytical expressions obtained by the two regression techniques.

3.3.4.1 Robustness to noise

We added experimentally realistic noise of $\pm 5\%$ in joint angles and $\pm 1\%$ in tendon excursions to the synthetic data generated by the 27 combinations of the three Landsmeer models (Tendon excursions are generally measured directly using a ruler or position encoders whereas joint angles are inferred from motion capture marker positions or measured using a goniometer. The latter are subject to larger variations due to errors in marker/segment positions, joint axes estimations, skin deformations, etc (Woltring et al. 1983, Cappozzo et al. 1996)). We then performed symbolic and polynomial regressions on the noisy datasets and compared how well they model the noisy data by testing with the cross-validation and extrapolation datasets.
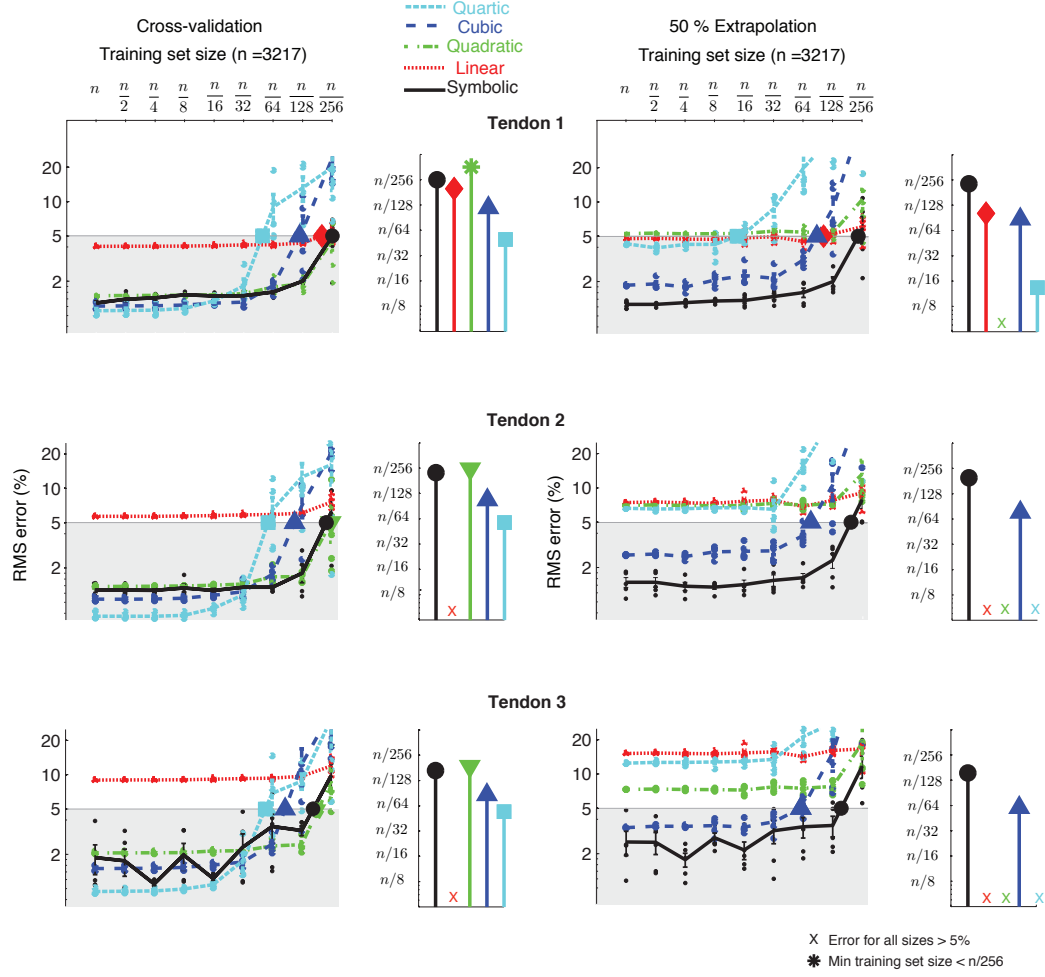
Figure 3.3: Effect of reducing the size of the training dataset : Comparison of RMS errors of symbolic and polynomial regressions with reduction in the number of training data points. The plots show mean and standard errors calculated across five runs for each regression type and training dataset size for the three tendons of the experimental robotic finger. When tested with the cross-validation dataset (interpolated from the same range as the training dataset), cubic and quartic regression had lower RMS errors compared to symbolic regression for large training datasets and quadratic regression had errors comparable to symbolic regression for small training datasets. But when tested with the extrapolation dataset (data points outside the range of training upto 50% of the volume of the training dataset), symbolic regression had lower errors than all polynomial regressions for all the different training dataset sizes. The stem plots show the training dataset size required to obtain a 5% RMS error using each of the regression techniques. Symbolic regression requires the fewest training data points compared to the different polynomial regressions for 5% cross-validation and extrapolation errors.

46

3.3.4.2 Number of free parameters

We compared the number of free parameters in the expressions inferred by symbolic regression against the number of coefficients in each form of polynomial regression. Expressions with fewer parameters are preferable not only because they are more computationally parsimonious and compatible with Occam's Razor, but also because expressions with a large number of parameters/coefficients tend to overfit to the training data, and naturally require larger training datasets.

3.4 Results

3.4.1 Results for the experimental tendon-driven robotic system

Symbolic regression could infer analytical expressions that had cross-validation and extrapolation RMS errors below 10% for each of the tendons of the experimental tendon-driven robotic system for all training dataset sizes and ranges of extrapolation. Table 3.1 shows examples of expressions obtained using the different regressions for one of the tendons of the robotic system in one of the cases. Below are the comparisons against polynomial regression:

3.4.1.1 Effect of reducing the size of the training dataset

We saw that symbolic regression was much more robust to reduction in the size of the training dataset (range being fixed) as compared to the polynomial regressions. As described above, this robustness was tested for cross-validation and extrapolation datasets.
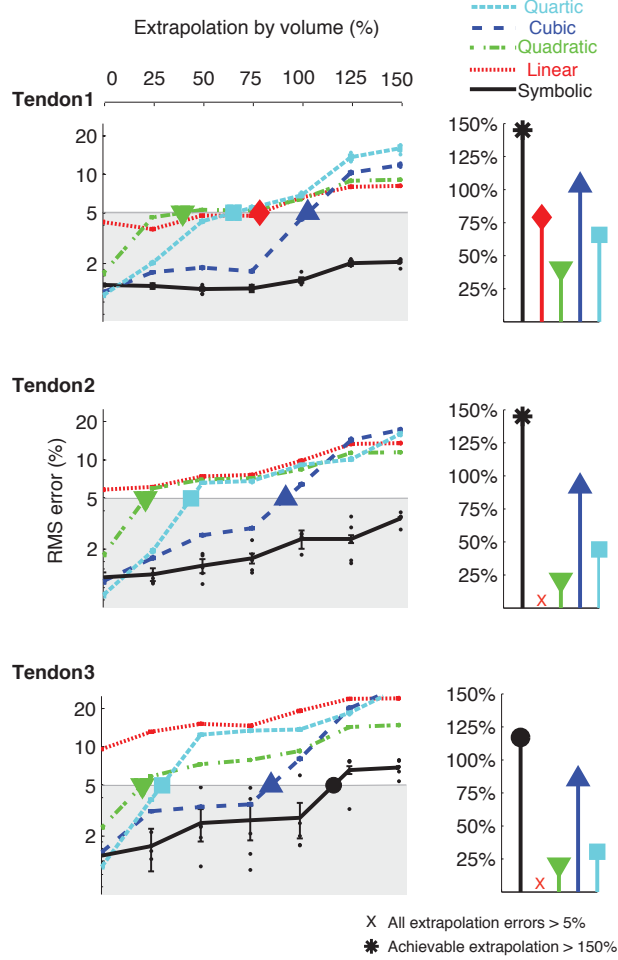
Figure 3.4: Effect of increasing the range of extrapolation: Comparison of RMS errors of symbolic and polynomial regressions across increasing ranges of extrapolation, expressed as a percentage by volume of the region in $\theta - \theta - \theta$ space enclosed by the training dataset. The plots show mean and standard errors calculated across five runs for each regression type and training dataset size for the three tendons of the experimental robotic finger. While cubic and quartic regressions have lower RMS errors for data points within the range of training (0% extrapolation), symbolic regression outperforms polynomial regressions for all ranges of extrapolation. The stem plots show the percentage of extrapolation achievable with each regression type to maintain the RMS error below 5%. Symbolic regression can extrapolate to much larger ranges of data compared to the different polynomial regressions for the same RMS prediction error.

In general, symbolic regression required fewer training data points than polynomial regressions to obtain RMS errors of 5% in tendon excursion predictions (Fig. 3.3). When tested with the cross-validation dataset, cubic and quartic regressions had lower RMS errors than symbolic regression for large training dataset sizes, but had much larger errors when the number of training data points was small. However, when tested with the extrapolation dataset, all polynomial regressions had much larger errors compared to symbolic regression, independent of the size of the training dataset (Fig. 3.3). These observations were consistent across all three tendons (S_1, S_2 and S_3 in Fig. 3.1).

3.4.1.2 Effect of increasing the range of extrapolation

Symbolic regression could extrapolate further away from the training datasets compared to polynomial regressions for the same RMS error in tendon excursion predictions. It could extrapolate to ranges beyond 150% of the range of the training dataset (by volume) for tendons one and two and up to 125% for tendon three and still maintain RMS errors below 5%. In comparison, linear, quadratic and quartic regressions could not extrapolate beyond 50-75% in most cases, and cubic regression up to 100% for the same RMS error of 5% in tendon excursion predictions (Fig. 3.4).

Figure 3.5 summarizes the comparison between symbolic and polynomial regressions for the experimental data from the tendon-driven robotic finger. It shows the achievable percentage extrapolation for the different regression techniques with reduction in training dataset size to obtain 5% RMS error in tendon excursion predictions. Symbolic regression could extrapolate to much larger ranges of data, compared to the polynomial regressions, for all the training dataset sizes.
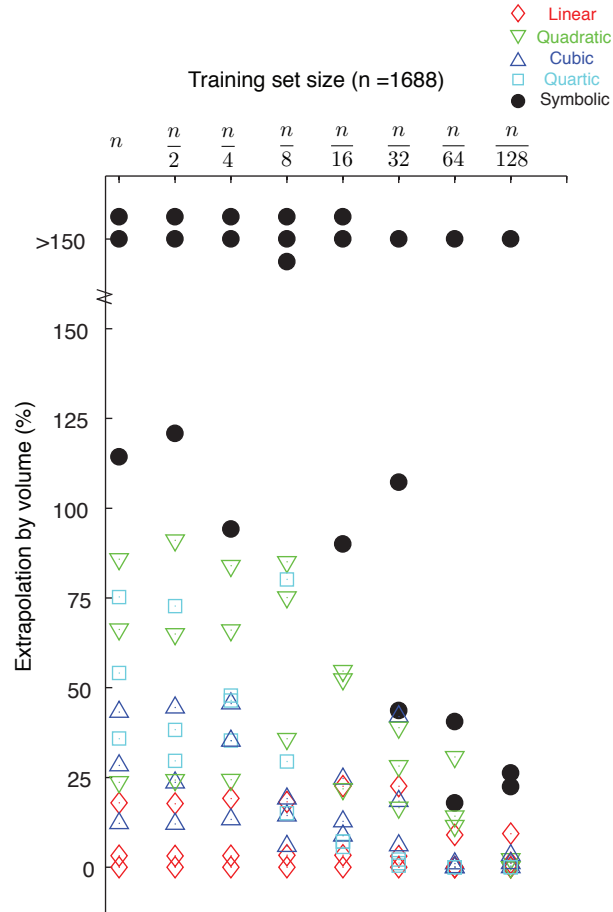
Figure 3.5: Summary of the comparison between symbolic and polynomial regressions in their ability to extrapolate and their performance with training dataset reduction. The achievable percentage extrapolation for models trained over different training dataset sizes to maintain RMS errors below 5% is shown for each regression technique for the three tendons of the planar robotic system. For each training dataset size, symbolic regression can extrapolate to larger ranges beyond the training dataset compared to polynomial regressions.

50

Landsmeer combination		Expressions	RMS errors (%)		
			Train.	Cross valid.	Ext.
I, I, I	Target	$1.8\theta_1 + 1.8\theta_2 + 1.8\theta_3$			
	Evolved	$1.8\theta_1 + 1.8\theta_2 + 1.8\theta_3$	0.001	0	0
I, II, III	Target	$1.8\theta_1 + 3.6sin(0.5\theta_2) + 0.6\theta_3 - (1.6\theta_3)/tan(0.5\theta_3) + 3.2$			
	Evolved	$1.8\theta_1 + 3.61sin(0.5\theta_2) + 1.54\theta_3 - 0.778sin(\theta_3)$	0.102	0.084	0.124
I, III, III	Target	$1.8\theta_1 + 0.6\theta_3 - (1.6\theta_3)/tan(0.5\theta_3) + 0.6\theta_2 - (1.6\theta_2)/tan(0.5\theta_2) + 6.4$			
	Evolved	$1.8\theta_1 + 0.61\theta_3 + 1.1\theta_3tan(0.24\theta_3) + 0.24\theta_2^2 + 2.15tan(0.287\theta_2)$	0.007	0.008	0.026
II, II, I	Target	$3.6sin(0.5\theta_1) + 3.6sin(0.5\theta_2) + 1.8\theta_3$			
	Evolved	$3.6sin(0.5\theta_1) + 3.6sin(0.5\theta_2) + 1.8\theta_3$	0.001	0	0
II, II, II	Target	$3.6sin(0.5\theta_2) + 3.6sin(0.5\theta_1) + 3.6sin(0.5\theta_3)$			
	Evolved	$3.6sin(0.5\theta_2) + 1.01(\theta_1 + sin(0.8\theta_1)) + 1.01(\theta_3 + sin(0.8\theta_3)) - 0.015$	0.043	0.041	0.318
III, II, I	Target	$1.8\theta_3 + 0.6\theta_1 - (1.6\theta_1)/tan(0.5\theta_1) + 3.6sin(0.5\theta_2) + 3.2$			
	Evolved	$1.8\theta_3 + 0.58\theta_1 + 0.31\theta_1^2 - 0.06sin(0.43\theta_1^2) + \theta_2 + 1.03sin(0.79\theta_2)$	0.031	0.034	0.165
III, III, III	Target	$0.6\theta_1 + 0.6\theta_2 + 0.6\theta_3 - (1.6\theta_1)/tan(0.5\theta_1) - (1.6\theta_2)/tan(0.5\theta_2) - (1.6\theta_3)/tan(0.5\theta_3) + 9.6$			
	Evolved	$0.58\theta_1 + 0.58\theta_2 + 0.55\theta_3 + 0.32\theta_1^2 + 0.32\theta_2^2 + 0.31\theta_3^2 - 0.13sin(0.32\theta_1^2) - 0.13sin(0.32\theta_2^2) + 0.018$	0.059	0.066	0.345

Table 3.2: Target and inferred expressions with training, cross-validation and extrapolation RMS errors(%) for some combinations of Landsmeer's models I, II, III

3.4.2 Results for the computer-generated synthetic data

All regressions produced very low errors for the computer-generated synthetic data when no noise or extrapolation was involved. We observed that of the 27 possible combinations of the three Landsmeer's models, symbolic regression tended to infer the exact target ground-truth expressions for joints with models I and II, and found expressions equivalent or closely related to the original expression (e.g., Taylor series terms or alternative trigonometric forms) for joints with model III (Table 3.2). The training, cross-validation and extrapolation RMS errors were below 0.4% for all 27 combinations.

3.4.2.1 Robustness to noise

When experimentally realistic noise was added to the training datasets, cubic and quartic regressions overfit to the noise and performed poorly when tested for cross-validation and extrapolation (Fig. 3.6). In contrast, symbolic regression outperformed the polynomial regressions for all tendons when tested with extrapolation datasets and matched quadratic regression when tested with cross-validation datasets. The box plot in Fig 3.6 shows that for the 27 combinations of Landsmeer's models with noise added, on average symbolic and quadratic regressions had equivalent cross-validation errors, whereas symbolic was 8% better than quadratic regression when tested with the extrapolation dataset. Hence, symbolic regression would be the regression of choice to model tendon excursions in physiological systems from experimental data, where measurement noise cannot be avoided.
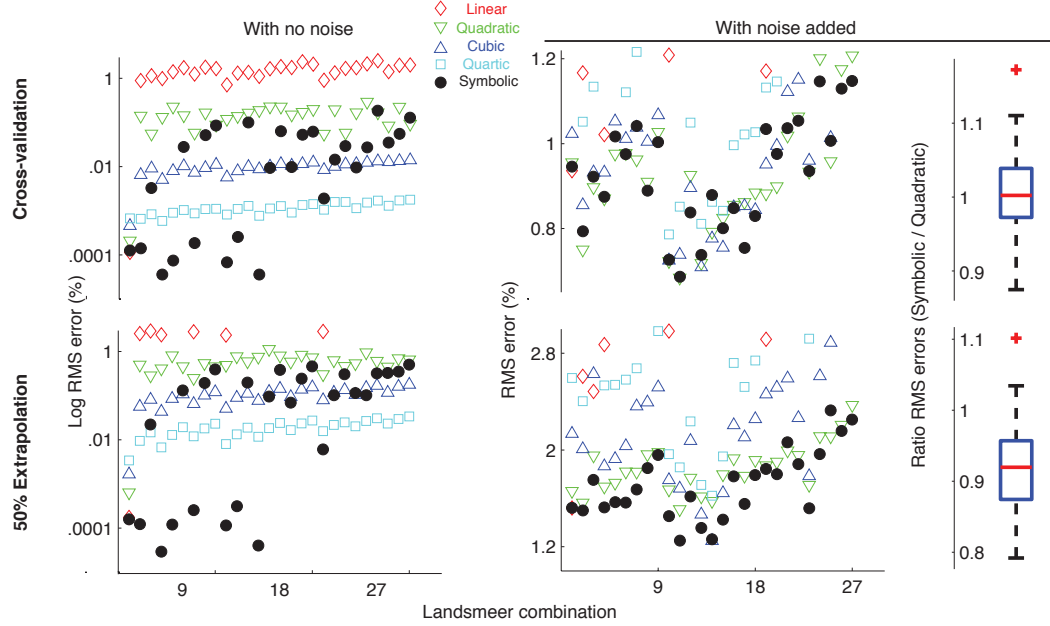
Figure 3.6: Comparison of root mean squared errors between symbolic and polynomial regressions for the 27 combinations of Landsmeers models with no noise and with ±5% noise added to joint angles and ±1% to tendon excursions. While cubic and quartic regressions have lower errors than symbolic regression for data with no noise, when experimentally realistic noise is added, symbolic regression has much lower errors than these polynomial regressions. The box plot on the right shows the ratio of RMS errors of symbolic to quadratic regression (best among polynomial regressions) for the data with noise. The median ratio is close to one for cross-validation testing demonstrating that symbolic and quadratic regressions are equivalent with respect to RMS errors in this case whereas for extrapolation testing, the median ratio is 0.92 indicating that on average, symbolic regression has 8% lower RMS errors than quadratic regression across the 27 models.
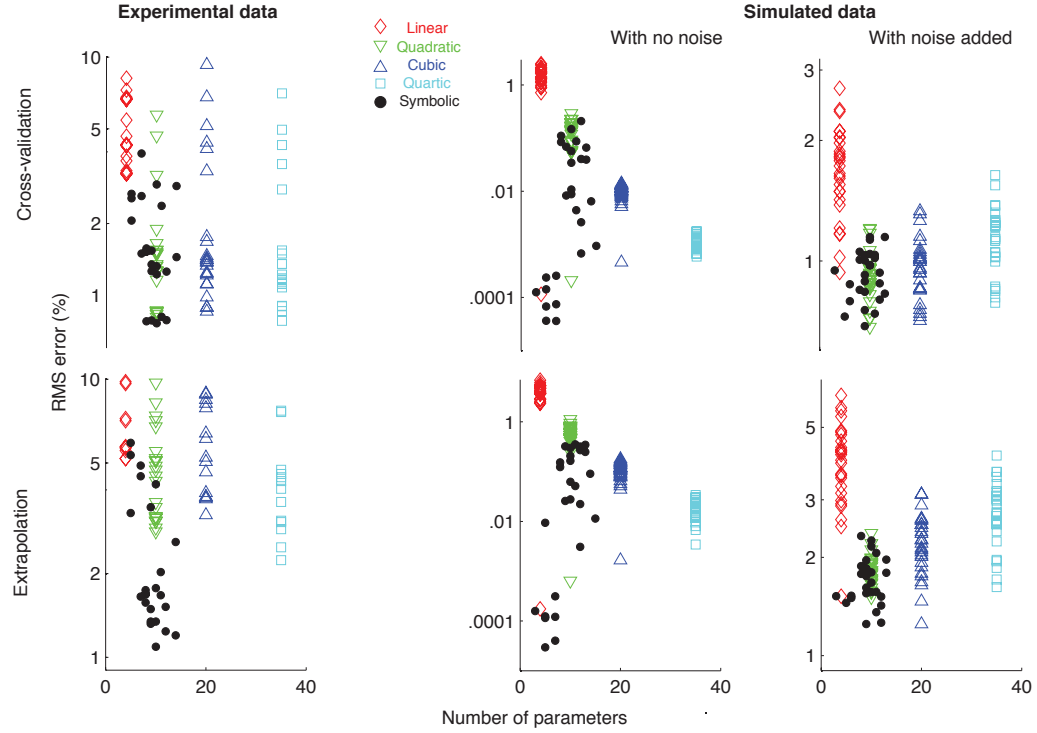
Figure 3.7: Comparison of RMS errors and number of parameters across symbolic and polynomial regression models for experimental data from the three tendons of the planar robotic system and synthetic data generated using the 27 combinations of Landsmeers models with no noise and with experimentally realistic noise added. In all cases, symbolic regression models have fewer parameters and lower RMS errors compared to the polynomial regressions.

3.4.2.2 Number of free parameters as a practical measure of the complexity of the analytical expression

Analytical expressions obtained using symbolic regression had fewer free parameters and lower cross-validation, extrapolation errors compared to polynomial regressions for experimental data from the tendon-driven robotic system as well as for the synthetic data with no noise and with noise added (Fig. 3.7).

3.5 Discussion

We have presented a novel method based on symbolic regression that can infer accurate analytical expressions mapping joint angles to tendon excursions from sparse datasets. Symbolic regression outperforms polynomial regression, the state-of-the-art technique used in musculoskeletal modeling, in that it requires smaller training datasets, can extrapolate to ranges outside that of the training dataset, and does not contain an arbitrary number of free parameters that can lead to overfitting the training datasets and/or their noise. We have demonstrated these advantages of symbolic regression using both experimental and synthetic data and strongly suggest that this approach may be a more suitable choice to model tendon mechanics for neuromuscular systems.

Obtaining the necessary experimental data to create valid analytical expressions to represent the musculoskeletal system is invariably difficult and costly. This is true for both cadaveric specimens and human subjects. Hence it is critical to be able to extract functionally accurate analytical expressions from as sparse a dataset as possible. Moreover, because the ground truth is not usually known, it is important to have confidence

that the expressions found are unaffected by unavoidable measurement noise, that enough data are available/used, that the form of the analytical expressions is appropriate and parsimonious, and that the analytical functions are valid for the entire natural workspace of the limb. We have demonstrated here that symbolic regression, as implemented in Eureqa (Schmidt & Lipson 2009), outperforms polynomial regression, the state-of-the-art in musculoskeletal modeling, with respect to these performance criteria.

For the physical system of tendons traveling over joints with smoothly varying mechanical behavior, it is critical that the tendon excursion expressions model data even outside the range of the experimentally obtained data points on which they are trained to ensure they capture the true behavior of the system, and not just overfit to the training data points. Moreover, obtaining data spanning the entire range of motion of a multi-degree of freedom biomechanical system is very difficult. It would also necessitate a larger training dataset. Polynomial models do not extrapolate well again due to their overfitting behavior whereas symbolic regression avoids this problem and can model points well beyond the range of training data.

Experimental data from biomechanical specimens is unavoidably polluted by measurement noise and/or uncertainty. These can arise from skin deformation, motion capture errors and/or estimation of axes of joint rotation, measurement errors and/or noise, etc. Small errors in these measurements lead to large errors in the inferred joint angle kinematics (Woltring et al. 1983, Cappozzo et al. 1996, Holden et al. 1997). While experimental data are often filtered, filtering introduces artifacts and reduces the resolution of the measurements. Hence it is important that the regression technique employed be robust to

noise and capture the true underlying system behavior with the highest resolution possible. We show that polynomial regression models, especially higher order polynomials, overfit to the noise and can be poor representations of the real underlying behavior of the system. In contrast, symbolic regression is seen to be robust to noise and is more accurate than polynomial regressions in modeling noisy data.

The form of the analytical function must also strike a balance between parsimony and accuracy. Functions with a large number of free parameters require a large training dataset for the estimation of the values of those parameters. They also have a greater tendency to overfit to the training dataset when compared to models with fewer parameters. On the other hand, analytical functions with too few parameters will fail to accurately represent the functional nonlinearities of the system. The symbolic regression algorithm in Eureqa explores multiple potential forms for the analytical function while also penalizing the number of parameters; and prioritizes low fitness error solutions with fewer parameters over those with more parameters. In many of the cases we present, polynomial functions of higher orders have a large number of free parameters compared to the more parsimonious analytical functions found by symbolic regression.

The ability of symbolic regression to infer the nonlinear target expressions of the Landsmeer models shows that our method can capture the underlying physics of the system directly from input-output data. This is particularly the case here because the target expressions were derived by Landsmeer by hand using principles of geometry and anatomy. As argued elsewhere (Schmidt & Lipson 2009), the fact that symbolic regression did not only infer adequate mathematical expressions but those target expressions is worth noting. At the very least, this says that those target expressions are parsimonious and

that Eureqa is able to favor parsimonious expressions. In addition, this demonstrates how the analytical expressions for tendon excursions or moment arm variations generated by symbolic regression may contain insight on the geometry of the tendon routing – and therefore capture the physics of the system.

Unlike conventional optimization that is based on a 'single line search' and finds the global optimum or one of the local optima of the fitness landscape, Eureqa converges on a family of optimal solutions that lie on the Pareto front of the fitness error-complexity plane. The user is then free to choose the solution they want based on the features of the analytical expressions most important to them such as (i) Observation and knowledge of the system being modeled, (ii) Fitness error alone, (iii) Cross-validation or extrapolation error (as we chose to in this chapter), etc. Polynomial regressions or other functional regressions do not offer this choice. Currently, selection of suitable functions is mostly driven by the properties and pitfalls of polynomial fitting as opposed to giving the freedom to the investigator to choose functions for scientific or computational reasons.

Until recently, measuring tendon excursions accurately was only possible in cadaveric specimens. But with advances in the field of magnetic resonance and ultrasound imaging, it has become possible to record moment arms in live subjects (Rugg, Gregor, Mandelbaum & Chiu 1990, Maganaris 2004, Blemker et al. 2007). While in this chapter we have demonstrated the use of symbolic regression to extract analytical functions mapping joint angles to tendon excursions assuming direct measurements in cadaveric systems, it will soon be possible to measure tendon excursions and moment arms non-invasively in vivo – and our techniques will be applicable to those measurements. This would enable estimation of accurate, subject-specific models of moment arm variation that are critical, for

example, in the cases of deformity, surgical modification, injury, or the development of functional electrical stimulation controllers (Khang & Zajac 1989) and for patient-specific diagnosis and rehabilitation.

The analytical functions obtained are selected to be computationally efficient for iterative or real-time use, but they can be costly to find off-line. One of the major limitations of symbolic regression is computational cost, since it uses genetic programming that involves searching a high dimensional space for optimal or near-optimal solutions. Eureqa was designed to execute on a cluster of parallel computers by automatically parallelizing the search process, where the computation time is reduced linearly with the number of processors available. Also, while it might be computationally expensive to infer these analytical expressions, it needs to be done only once. The resulting analytical expressions can then be used as part of the model in the research of interest. In fact, once inferred, the computational cost of implementing the expressions is lower given that parsimony (and therefore computational efficiency) is an explicit fitness criterion. Eureqa's graphical user interface allows the user to continuously monitor the fitness error as well as the family of optimal analytical functions throughout a search. The user can pause and continue, or terminate the search at any point. In addition, the user has the flexibility to select the set of mathematical operations that are to be the possible options defining the space of feasible functions to be generated. While choosing more operations would make the search more generic and thus increase computational cost for function inference, restricting the solution space too much can also lead to inappropriate or inaccurate analytical functions. Hence an informed choice needs to be made based on knowledge of the system

being modeled, the purpose of the analytical functions, and availability of computational power.

State-of-the-art biomechanical modeling involves assuming a fixed topology/form for the system being modeled and estimating the parameter values from experimental data. In our previous work (Valero-Cuevas, Anand, Saxena & Lipson 2007), we have demonstrated that modeling of certain complex biomechanical systems requires simultaneous inference of both model topology and parameter values directly from experimental data. Here, as a continuation of that work, we have demonstrated that the conventional method of assuming a fixed polynomial form and regressing coefficients from experimental data, suffers from certain drawbacks which can be overcome by using symbolic regression that simultaneously infers both the form and the parameter values of the analytical expressions directly from experimental data.

We have demonstrated the advantages of using this method in a tendon-driven robotic system. We are currently applying it to infer analytical expressions modeling tendon excursions in the human fingers from cadaveric data.

Acknowledgment

robotic finger. This material is based upon work supported by NSF Grants EFRI-COPN 0836042 and NIH Grants AR050520 and AR052345 to FVC.

Chapter 4

Simultaneous inference of the form and parameters of analytical models describing tendon routing in the human fingers.

4.1 Abstract

Control of finger movement and force is made possible by a complex network of tendons. Analytical models for the excursions and moment arms of these tendons have been used extensively in the literature to understand finger motion and force, to understand the changes in actions of different muscles with joint posture, and more recently, to model finger dynamics to test theories of motor control. The analytical models used in the literature are mostly of two kinds: i. Polynomial regressions and ii. Functions consisting of Landsmeer's models which are based on approximate geometry of tendon routing. Both these types of models assume a fixed form for the mathematical expressions while the parameter values are either regressed from experimental data or calculated based on assumptions about the anatomy or some optimization criteria. Here we demonstrate a

novel method based on symbolic regression that simultaneously infers both the mathematical form and the parameter values of these models directly from experimental data. We use this technique to infer analytical models for the seven tendons controlling the index finger. We demonstrate that these models are more accurate and have fewer parameters than both polynomial regressions as well as models consisting of Landsmeer's models when tested with i. data from multiple trials from the same cadaveric hand and ii. data from different cadaveric hands. Hence, our symbolic regression approach would be the method of choice whether the goal is to obtain subject-specific analytical models representing these systems or models that generalize across the population.

4.2   Introduction

Tendon routing in the human fingers is complex with the presence of networks of interconnections that connect multiple muscles to multiple joints. The actuation of these tendons by the muscles to bring about movement and force is not fully understood (Zancolli 1979, Brand & Hollister 1999). Computational modeling of these systems have been extensively used in the literature to understand the role of these networks in human manipulation including grasp, climbing, playing music (Leijnse 1996, Vigouroux, Quaine, Labarre-Vila & Moutet 2006, Sancho-Bru et al. 2001, Sancho-Bru, Perez-Gonzalez, Vergara & Giurintano 2003), to understand changes upon injury (Valero-Cuevas et al. 2000), neuromuscular control(Esteki & Mansour 1996, Valero-Cuevas 2000b) and to develop functional electrical stimulation controllers (Esteki & Mansour 1997).

Many of these computational models often rely on explicit analytical expressions representing changes in tendon excursions with joint angles. Instantaneous moment arms (and hence, moment arm matrices) can then be calculated using the tendon excursion-joint displacement technique (An et al. 1984) by taking partial derivatives of these expressions with respect to the joint angle changes. Such models have been used in the literature not only in the fingers but in different musculoskeletal systems in the body, to understand how the action of muscles changes with joint posture(Eg. (An et al. 1983, Spoor et al. 1990, Herzog & Read 1993, Liu et al. 1997)). They have been used to validate anatomical models explicitly representing the physics of interactions of tendons with bones (Eg. (Murray et al. 1995, Buford Jr et al. 1997)). These analytical models are particularly important for the simulation of musculoskeletal dynamics to test theories of motor control where moment arms (part of the system dynamics) need to be evaluated iteratively several thousand times(Theodorou et al. 2011). In such simulations, compact, simple representations which can be easily differentiated and evaluated quickly are critical.

The most commonly used analytical models representing tendon routing in the fingers are based on Landsmeer's models I, II and III (Landsmeer 1961) where the tendon excursions for the different tendons are represented as combinations of the different Landsmeer models based on geometry of the joints they actuate. The parameter values for the Landsmeer models in these cases are obtained from force optimizations in simulation and ratios of distribution of forces in the different bands of the extensor mechanism (Brook et al. 1995, Berme, Paul & Purves 1977, Purves & Berme 1980). The other type of analytical model consists of polynomial regression models where tendon excursions are assumed

to be of polynomial form (linear, quadratic, cubic, etc.) and the coefficients are regressed from experimental data obtained from cadaveric specimens (Eg. (Franko et al. 2011)). Both these types of models rely on fixed mathematical forms for the expressions. In the previous chapter, we introduced a new approach to infer simultaneously both the form and the parameter values of analytical expressions representing tendon excursions as models of joint angles(Kurse et al. 2012). We demonstrated the success of this approach using data generated by simulating combinations of Landsmeer models(Landsmeer 1961) and also using experimental data generated using a robotic tendon driven system. Here we apply this novel approach to infer analytical models mapping joint angles to tendon excursions from experimental data obtained from a human cadaveric index finger. We compare the models generated using this approach to polynomial expressions regressed from experimental data and also trigonometric functions generated using combinations of Landsmeer's models as presented in (Brook et al. 1995).

4.3   Methods

4.3.1   Experimental setup and data collection

We dissected a freshly frozen human cadaveric hand and attached the seven tendons of the index finger (*flexor digitorum profundus (FDP), flexor digitorum superficialis (FDS), extensor indicis (EIP), extensor digitorum communis (EDC), first lumbrical (LUM), first dorsal interosseous (FDI), and first palmar interosseous (FPI)*) to nylon strings that were connected to seven dc servo motors (Fig 4.1). We applied constant tensions on each tendon equal to 5% the maximum force its corresponding muscle can apply(Valero-Cuevas
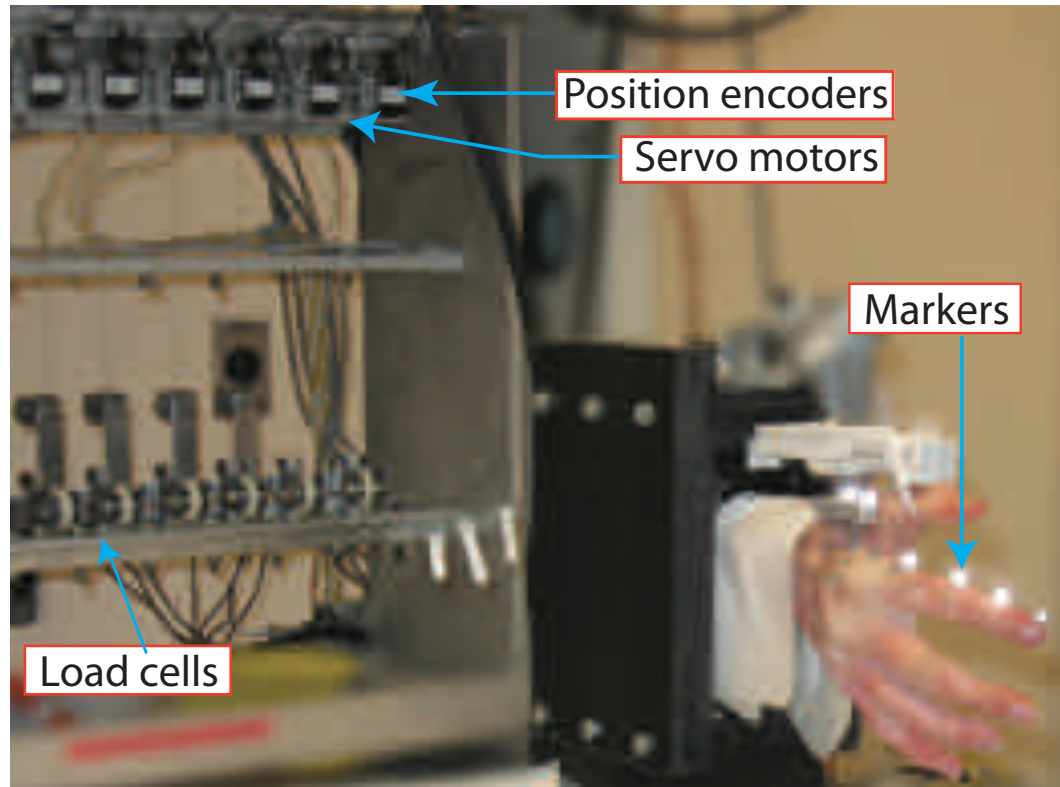
Figure 4.1: The index finger of a freshly frozen cadaveric finger was moved manually to span a range of joint angles. The excursions of the seven tendons were recorded and joint angles calculated from motion capture data.

et al. 2000). This prevented the tendons from going slack. We then moved the finger manually to span the full four-dimensional joint configuration space (ad-abduction and flexion-extension at the metacarpophalangeal joint (MCP), and flexion-extension at the the proximal interphalangeal joint (PIP) and the distal interphalangeal joint (DIP) of the index finger. A single movement trial lasted for five minutes. As we moved the finger, optical encoders measured tendon excursions at a sampling frequency of 10Hz. We used a 6-camera optical motion capture system, manufactured by Vicon (Lake Forest, CA), to track reflective markers adhered to each segment of the finger, at a frequency of 30 Hz. The mean calibration residual error of the marker position reconstruction was less than 0.2 mm. We processed the 3D coordinates of the markers generated by the Vicon Nexus software to obtain the four sets of joint angle changes for the entire duration of movement and then downsampled them to 10 Hz. This provided us a dataset consisting of a set of joint angles of the four degrees-of-freedom for the index finger and corresponding tendon excursions of the seven tendons. We divided this complete dataset into a training, cross-validation and extrapolation datasets. Please see chapter 3 for descriptions of these datasets. We repeated the movement trial with the same set of tensions on all the tendons to obtain a second dataset of joint angles and tendon excursions. We also repeated the above experimental procedure with a second cadaveric index finger to obtain a third dataset of joint angles and tendon excursions. While we moved the finger to span the full four-dimensional space in all trials, the actual movement time profiles were different in each case.

4.3.2 Symbolic regression implementation using Eureqa

We used a software program called Eureqa(Schmidt & Lipson 2009) that implements symbolic regression using genetic programming to learn the analytical models that map joint angle changes to the tendon excursions of the seven tendons of the index finger. The objective function defined in the Eureqa environment was to find explicit analytical models of the form $s = f(\boldsymbol{\theta})$, where s is each tendon's excursion and $\boldsymbol{\theta}$ is the vector of the four joint angles at every time step, minimizing the root mean squared errors between predicted and experimentally measured values for tendon excursions (*fitness error*). Only the data points from the training dataset were used to infer the analytical models. In addition to minimizing the error criterion, Eureqa also penalizes *model complexity* defined by the number of mathematical operators and parameter values in the function. Using this multi-objective optimization approach, Eureqa produced a family of multiple 'optimal' analytical models (15-20 functions) that map joint angles to the tendon excursions and lie on the Pareto front of the fitness error vs. complexity (defined above) plane. The advantage of this approach is that the user now has the choice to pick a solution based on the criterion of interest: minimizing cross-validation error, extrapolation error or based on inspection. Please see (Kurse et al. 2012) and Chapter 3 for more details about Eureqa implementation in tendon driven systems. Here, we chose the expressions that gave the lowest RMS error when tested on all the data points in the dataset(s) of interest. On average, we ran each search in parallel for 150 core hours on a cluster of computers(Dual Dualcore AMD Opteron 2.0 GHz) at the USC High-Performance Computing and Communications (www.usc.edu/hpcc) computer cluster.

4.3.3 Comparison against polynomial regression and Landsmeer based models

The state-of-the-art technique in musculoskeletal modeling is to regress tendon excursions as polynomial functions of joint angles (Eg. (Spoor et al. 1990, Visser et al. 1990, Pigeon et al. 1996, Liu et al. 1997, Menegaldo et al. 2004, Franko et al. 2011)). We regressed the coefficients of multivariable linear, quadratic, cubic and quartic polynomials (all cross terms considered) using MATLAB © (Version R2009b, MathWorks, Natwick, MA). We did not consider polynomials of order greater than four because they tend to overfit to the training data and perform worse than polynomial regressions of lower orders. Spline functions, which are piecewise polynomials stitched together (Murray et al. 1995) would also overfit to the data. Please see 3 for more reasoning on why we chose only these polynomials. We also implemented the analytical models proposed in (Brook et al. 1995) consisting of combinations of Landsmeer's models and whose parameter values are based on force distribution in the extensor mechanism suggested in earlier papers including (Chao & An 1978a). We uniformly scaled these Landsmeer-based model expressions using the training dataset to minimize the RMS errors between the experimentally recorded and model predicted tendon excursions. This was done to account for differences in hand size across specimens.

While all the analytical models (symbolic, polynomial and Landsmeer-based) were obtained using only the training data points from the first dataset, they were compared against each other with respect to i Mean errors across two movement trials from the

same cadaveric hand and ii. Mean errors across two trials from two different cadaveric hands.

4.3.3.1   Two movement trials from the same cadaveric specimen

We calculated the RMS errors between model-predicted and experimentally measured tendon excursions over all the data points in the two datasets from the same cadaveric specimen. We compared the mean of the two RMS errors for the different analytical models. In other words, we wanted to see which models had lowest error across the two datasets. Since symbolic regression gave us a family of multiple analytical models, we chose the function with the least error across the two datasets for comparison.

4.3.3.2   Two trials with two different cadaveric specimens

We repeated the above procedure using : the first dataset (same movement trial used for training) and the dataset obtained from the second cadaveric specimen. We again compared the mean of the two RMS errors for the different analytical models to see which models had the lowest error across the two specimens. For symbolic regression, we chose the analytical expression with the smallest error among the family of functions obtained. When testing against data points from the second hand specimen, we scaled all the models (symbolic, polynomial and Landsmeer-based) uniformly to account for differences in hand size.

$$s_{fdp} = 10.36\theta_{mcp} + 10.95\theta_{pip} + exp(1.84\theta_{dip})$$
$$s_{fds} = 12.47\theta_{mcp} + 7.22\theta_{pip} - exp(1.49 - 4.22\theta_{pip} - 24.15\theta_{mcp}\theta_{pip} - 26.03\theta_{add}) - \theta_{dip} + 5.34$$
$$s_{ei} = 5.86sin(1.97\theta_{add} - \theta_{mcp}) - 3.92\theta_{pip} + 0.8$$
$$s_{edc} = -6.99sin(\theta_{mcp} - \theta_{add}) + 5.09cos(0.23 + \theta_{pip}) - 4.39$$
$$s_{lum} = 2.54\theta_{mcp} - 0.71cos(39.7\theta_{add}\theta_{mcp} - 3.1\theta_{mcp}) - 13.05\theta_{add} - 4.83\theta_{pip}$$
$$s_{fdi} = -5.64\theta_{add} - 4.4\theta_{add}sin(4.94\theta_{mcp}) + 1.27sin(3.4\theta_{mcp}) + 1.45cos(1.02 - 1.96\theta_{pip}) - 4.83\theta_{add}\theta_{pip}$$
$$s_{fpi} = 9.38\theta_{mcp} + 9.25sin(3.01\theta_{add}) - 11.29\theta_{add}\theta_{mcp} + 4.12cos(\theta_{pip} + 4.12\theta_{add}) - 3.01$$

Table 4.1: Analytical models obtained using symbolic regression for the excursions of the seven tendons of the index finger (FDP,FDS,EIP,EDC,LUM,FDI,FPI) that generalize best across trials from the same cadaveric hand.

$$s_{fdp} = 10.36\theta_{mcp} + 10.95\theta_{pip} + exp(1.84\theta_{dip})$$
$$s_{fds} = 12.17\theta_{mcp} + 8.14\theta_{pip} - \theta_{dip} + 4.46$$
$$s_{ei} = -9.61\theta_{mcp} - 2.85\theta_{pip} + 1.19$$
$$s_{edc} = -9.13\theta_{mcp} + \theta_{add} - 3.34\theta_{pip} + 1.47$$
$$s_{lum} = 2.54\theta_{mcp} - 13.05\theta_{add} - 0.71cos(39.7\theta_{add}\theta_{mcp} - 3.1\theta_{mcp}) - 4.83\theta_{pip}$$
$$s_{fdi} = 4.51\theta_{mcp}$$
$$s_{fpi} = 9.48\theta_{mcp} + 8.08sin(2.99\theta_{add}) - sin(13.95\theta_{add}\theta_{mcp}) + 4.31cos(\theta_{pip} + 2.99\theta_{add}) - 3.2$$

Table 4.2: Analytical models obtained using symbolic regression for the excursions of the seven tendons of the index finger (FDP,FDS,EIP,EDC,LUM,FDI,FPI) that generalize best across trials from different cadaveric hands.

4.4   Results

Table 4.1 shows the 'best' analytical models obtained using symbolic regression that had lowest mean RMS errors across the two movement trials from the same cadaveric specimen. These are the expressions that would best describe this specific cadaveric specimen. The expressions consist mostly of linear, trigonometric and exponential terms. Table 4.2 shows similar analytical models obtained using symbolic regression with lowest mean RMS errors across the two specimens from among the family of multiple solutions. Note that both these sets of expressions are from the same family of solutions inferred using the training data points from the first movement trial. The expressions that generalized across the two specimens had more linear components, fewer parameters and hence may be termed simpler than the functions in Table 4.1.
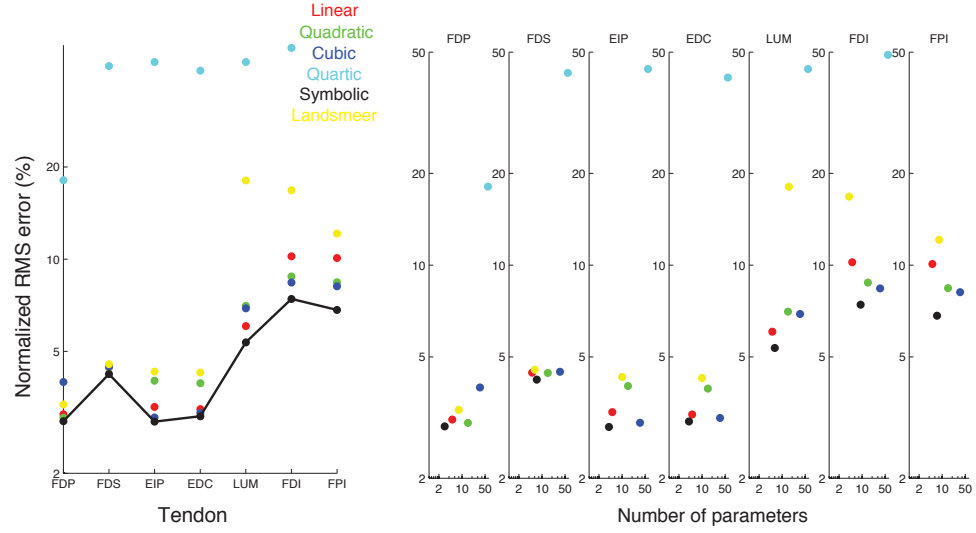
(a) Mean of normalized RMS errors of the different models across two movement trials from the same cadaveric specimen. The best symbolic regression function (picked from the family of functions generated) had lower errors across the two trials compared to the polynomial regressions and the Landsmeer based models.

(b) Normalized RMS errors vs. the number of parameters in the functions generated using the different techniques. Symbolic regression expressions had fewer parameters and lower RMS errors compared to the other functions.

Figure 4.2: Comparison of symbolic, polynomial and Landsmeer functions when tested on datasets from two different movement trials from the same cadaveric specimen to compare generalizability of functions across experimental trials.
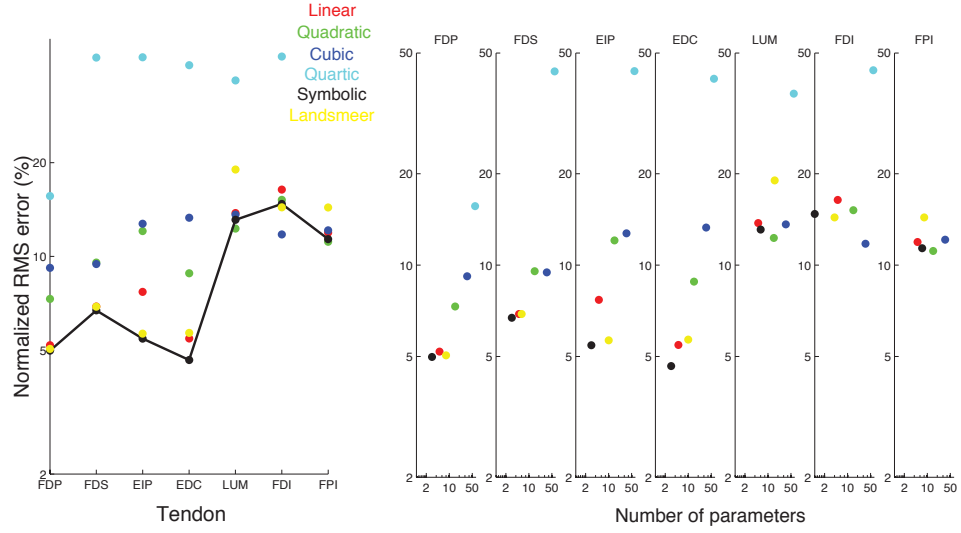
(a) Mean of normalized RMS errors of the different regressions across two movement trials from two different cadaveric specimens. The models were all trained on dataset from one specimen but uniformly scaled when tested on the other specimen. The best symbolic regression model (picked from the family of functions generated) had lower mean errors across the specimens, compared to the other functions.

(b) Normalized RMS errors vs. the number of parameters in the models generated using the different techniques. Symbolic regression expressions had fewer parameters and lower RMS errors compared to the other models.

Figure 4.3: Comparison of symbolic, polynomial and Landsmeer models when tested on datasets from two different cadaveric specimens to compare generalizability of models across hands.

Fig. 4.2a shows the comparison of performance of the analytical models for symbolic regression against other analytical models upon testing with data points from the two movement trials from the same cadaveric hand. The symbolic regression functions had the lowest RMS errors. While the errors for the flexor tendons (FDP, FDS) were comparable across the different models, the models had more varying errors for the extensor (EIP, EDC) and intrinsic tendons (LUM, FDI, FPI). The intrinsic tendons also had much larger errors compared to the other tendons. Quartic regression in all cases had very large errors. Quartic regression tends to overfit to the training data points and has been observed to perform badly with cross-validation and extrapolation data 3.

Fig. 4.2b shows the RMS errors of the models vs. the number of parameters in each. Expressions with fewer parameters may be considered simple, have lesser tendency to overfit to the data and hence, are more desirable. Symbolic regression expressions had lower RMS errors as well as fewer parameters than the other models.

Fig. 4.3a shows the comparison of the different models when tested with data points from two different specimens. The errors for all models were larger than before as expected. Symbolic regression solutions again had lower errors than the other models (except for the FDI where cubic regression model had a lower RMS error). The models disagree much more in this case with respect to one another for all the tendons in comparison to the previous case. The intrinsic tendons (LUM, FDI, FPI) were observed to have larger errors in all models in comparison to the extrinsic tendons (FDP,FDS, EIP and EDC). Fig. 4.3b compares the RMS errors of the models vs. the number of parameters. Symbolic regression expressions had fewer parameters and lower errors than the other models.

4.5 Discussion

We have implemented a novel method based on symbolic regression to simultaneously infer the mathematical form and parameter values of analytical models representing the tendon excursions of the index finger. We have demonstrated that these models are more accurate than both polynomial regressions (linear, quadratic, cubic and quartic) as well as Landsmeer-based models in representing tendon routing, whether our goal is to obtain i. subject-specific models of these systems or ii. models that generalize across specimens. We also show that these symbolic regression models have fewer parameters than the other models which is important to ensure they do not overfit to the training data points.

The analytical models obtained using symbolic regression that best fit the data from a single cadaveric hand mostly consisted of linear, exponential and trigonometric components. The expressions for the tendon excursions give some insight into the physics of interaction and routing of these tendons. For example, the expressions for the lumbrical and the FPI contain coupling terms $\theta_{mcp}\theta_{add}$ reflecting on the way these tendons are routed about the MCP joint whereas tendons like the FDP and FDS do not contain this term and are known to produce a more straightforward flexion-extension motion at the joints. This insight is not available in case of polynomial regressions. The analytical models that generalize well across the two hand specimens are more 'simpler' than the functions in the previous case with the latter consisting of a larger number of linear terms. While we know that these functions generalize best across the two cadaveric specimens in comparison to the other models, whether they are sufficiently accurate would have to

be decided by the modeler looking at the RMS error values presented in Fig. 4.3a and the problem they are trying to solve.

As we have shown in chapter 3, polynomial regressions tend to overfit to the training dataset. This results in very large errors when tested on data points either not in the training dataset but lying in the range of the training data (cross-validation dataset) or data points outside the range of training (extrapolation dataset). Hence when tested on the complete dataset as we have done here, the errors of functions like quartic regression are very high.

All models are more accurate for the 'simpler' tendons, the FDP, FDS, EIP and EDC, in comparison to the intrinsic muscles (LUM, FDI, FPI). These larger errors could be attributed in part to the joint model of the MCP where the orientation of the ad-abduciton axis to the flexion-extension axis has been long debated (Berme et al. 1977, Youm, Gillespie, Flatt & Sprague 1978, Valero-Cuevas 1997) and in part because these tendons do not independently control the finger joints but attach to the extensor mechanism which in turn controls joint motion. Again the complexity of the extensor mechanism is well known (Eg. (Landsmeer 1949, Garcia-Elias, An, Berglund, Linscheid, Cooney Iii & Chao 1991),etc.). Also, there have been variations observed across the population in terms of attachment points of the intrinsic muscles (Salsbury 1937). This could also explain why all models performed much worse for the intrinsics when tested across datasets from two different hand specimens.

Models with fewer coefficients are preferable to models with a large number of coefficients to reduce overfitting (Kurse et al. 2012). They may also be considered as 'simpler' and more elegant representations of the system. Symbolic regression functions had much

fewer parameters than the other models. This is because Eureqa (the symbolic regression program used here) explicitly favors solutions that have fewer mathematical components (parameters and mathematical operators) to those with a larger number of mathematical components.

Most existing studies use cadaveric testing to obtain analytical models for moment arms and tendon excursions. But, with advances in imaging, it is becoming possible to measure tendon excursions and moment arms in live subjects(Rugg et al. 1990, Maganaris 2004, Blemker et al. 2007). We can then apply our methodology to datasets from these imaging studies to obtain accurate, subject-specific models of tendon routing that would be critical to developing functional electrical stimulators or for diagnosis and repair.

While the analytical models obtained using symbolic regression are selected to be computationally efficient for iterative or real-time use, they can be computationally expensive to find. But this needs to be done only once. Please see 3 for the limitations of Eureqa and how some features built in Eureqa help to minimize those limitations.

Acknowledgment

material is based upon work supported by NSF Grants EFRI-COPN 0836042 and NIH

Grants AR050520 and AR052345 to FVC.

Chapter 5

Experimental cadaveric actuation gives insight on control of human finger movement

5.1 Abstract

Human finger movement is produced by the coordinated actuation of several tendons interacting with one another. The control mechanisms that produce this movement are not well understand. In this chapter, we describe the use of computer controlled servo motors to actuate the seven tendons of a cadaveric index finger to produce a simple tapping motion. We observe that controlling the motors as tunable springs, similar to human muscles, is an effective way to control finger movement in comparison to simple force or position control. We also observe that two types of equilibria can be demonstrated in the cadaveric finger: i. stable equilibrium where the displacement of the finger brings it back to a specific posture and ii. what we describe as neutral equilibrium observed in a specific range of postures and tendon tensions where the finger when disturbed from equilibrium stays in the new displaced posture. We show that the tendon tensions in the

latter type of equilibrium lie close to the null space of the moment arm matrix that maps tendon tensions to joint torques.

5.2 Introduction

Slow and accurate finger movements are critical to human manipulation. There have been several studies in the literature that have described these movements in different activities of daily living, like typing, movement to grasp, etc (Eg. (Dennerlein, Mote Jr & Rempel 1998, Santello, Flanders & Soechting 2002)). But how the nervous system controls the complex musculature that actuates the human fingers to produce these movements is not completely understood. Understanding control of finger movement is important to be able to predict and correct changes that happen during injury and disease, to develop functional electrical stimulation controllers and to build better robotic and prosthetic hands.

Accurate measurement of the excursions of the tendons actuating the fingers and the corresponding muscle forces during these simple finger movements would give insight on how the nervous system is controlling them. Unfortunately, it is currently impossible to measure both forces and tendon excursions accurately in a live person. While electromyography (EMG) is useful to determine when a particular muscle or groups of muscles are turning on and off, how the signal can be related to either muscle force or tendon excursions is not clearly understood (Inman, Ralston, De CM Saunders, Bertram Feinstein & Wright Jr 1952, Disselhorst-Klug, Schmitz-Rode & Rau 2009). On the other hand, artificially actuating a human cadaveric specimen makes it possible to completely measure

inputs (the tendon excursions and forces) and outputs (fingertip forces and joint angle changes). In this chapter we describe the cadaveric actuation system we have developed, that enables us to selectively control the tendons of a human cadaveric hand. We use this setup to control the tendons of the index finger to produce a slow tapping motion (flexion-extension movement) and to study finger equilibrium at different postures and input tendon tensions. This cadaveric actuation gives us a better understanding of the problems the nervous system faces when actuating the complex musculature of the fingers.

5.3   Methods

We dissected a freshly frozen human cadaveric hand and mounted it on a fixed support using an external fixator (Agee-WristJack, Hand Biomechanics Lab, Inc., Sacramento, CA). We attached the seven tendons of the index finger (flexor digitorum profundus (FDP), flexor digitorum superficialis (FDS), extensor indicis (EI), extensor digitorum communis (EDC), first lumbrical (LUM), first dorsal interosseous (FDI), and first palmar interosseous (FPI)) to nylon strings that were connected to seven dc servo motors (Fig. 5.1). We measured the tension exerted on each tendon using one degree-of-freedom load cells and the tendon excursions using optical encoders attached to the motors. We used a real-time controller (PXI 8108, National Instruments, Austin, TX) to control the motors in three different modes : i. *position control mode* where the motors were commanded to apply specific tendon excursions on each of the tendons, ii. *force control mode* where the motors were commanded to apply specific tension on each tendon, and iii. *sping control mode* where the motors were made to behave like tunable springs whose spring constant
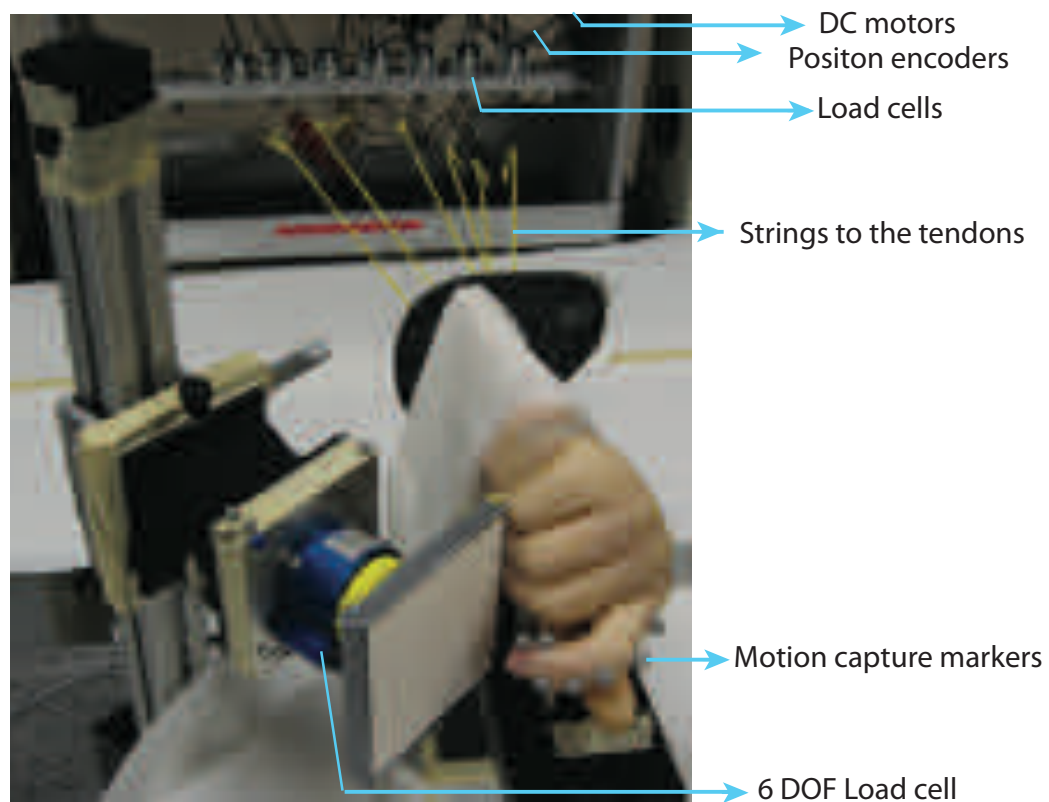
Figure 5.1: Experimental setup to control the index finger of a freshly frozen cadaveric hand to produce flexion-extension motion. The seven tendons of a freshly frozen human cadaveric hand were attached to strings connected to servo motors. The finger was moved by the experimenter to produce a flexion extension motion of the index finger in force control mode. The tendon excursions were recorded and played back in spring control mode, where the motors were controlled to behave like tunable springs.

could be adjusted and the command to each motor was in the form of change in resting length of the spring.

5.3.1 Control of finger tapping motion

The first phase of the experiment was the *recording phase*. In this phase, we maintained a constant tension of 5N on all the tendons of the cadaveric finger using force control mode and moved the finger manually to produce a motion that resembled a simple finger tap (Venkadesan & Valero-Cuevas 2008). We recorded tendon tensions and excursions throughout the movement. The next phase of the experiment was the *playback phase* where we played back the excursions recorded in the first phase as changes in resting lengths of the tunable springs corresponding to each tendon in spring control mode. This helped us to replicate the tapping motion produced in the first phase.

5.3.2 Finger equilibrium study

We applied a constant tension of 3N to each of the seven tendons of the index finger in force control mode (coordination pattern 1). The finger came to a stable equilibrium position. We then perturbed the finger from this position and the finger returned to the equilibrium posture. Then, keeping the finger in a specific posture (neutral ad-abduction and approximately 20 degrees flexion at the metacarpophalangeal (MCP), proximal interphalangeal (PIP) and distal interphalangeal (DIP) joints), we adjusted the tensions on the tendons by trial and error to find a specific set of tensions that maintained the finger in that posture in equilibrium (coordination pattern 2). We then moved the finger to a different posture keeping the tension on each of the tendons the same (using
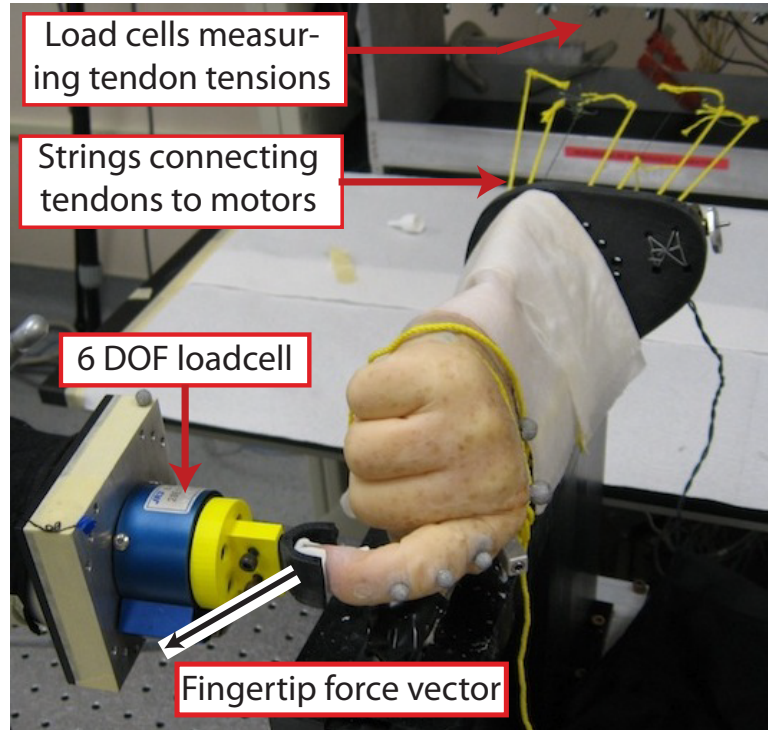
Figure 5.2: The experimental setup used to record fingertip forces from a freshly frozen cadaveric hand. We applied all possible combinations of high and low tensions to the seven tendons of the index finger (there are 128 such combinations) and recorded corresponding fingertip forces. We repeated this in three different finger postures : *fully flexed*, *tap* and *fully extended*.

force control) and the finger stayed in equilibrium even in the new posture. We observed a range of finger postures where the finger remained in this equilibrium. We call this state of equilibrium, neutral equilibrium and describe more in section 5.5. Movement beyond this range resulted in the finger attaining the posture that formed the boundary of this neutral equilibrium. We then increased the tension on one of the finger tendons (FDS) (coordination pattern 3) and this neutral equilibrium was lost. The finger now reached a new equilibrium, in a new posture. Changing the finger posture manually resulted in the finger coming back to this new equilibrium in a spring like behavior.

We then performed an isometric force production experiment where we adjusted the finger segments to a posture in the range where the neutral and stable equilibrium had been observed in the previous scenario, and attached the cadaver fingertip to a six degree-of-freedom load cell 5.3. We applied multiple combinations of tendon tensions consisting of a low force of 1N and high force of 11N (using force control mode) and recorded the corresponding fingertip forces. We then regressed a matrix mapping tendon tensions ($\mathbf{F_m}$) to fingertip force ($\mathbf{F_{tip}}$) which we call the action matrix (A). We can then obtain the moment arm matrix, R from the action matrix as demonstrated below. We then multiplied this matrix with the transpose of the jacobian ($J(\theta)$) transforming joint angle velocities to fingertip velocities, to obtain the moment arm matrix (R) of the finger in this posture. We did not use the entire fingertip wrench (force and torque at the endpoint (Valero-Cuevas et al. 1998)) but only the fingertip force. Hence the action matrix is only an approximation of the actual action matrix.

It can be shown using Principle of Virtual Work (Yoshikawa 1990, Valero-Cuevas 2009),

$$\mathbf{F_{tip}} = J(\theta)^{-T}\boldsymbol{\tau}$$

where $\mathbf{F_{tip}}$ is the wrench vector at the fingertip, $J(\theta))$ is the Jacobian transforming joint angle velocities to fingertip velocity and the $\boldsymbol{\tau}$ is the vector of joint torques. However,

$$\boldsymbol{\tau} = R\mathbf{F_m}$$

where R is the moment arm matrix and $\mathbf{F_m}$ is the vector of tendon tensions. Hence,

$$\mathbf{F_{tip}} = J(\theta)^{-T}R\mathbf{F_m}$$

$$\mathbf{F_{tip}} = A\mathbf{F_m}$$

$$A = J(\theta)^{-T}R$$

$$R = J(\theta)^{T}A$$

We then calculated joint torques ($\boldsymbol{\tau} = R\mathbf{F_m}$) using the moment arm matrix R. The null space of the 4×7 moment arm matrix is 3 dimensional. We calculated the distance of the three coordination pattern vectors from the null space of the moment arm matrix to see how far each of these patterns were from being in the null space. Here is how we determined the distance from the null space:

$$\mathbf{w} = U(U^{T}(U))^{-1}U^{T}\mathbf{F_m}$$

$$d = \|\mathbf{F_m} - \mathbf{w}\|$$

where U is the matrix formed by the bases vectors of the null space of the action matrix A and $\mathbf{w}$ is the projection of F_m on the null space.

5.4   Results

We were able to successfully control the motion of the human cadaveric finger and record tendon excursions and tendon tensions for all movements.

5.4.1   Results from control of finger tapping motion

Fig. 5.3 shows the start and end posture of the cadaveric finger during the tapping motion as well as the time history of excursions and tensions of the seven tendons. The playback of the finger tapping motion using the spring control mode produced smooth, repeatable movements at all the joints. Even though the motion produced was a simple flexion-extension, a coordinated set of excursions of all tendons were required. This is due to the routing of the seven tendons around the four degrees-of-freedom of the index finger. The tension profiles observed were based on the spring stiffness chosen to produce the movement and are not unique.

5.4.2   Results from finger equilibrium study

We observed that the finger exhibited two kinds of equilibria when the tendons were held at constant tension in force control mode: i. Stable equilibrium where the displacement of the finger posture resulted in its coming back to the same posture, and ii.   what
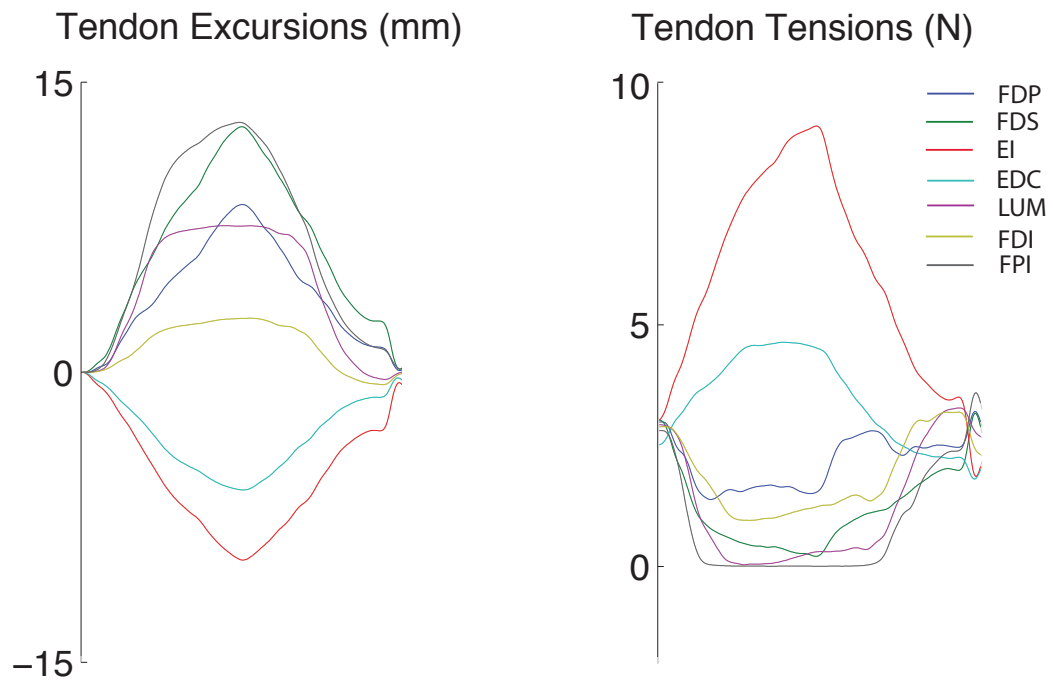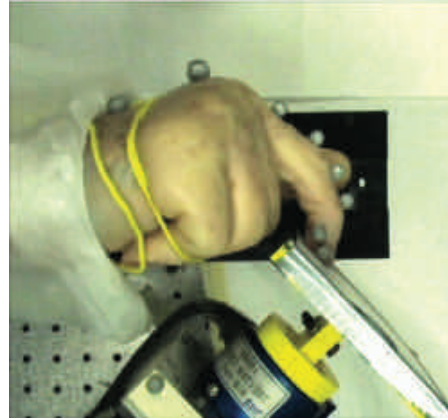
Figure 5.3: Tendon excursions and tendon tensions for a single tap. The figure shows the cadaver finger in the start and end of a single tap. Even a simple flexion-extension motion of the finger requires a coordinated set of excursions of all the seven tendons controlling the index finger. The tendon tension profile shows the tensions in the corresponding tendons during this movement which are not unique.
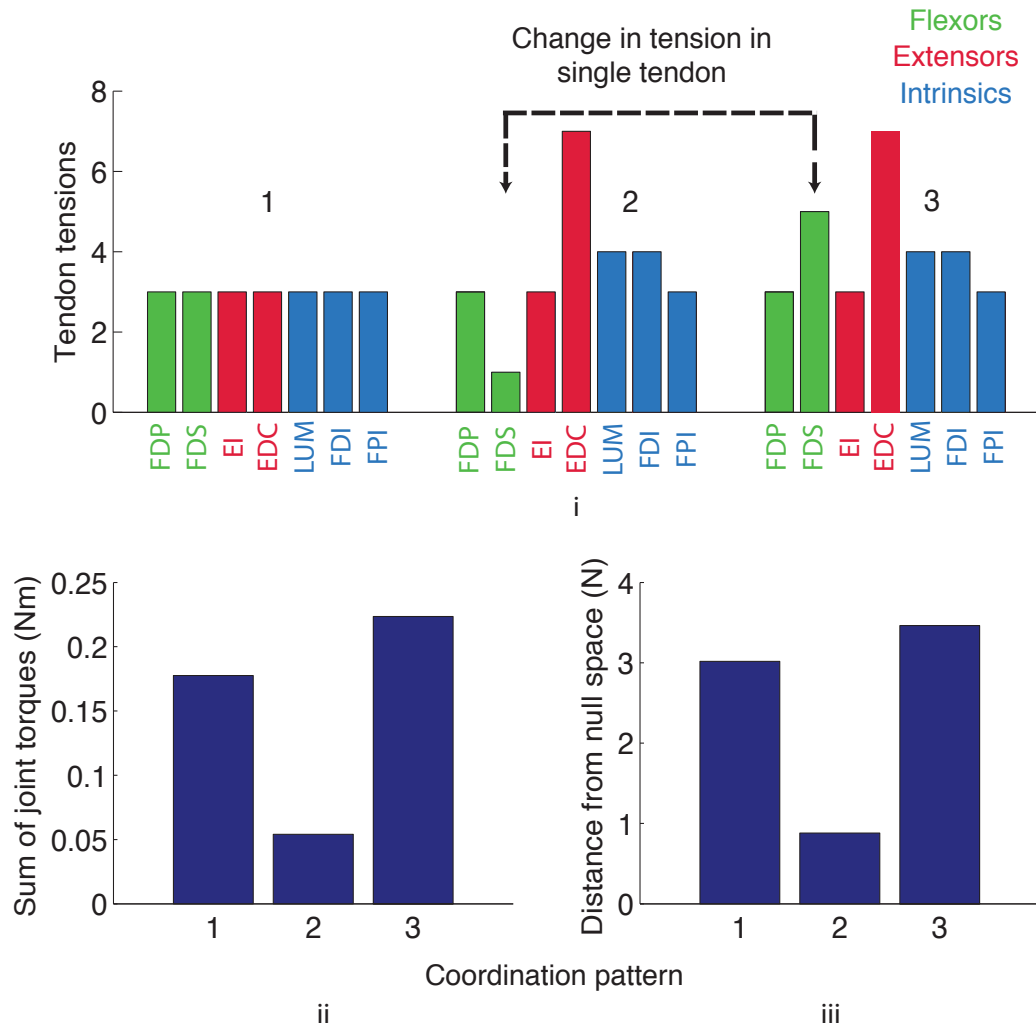
Figure 5.4: Results from the finger equilibrium study. i. Three different coordination patterns were applied to the seven tendons. The only difference between coordination pattern 2 and 3 is the tension applied to the FDS tendon. ii. The sum of joint torques was calculated for each of the three coordination patterns based on a constant moment arm matrix regressed from experimental data consisting of tendon tensions and fingertip force outputs in an isometric test. The calculated joint torque was smallest for the second coordination pattern that produced neutral equilibrium in the finger. iii. Calculating the distance of the coordination patterns from the null space of the moment arm matrix showed that the second pattern producing the neutral equilibrium was closest to the null space.

we describe as neutral equilibrium where the displacement of the finger results in a new posture and the finger stays in equilibrium in this new posture. In section 5.5, we describe how we believe these equilibria are being attained.

Fig 5.4 shows the three coordination patterns applied and the results from the calculation of the joint torques and distances from the null space. The sum of joint torques in the four-degrees of freedom was smallest in coordination pattern 2 compared to the other two coordination patterns. The distance of coordination pattern 2 from the null space of the moment arm matrix was also the smallest, implying that coordination pattern 2 which produced the neutral equilibrium pattern in the finger was closest to the null space of the moment arm matrix among the three patterns.

5.5 Discussion

We have demonstrated the successful control of a cadaveric index finger to produce a simple tapping motion consisting of flexion-extension of the MCP, PIP and DIP of the index finger. We have also demonstrated that the finger exhibits neutral equilibrium in a specific range of joint postures and tendon tension combinations and stable equilibrium in others, when the tendon tensions are maintained at a constant set of values.

Even a simple motion like finger flexion-extension requires a coordinated set of tendon excursions in all the tendons. But this does not necessarily mean that all the muscles attached to these tendons need to be activated. Muscles not activated would be stretched passively by the actions of the other muscles and the joint motion. The tendon tension profile we recorded in our cadaveric actuation setup is again the force that in a living

person would come from both active contraction and passive stretching. These force profiles are not unique due to redundancy in the system (Bernstein 1967, Kutch & Valero-Cuevas 2011). Multiple sets of muscle forces can lead to the same tendon excursions and joint motion. The nervous system could pick a coordination pattern depending on the task and the cost function being considered.

We tried to implement the finger tapping motion in force control, position control and spring control modes. Force control, where the command consists of specific sets of tendon tensions requires a good model of the plant to execute successfully. Otherwise the specimen could be damaged if a specific force is being commanded on a tendon and that cannot be produced due to kinematic restrictions or action of other muscles. Simple position control again requires a perfect model of the plant to avoid tendons from going slack. Also demanding a specific set of tendon excursions could result in very high tendon tensions resulting in the system getting locked leading to damage. The spring based control where inaccuracies in the model of the plant are accounted for by simulated passive compliance in the controller proved most effective in the control of the index finger. The spring based control has parallels to muscles in the human system. Command from the alpha motor neuron can be considered as a command that reduces the resting length of a spring resulting in force being generated. The force-length and force-velocity properties of the muscle would effectively change the stiffness of this viscoelastic structure. Together the finger can be considered to being displaced from one equilibrium position to another. See Section 5.7 for a simulation study discussing this in more detail.

Joint equilibrium upon loading of tendons has been discussed with respect to the fingers and also other joints in the body(Landsmeer 1961, Zdravkovic, Jacob & Sennwald

1995). But, to the best of our knowledge, equilibria of finger joints at different tendon tension combinations and joint postures has not been studied experimentally in cadaveric specimens. Our cadaveric setup allowed us to tune in different tendon tensions easily and observe changes in different postures. We observed both stable equilibrium discussed in the literature before (Landsmeer 1961) where the finger upon external perturbation to posture returned to a specific posture, as well as neutral equilibrium where the finger upon displacement stayed in the new posture.

There is a natural equilibrium of the finger that is stable : produced by the stiffness created by the skin, the ligaments, etc. This stiffness is larger at the boundaries in comparison to the working range of the finger (Esteki & Mansour 1996). When perturbed with no tendon tension inputs, the finger comes to this equilibrium posture. When a control input is applied in the form of joint torque produced by tendon forces, then depending on the tendon tension pattern, different behavior is observed: i. If the tendon tension profile is in the null space of the moment arm matrix of the finger (in that posture), the finger exhibits 'neutral equilibrium' where any perturbation in posture results in the finger staying in this new posture because the equilibrium conditions are satisfied in this new posture. This kind of behavior is seen in the working range of the finger motion where the torque due to ligaments, skin, etc. is very small compared to the torque produced by tendon tension. ii. For tendon tension profiles that do not lie in the null space of the moment arm matrix, the equilibrium posture is closer to the boundaries of the range of finger motion where the torque due to the passive stiffness (skin, ligaments, etc.) balances the torque produced by the tendon tensions. See the Appendix (Section **??**) for a mathematical description of this equilibrium.

I have corrected this in the final version :)

92

We only considered the fingertip force output and not the torque that the four degree-of-freedom finger produces at the fingertip (Valero-Cuevas 2009). We need to include the measured fingertip torque when regressing the action matrix from finger output and tendon tensions. It is possible that the sum of torques at the joints as well as the distance from the null space would be much smaller than that calculated here if this fingertip torque were included in the analysis.

In this study the tendons were being held at a constant tendon tension pattern (using force control). This is not exactly true in the human system, since changes in posture result in changes in muscle lengths and hence, in tendon tensions (force-length relationship). However, for small finger movements the length changes of the muscles would be relatively small and hence keeping the tension profile also relatively fixed.

The existence of neutral equilibrium could be used by the central nervous system in finger grasp. While the nervous system sends a simple finger flexion command, the finger posture would be adjusted based on the shape of the object being grasped. Experiments with EMG recordings in live subjects from the finger muscles during grasp would need to be performed to test if this is true.

Acknowledgment

5.6   Appendix: Mathematical explanation of finger equilibria

We describe here in more detail using a dynamical systems perspective, the two states of equilibria of the finger. The finger can be described as a second order dynamical system. Then the equation of motion of the system would be:

$$I\ddot{\boldsymbol{\theta}} + C\dot{\boldsymbol{\theta}} + K\boldsymbol{\theta} = \boldsymbol{\tau}$$

where I is the moment of inertia of the finger, $\boldsymbol{\theta}$ represents the vector of joint angles at the four degrees of freedom in the finger, C is the viscosity coefficient, K is the stiffness coefficient and $\boldsymbol{\tau}$ is the vector of joint torques produced by the tendons. Suppose the states of the system are $\mathbf{x_1},\mathbf{x_2}$ where $\mathbf{x_1} = \boldsymbol{\theta}$ and $\mathbf{x_2} = \dot{\boldsymbol{\theta}}$

$$\dot{\mathbf{x_1}} = \mathbf{x_2}$$

$$\dot{\mathbf{x_2}} = \ddot{\boldsymbol{\theta}} = I^{-1}(\boldsymbol{\tau} - K\boldsymbol{\theta} - C\dot{\boldsymbol{\theta}})$$

In equilibrium,

$$\dot{\mathbf{x_1}} = 0$$

$$\dot{\mathbf{x_2}} = 0$$

which implies,

$$\dot{\boldsymbol{\theta}} = 0$$

$$I^{-1}(\boldsymbol{\tau} - K\boldsymbol{\theta} - C\dot{\boldsymbol{\theta}}) = 0$$

$$I^{-1}(\boldsymbol{\tau} - K\boldsymbol{\theta}) = 0$$

$$(\boldsymbol{\tau} - K\boldsymbol{\theta}) = 0$$

But,

$$\boldsymbol{\tau} = R\mathbf{F_m}$$

$$R\mathbf{F_m} - K\boldsymbol{\theta} = 0$$

But in the central region of the workspace of the finger, K is negligible compared to $R\mathbf{F_m}$. Hence, if $\mathbf{F_m}$ lies in the null space of R, then there is 'neutral equilibrium'. And when it is not in the null space of R, then there is a net torque at the joints which displaces the finger till it reaches the boundary where the K is not negligible. The new equilibrium then corresponds to a posture, $\boldsymbol{\theta}$ such that $R\mathbf{F_m} - K\boldsymbol{\theta} = 0$.

5.7 Appendix: A strain-energy approach to simulating slow finger movements and changes due to loss of musculature

5.7.1 Introduction

The neuromuscular interactions that produce slow and accurate finger movements are not understood. The geometry of finger anatomy is such that a slow finger movement (i.e., sequence of joint rotations) completely defines the necessary excursions of all tendons. Given that muscle tone prevents tendons from becoming slack, all tendons must undergo eccentric or concentric excursions during functional finger movements. Here, we describe a novel computational solver to model slow finger movements, and report how the mathematics of strain-energy of over-constrained systems can predict the impairment in finger motion that accompanies partial paralyses.

5.7.2 Methods

A slow moving finger is best modeled as a first order dynamical system having low mass and performing quasi-static motion (which is not the case for fast finger movements (Darling et al. 1994)). Our 3-D model consists of a kinematic 3-link mechanism with 2 degrees of freedom (ad-abduction and flexion-extension) at the metacarpophalangeal joint (MCP) and 1 degree of freedom (flexion-extension) at the proximal interphalangeal (PIP) and the distal interphalangeal (DIP) joints. All seven muscles of the index finger were included: flexor digitorum profundus (FDP), flexor digitorum superficialis (FDS), extensor indicis proprius (EIP), extensor digitorum communis (EDC), first lumbrical (LUM), first dorsal interosseous (FDI), and first palmar interosseous (FPI). The routing

of the tendons across finger joints is represented by the moment arm matrix obtained from (An et al. 1983). Our focus here is the computational engine, thus for now we have neglected the extensor mechanism, but its effects will be considered in subsequent work. Torsional springs at the joints simulate the known passive stiffness arising from skin and soft tissue. The muscles actuating the index finger are modeled as tunable linear elastic springs that only exert force in tension. Changing the latent resting length of a spring, l0 , results in a muscle force that is proportional to the difference between its current and resting lengths. Therefore the activation signal to a muscle is simulated as a change in resting length, Δl_0 (Fig. 1). Here, we are only interested in understanding how finger movement arises from Δl_0 , and simply assume that Δl_0 can arise from a neural command. A set of commanded resting lengths to all muscles defines the posture attained by minimizing the strain-energy of the finger at equilibrium: where the net joint torques produced by the muscles, $\boldsymbol{\tau}_{ext}$, are exactly balanced by the torques produced by joint-stiffness, $\boldsymbol{\tau}_{in}$.

$$\Delta s = R^T (\Delta \boldsymbol{\theta})$$

$$\boldsymbol{\tau}_{ext} = R K_m (\Delta l_0 - \Delta s)$$

$$\boldsymbol{\tau}_{in} = K_\theta (\Delta \boldsymbol{\theta})$$

where Δs is the change in tendon excursions, R is the moment arm matrix, K_m is the matrix of muscle spring constants, Δl_0 is the change in spring resting lengths, K_θ is the

matrix of torsion spring constants at the joints and $\Delta\boldsymbol{\theta}$ is the resulting change in joint angles.

Given that muscles behave like nonlinear springs that do not exert compressive force, there is an extra constraint defined by,

$$K_m \approx 0 \qquad\qquad if\ \Delta l_0 < R^T \Delta\boldsymbol{\theta} \qquad\qquad (5.1)$$

Also, we ensure that $\Delta l_0 > 0$ since muscle activation always leads to a net force greater than passive stretch force. We solve the forward kinematic problem iteratively using a Newton-Raphson iteration method.

As a first demonstration of our system, we simulated a simple quasi-static tapping motion by finding an appropriate trajectory of muscle resting length changes. The movement consisted of an initial retraction of the index finger followed by a downward flexion motion (Fig. 5.5). In addition, we simulated the resulting trajectory for acute radial, median and ulnar nerve palsies by removing the muscle commands to the i) two extensors, ii) the two flexors, and iii) the two interosseii and lumbrical, respectively and applying the same resting length change commands as before to the unaffected muscles. This simulates effects prior to neuromuscular adaptation (i.e., the robustness of finger trajectories to acute loss of some muscles). Note that the affected muscles continue to exert passive stretch forces even without the activation command.
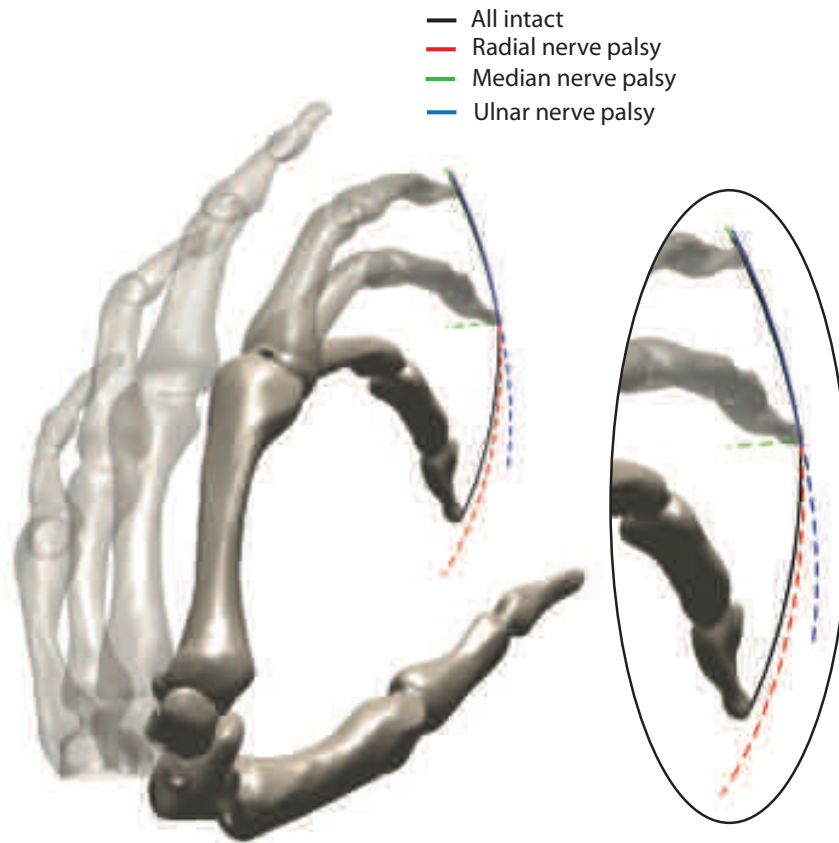
Figure 5.5: Fingertip trajectories for a simple tapping motion in unaffected and impaired cases.

5.7.3 Results and Discussion

Not surprisingly, the fingertip deviates from the original trajectory when some muscle commands are removed (Fig. 5.5). Some postures and directions of movement become impossible without the presence of specific muscles. However, the value of these simulations is that they begin to explain the relative effect of different deficits and indicate which muscles are more or less critical to the execution of accurate and slow finger movements. In addition, finger movements are typically modeled using second order dynamics(Sueda et al. 2008, Venkadesan & Valero-Cuevas 2008). Here we are proposing that a simple quasi-static solver based on strain-energy equilibrium can model slow finger movements since mass and inertia properties of fingers are small. While muscle mechanics depends on neural activation and a muscles force-length and force-velocity properties, the end product is a force command, which we generate by the adjustment of resting lengths of fictitious springs.

Chapter 6

Experimental validation of existing models of the index finger

6.1 Introduction

The role of the different components of the extensor mechanism in finger function has been long debated in the literature. While several simplistic computational models have been suggested over the years, the normative model developed by An et al. 1979 (Chao & An 1978a, An et al. 1979) remains the most comprehensive 3D anatomical model of the index finger to date. Though this model has been employed in several research studies (Eg. (Harding et al. 1993)), it has never been rigorously validated with experimental data. The model assumes bowstringing of all tendons with joint rotation and a constant force distribution within the different bands of the extensor mechanism, independent of joint posture. Both the above assumptions are modeling simplifications and are contrary to experimental observations. Valero-Cuevas et al. in 1998 (Valero-Cuevas et al. 1998) emphasized the importance of including changes in force distribution through the extensor mechanism, with finger posture. They modified a constant moment arm model proposed

by An et al, 1983 (An et al. 1983), obtained by regression of tendon excursion-joint angle data from cadaveric specimens, to include changes in force distribution through the extensor mechanism with posture. But the validity of fingertip force predictions of neither of these models has been tested with experimental data. In this chapter, we rigorously validate the normative model of the index finger as well as the constant moment arm models described in An et al, 1983 and Valero-Cuevas et al. 1998, with experimental data collected from a cadaveric index finger in multiple postures.
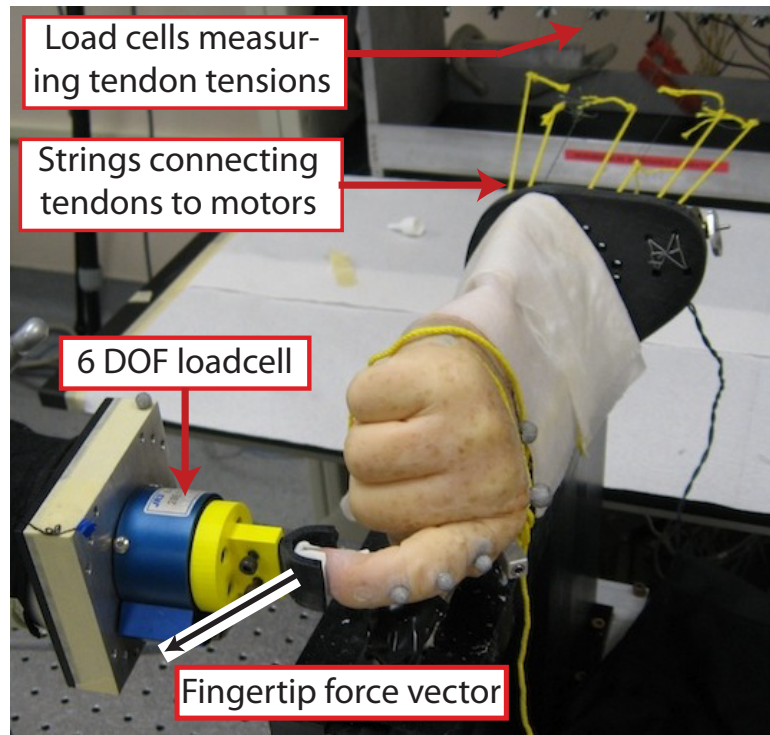
Figure 6.1: The experimental setup used to record fingertip forces from a freshly frozen cadaveric hand. We applied all possible combinations of high and low tensions to the seven tendons of the index finger (there are 128 such combinations) and recorded corresponding fingertip forces. We repeated this in three different finger postures : *fully flexed*, *tap* and *fully extended*.

6.2 Methods

The seven tendons of the index finger: flexor digitorum profundus (FDP), flexor digitorum superficialis (FDS), extensor indicis (EI), extensor digitorum communis (EDC), first lumbrical (LUM), first dorsal interosseous (FDI), and first palmar interosseous (FPI), in a freshly frozen cadaveric hand were actuated using dc motors controlled by a National Instruments PXI real-time control system (Fig. 6.1). All possible combinations of low (2N) and high (10N) tendon tensions were applied to the cadaveric specimen and corresponding fingertip forces and torques were recorded using a 6 DOF load cell attached to the fingertip. This procedure was repeated at three different postures in one cadaveric specimen.

A matrix transforming tendon tensions to fingertip forces (the action matrix) was regressed from the experimental data in each posture (mean $R^2 = 0.96$). The normative model of the index finger was implemented in MATLAB. The moment arm matrix corresponding to each finger posture was calculated based on rotations of tendon positions as described in (An et al. 1979) and using equations for force distribution through the extensor mechanism described in (Chao & An 1978a). The action matrix was calculated by multiplying the inverse transpose of the Jacobian mapping joint angle velocities to fingertip velocities, with the moment arm matrix (Valero-Cuevas et al. 1998). Similar action matrices were determined for the constant moment arm models of An et al, 1983 (An et al. 1983) and Valero-Cuevas et al, 1998 (Valero-Cuevas et al. 1998). All moment arm matrices were scaled to the length of the middle phalanx to reduce the effect of

inter-subject variability (An et al. 1979). Each column of the action matrix (action vector), represents the fingertip force resulting from 1N tension applied to the corresponding tendon. The sensitivity of the models to variations in moment arm values was then tested by applying ±10% randomly distributed noise to the moment arm matrices in the three models.
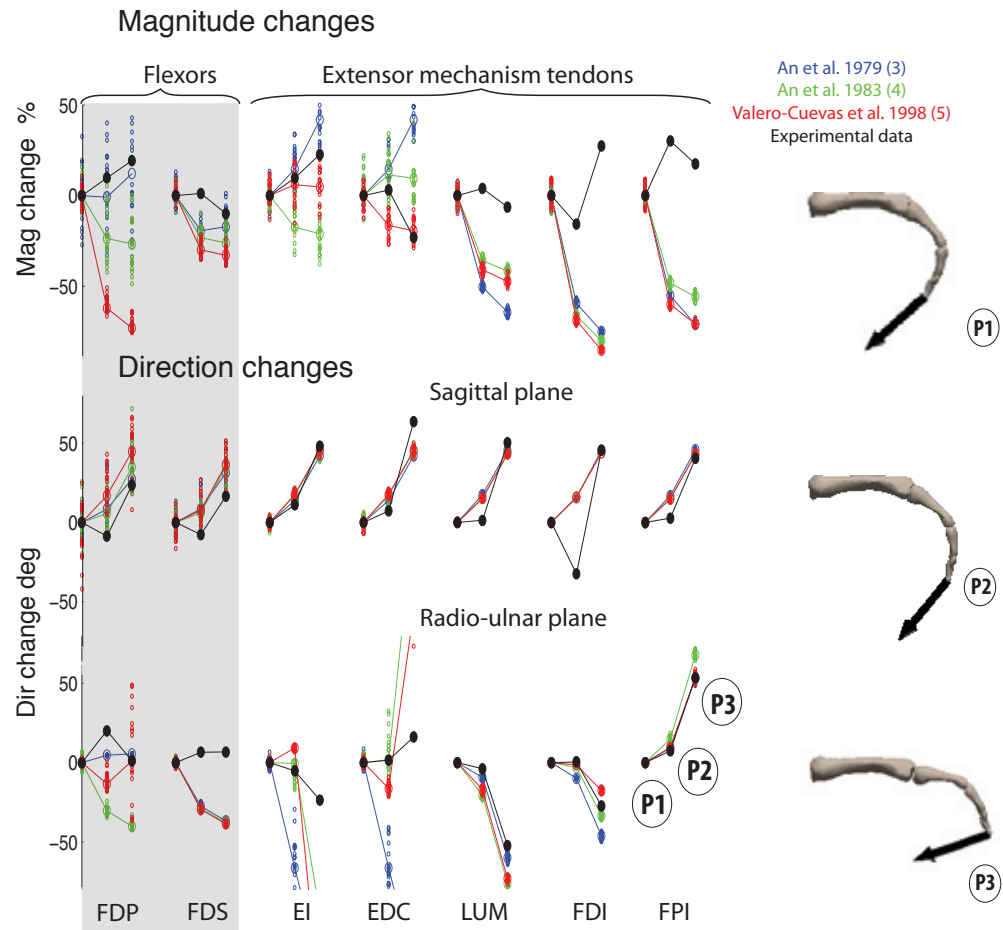
Figure 6.2: Results of experimental evaluation of existing biomechanical index finger models

6.3　Results

Fig. 6.2 shows the changes in magnitude and direction of each tendons action vector relative to the first posture for all models (and data). The changes in magnitude observed in all three models disagree with one another and with those observed in experimental data. The changes in direction for tendons other than EI and EDC (sagittal plane) and LUM, FDI and FPI (radio-ulnar plane) also do not match with corresponding changes in experimental data. The components of the action vector for the EDC and EI in the radio-ulnar plane are very small and hence corresponding directional errors can be neglected.

Fig 6.3 shows the absolute magnitude and direction errors for the An-Chao normative model (An et al. 1979), which is the only one of the three models here that explicitly represents the extensor mechanism. The figure shows the errors for each tendon's action vector when evaluated against the experimental data in the three finger postures. The absolute errors in magnitude are very large. The direction errors for some of the intrinsic tendons is smaller compared to the errors for the EDC and EIP. This is a little counterintuitive considering that these are relatively 'simple tendons'. Also the errors are different in different postures as can be expected since the tension distribution in the extensor mechanism is known to change with posture.

The flexors with larger moment arms are more sensitive to variations as compared to the extensors and the intrinsics. A $\pm 10\%$ change in moment arm values in these tendons results in 30-40 degree change in fingertip force direction and around 50% change in magnitude.
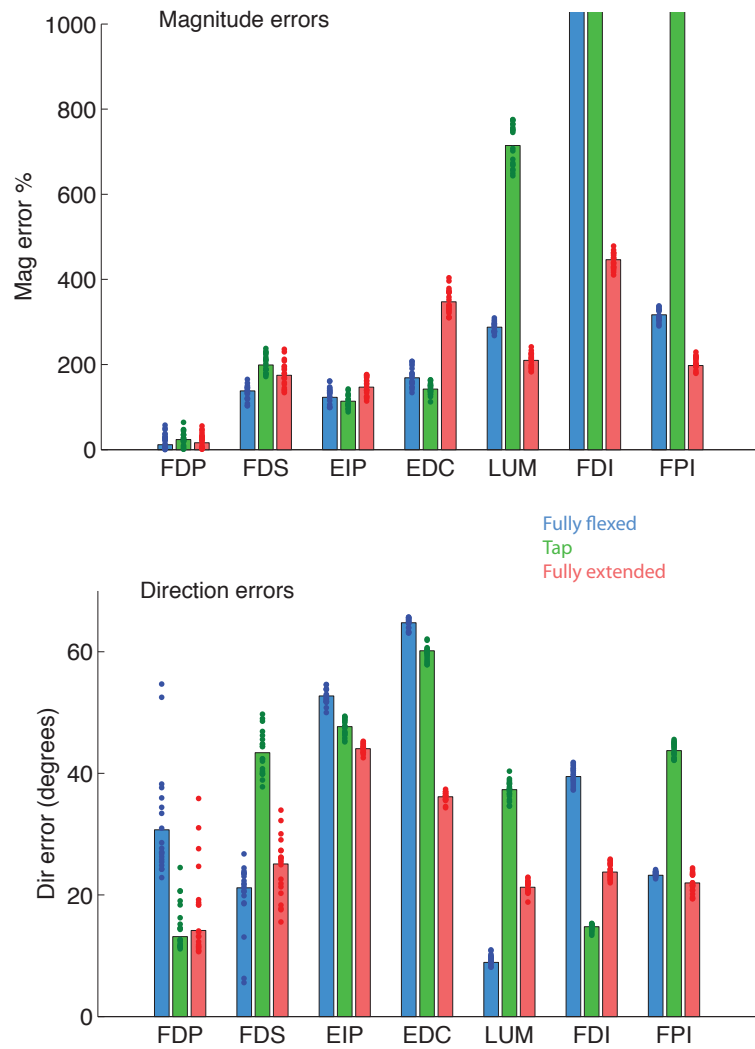
Figure 6.3: Absolute magnitude and direction errors for the An-Chao Normative model when tested with experimental data from a cadaveric index finger

The three models of the index finger disagree with one another and with the experimental data. They are sensitive to perturbations and result in large variations in fingertip force output. Hence it is important to develop subject-specific models of these complex systems that have been informed by experimental data.

6.4 Discussion

Our experimental validation of the existing models of the index finger revealed that existing models have large magnitude and directional errors. More detailed and accurate representations of the topology and parameters of the extensor mechanism, inferred from experimental data, are necessary to develop reliable biomechanical models of the finger to understand motor control of manipulation and changes upon damage.

Acknowledgment

Chapter 7

Study of the sensitivity of fingertip force output to topology and parameters of the extensor mechanism using a novel finite element analysis simulator

7.1 Abstract

How the extensor mechanism of the fingers distributes forces from multiple muscles to multiple joints resulting in fingertip force is not clearly understood. Existing musculoskeletal modeling software cannot model interactions of complex tendon networks with bones. Here we present a novel simulator based on the finite element method that models the mechanics of interactions of any elastic network of strings with arbitrarily shaped solids like bones. We validated this simulator using experimental data from the actuation of a latex rubber network draped on a solid hemispherical dome and observed that the model matches the experimental data closely with an overall RMS error of 11.5% in forces. We then simulated the extensor mechanism of the index finger as an elastic tendon network of strings draped over an MRI scan of the finger bones. Since the properties of the

extensor mechanism and its influence on fingertip force are poorly understood, we performed a sensitivity analysis where we varied the positions of connectivity of the network, the cross sectional area of the different bands, the resting lengths of these components and the topology (or connectivity) of the network itself. We simulated these changes in three different finger postures. We observed that the fingertip force output is sensitive to the posture, the positions of the nodes, the resting lengths of the components and the topology of the extensor mechanism and less sensitive to the cross sectional areas of the different bands.

7.2 Introduction

Forces generated by the muscles actuating the fingers are transmitted to the joints through a complex network of tendons called the extensor mechanism. The role of the extensor mechanism in human manipulation is not clearly understood (Valero-Cuevas $2000a$, Lee, Chen, Towles & Kamper 2008, Landsmeer 1949, Haines 1951, Littler 1967, Harris Jr & Rutledge Jr 1972). Studies have shown that the extensor mechanism transmits forces differently at different finger postures. It has also been shown that the different components of the extensor mechanism have different elastic properties (Garcia-Elias, An, Berglund, Linscheid, Cooney & Chao 1991). While most studies of the extensor mechanism use the Winslow's rhombus representation, other representations have also been suggested in the literature (Garcia-Elias, An, Berglund, Linscheid, Cooney Iii & Chao 1991). How fingertip force output changes with these parameters: locations of the network nodes, the

elastic properties of the network or the topological representation (the network connectivity) itself, has not been studied.

Computational modeling can be a useful tool to understand the mechanical behavior of the extensor mechanism and its sensitivity to the properties mentioned above. Most existing computational models of the fingers do not represent the interactions of the various components of the extensor mechanism. They either consist of combinations of Landsmeer models for tendon routing (Sancho-Bru et al. 2001) or are represented as constant moment arm matrices (An et al. 1983, Spoor 1983, Leijnse et al. 1992, Leijnse 1996, Valero-Cuevas et al. 1998). The An-Chao model (Chao & An 1978a, An et al. 1979), one of the earliest developed mathematical representations of the finger, which has been used in several studies in the literature (Li et al. 2001, Harding et al. 1993, Dennerlein, Diao, Mote Jr & Rempel 1998, Weightman & Amis 1982), explicitly modeled the distribution of forces within the extensor mechanism. But it assumed a fixed distribution of tendon tensions among the different bands of the extensor mechanism for all postures. However, earlier studies had shown that the geometry of the bands as well as the force distribution through them, change significantly with posture (Garcia-Elias, An, Berglund, Linscheid, Cooney Iii & Chao 1991, Sarrafian et al. 1970, Micks & Reswick 1981). Recently, a dynamic simulator of the hand has been developed (Sueda et al. 2008) that simulates the interactions of these tendon network interactions. But it is aimed at producing realistic hand motion for graphics applications and the force transmission capability of this model has not been validated with experimental data.

Most existing musculoskeletal modeling software like SIMM (Motion Analysis Corporation) (Delp & Loan 1995), AnyBody (AnyBody Technology) (Damsgaard et al. 2006)

or MSMS (Davoodi et al. 2007) do not have the capability to model tendinous networks. They are based on single line of action models for the musculotendons or use of wrapping surfaces and via points to model the routing of musculotendons around joints. See chapter 2 for more details about these models. These techniques do not suffice to model the wrapping of a network of tendons on solid bony surfaces. Hence, we developed a novel finite element method based simulator that models the mechanical force transmission by an elastic network of tendons draped on any arbitrary solid (like bones) which we present here. It is an advancement of the relaxation algorithm based simulator presented earlier (Lipson 2006, Valero-Cuevas & Lipson 2004). It can be effectively used to model isometric force production in complex biomechanical systems. We validate this solver by actuating a latex network draped on a hemispherical dome. We then use this simulator to model the finger extensor mechanism to study the sensitivity of fingertip output to variation in the parameters and topology of the extensor mechanism.

7.3 Methods

7.3.1 The tendon network simulator

Previously, a relaxation algorithm was used to simulate mechanics of tendon networks in 2D and for networks on simplified models of bones in 3D(Valero-Cuevas & Lipson 2004). Here we use the finite element method to expand this work to develop a simulator of elastic networks interacting with arbitrarily shaped rigid objects. The solver assumes the solid surface to be fixed and frictionless, and the elastic network is free to deform and slide over the surface while the resulting contact forces can be determined.
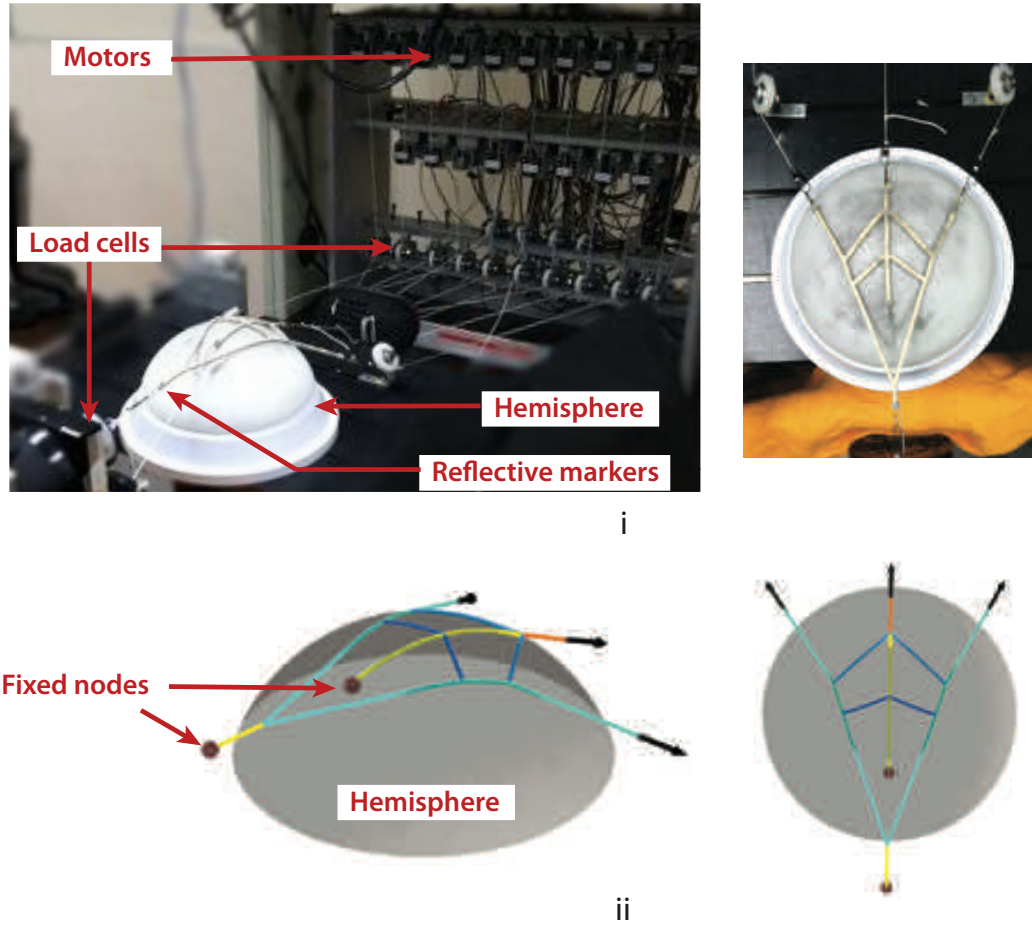
Figure 7.1: Validation of the tendon network simulator. i.A latex network was draped on a hemispherical dome.The network had three input nodes that were connected to nylon strings and were actuated using dc servo motors and 2 output/fixed nodes that were attached to load cells fixed to the ground. Reflective markers tracked by a four-camera motion capture system, were attached to the strings actuating the network to measure the direction of the input and output force vectors.The hemisphere was coated with graphite powder to reduce friction. ii.The latex network draped on a hemisphere was simulated using the tendon network simulator. The same input force vectors applied in the experimental setup was used to actuate the network and the output forces were calculated at the fixed nodes using the non-linear finite element method.

We model the elastic tendon networks using cable elements that transmit forces in tension but not in compression, that are connected at nodes that only have displacement degrees of freedom (three, similar to a 3D truss). The solid surface on which this network is draped is modeled as a rigid tessellated solid. The boundary conditions include the input force vectors applied on the network (by muscles in the body) in 3D and zero displacements at the nodes where the elastic network attaches to the solid (the tendon slips). We used the incremental-iterative Newton-Raphson (NR) technique to solve the non linear finite element problem (Crisfield 1991). First the initial configuration of the network was defined in the same 3D coordinate space as the rigid polygon model of the bones. Then in every large iteration of the process, we performed i. a *node penetration* test – If a node was inside the tessellated solid, we pushed it to the surface and held it there by a *constraint spring* and ii. an *element penetration* test –We tested multiple points along the length of the element and created new nodes at points penetrating the solid and pushed them to the surface. Once node and element-penetration tests were performed, the tangent stiffness matrix and residue vector were calculated for every element. These were assembled and the displacements of the nodes were calculated for small increments in load using the iterative Newton-Raphson method. The node- and element-penetration tests were repeated for every load increment. Please see the appendix for more details.

7.3.2   Experimental validation of the tendon network simulator

We draped a network made of latex rubber on a plastic surface which formed a part of a hemisphere. The network had three input nodes and two output nodes (Fig. 7.1). We connected the input nodes using nylon strings to dc servo motors. The strings were

routed around pulleys connected to 1DOF load cells that measured the tension in these strings. The output nodes were connected to fixed load cells attached to the ground, also using nylon strings. A 4-camera optical motion capture system, manufactured by Vicon (Lake Forest, CA), tracked reflective markers adhered to each of the input and output strings, from which we determined the bases for the input and output force vectors. We applied different sets of tensions on the input strings using a PXI controller (National Instruments) connected to the dc servo motors and measured the force magnitudes in the output nodes. We obtained a dataset of experimentally recorded input-ouput force vectors. We then simulated the latex network draped on the hemispherical surface in our tendon network simulator and calculated the output force vectors for the same set of input force vectors that we had applied in the experiment thus obtaining a dataset of input-output force vectors in simulation.

7.3.3 Simulating the extensor mechanism

We modeled the extensor mechanism using the Winslow's rhombus topology (originally described by Winslow and reproduced in drawing by Zancolli (Zancolli 1979)) that has been used in several studies previously (Eg. (Chao & An 1978*a*, An et al. 1979, Valero-Cuevas et al. 1998)). We obtained the resting lengths of the elastic elements forming the extensor mechanism by draping the network on the finger bones rotated to a neutral ad-abduction posture with 40 degrees flexion at the metacarpophalangeal (MCP) joint, 30 degrees flexion at the proximal interphalangeal (PIP) joint and 5 degrees flexion at the distal interphalangeal (DIP) joint. We modeled all the tendons using the same nonlinear stress-strain relation obtained from (Zajac et al. 1989). Since these tendons are all made

of collagenous fibers, this is a valid assumption. We calculated the element cross-sectional areas for each of the bands of the extensor mechanism using values for the force length relationship provided in (Garcia-Elias, An, Berglund, Linscheid, Cooney & Chao 1991). We obtained the polygonal surface model of scanned hand bones from the Stereolithography Archive at Clemson University. We studied the finger in three postures, all in neutral ad-abduction : i. *Fully flexed* (50 60 20) ii. *Tap* (40 30 5) and iii. *Fully extended* (20 20 10). (Note that the values in the parentheses represent the flexion joint angles, in degrees, at the MCP, PIP and DIP, respectively for each of the postures.) There were three inputs to the model representing forces from four of the muscles actuating the index finger- the *first palmar interosseous* (FPI), *extensor indicis* (EI), *extensor digitorum communis* (EDC) and the first *lumbrical* (LUM). The EI and the EDC which have a very similar line of action (An et al. 1983) were modeled as one input. The extensor mechanism attached to the finger bones at two points, the central and the terminal slips on the middle phalanx and distal phalanx respectively (Fig. 7.2a). We did not model the retinacular and the oblique retinacular ligaments (Bendz 1985). Solving the non linear finite element problem gave us the displacements of all the nodes of the network and the reaction forces at the two slips. We obtained joint torques from tendon tensions and calculated fingertip force output using the formulation $F = J^{-T}\boldsymbol{\tau}$ (Valero-Cuevas 2009) where F is the fingertip force output, J is the jacobian transforming joint angle velocities to fingertip velocities and $\boldsymbol{\tau}$ is the vector of joint torques (Fig. 7.2a).

7.3.4 Sensitivity analysis

Sensitivity analysis is a common procedure in computational modeling to see the effect of changes in parameter values or inputs on the output of the model. Local sensitivity analysis is one of the simplest forms where the parameters/inputs to the model are varied one at a time keeping the others fixed at the base value (Scovil & Ronsky 2006, Raphael, Tsianos & Loeb 2010). We tested the local sensitivity of the fingertip force output to four different properties of the extensor mechanism : i. Node positions of eight nodes forming the extensor mechanism, ii. Cross-sectional areas of 10 elements, iii. Resting lengths of 10 elements iv. Topology of the network (Fig. 7.2b). We assumed palmar-dorsal symmetry for all properties (so number of parameters were reduced to half their total number). We varied each property individually and measured changes in fingertip force magnitude and direction in reference to those generated using the base network with nominal values for the properties (defined in the previous section). For the first three properties, we generated 100 samples each, consisting of random combinations of parameter values lying between $\pm25\%$ of the range of possible values for the parameter of interest (i.e. 100 combinations of node positions, 100 combinations of cross sectional areas, etc.) To understand the effect of topology, 16 discrete topologies were studied, formed by different combinations of inclusion and removal of four bands of the extensor mechanism (Fig. 7.2b).
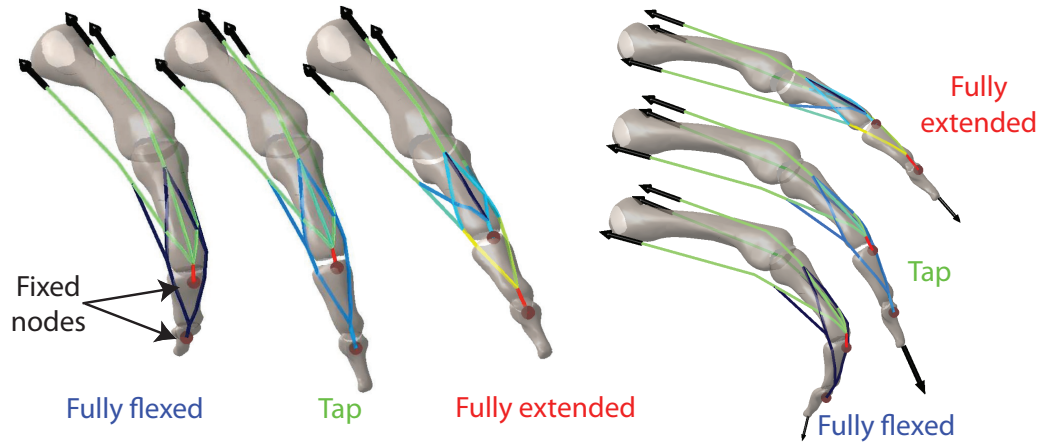
(a) The figure shows the three postures that were simulated : fully flexed, tap and fully extended. The tension distribution in the different bands of the extensor mechanism was obtained by solving the nonlinear finite element problem of an elastic cable network draped on a tessellated solid. Fingertip force vectors were calculated from the torques produced at the four joints (two at the MCP and one each at the PIP and the DIP) using the jacobian transforming joint angle velocities to fingertip velocities.
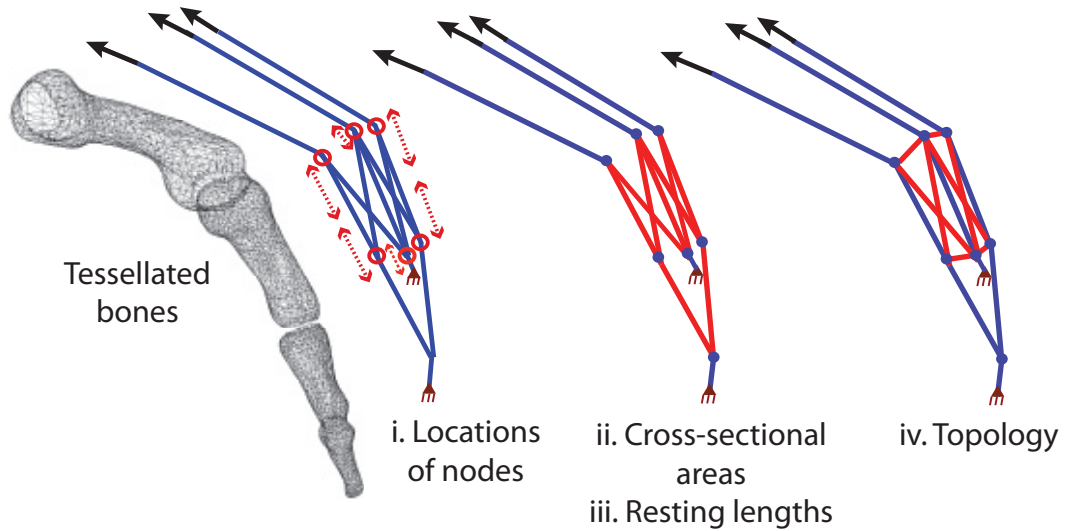
(b) The figure shows the tessellated bone structure and the elastic tendon network with base values for its properties, that was draped on the bones. The local sensitivity of fingertip force output to four properties were studied : i. node locations of eight nodes, ii. Cross-sectional areas of 10 elements, iii. Resting lengths of 10 elements, iv. topology of the network (16 topologies obtained by combinatorial addition and removal of 4 pairs of bands).

Figure 7.2: Sensitivity analysis of fingertip force output to properties of the extensor mechanism

7.4 Results

7.4.1 Results of validation of the tendon network

The reaction forces determined using the tendon network simulator matched the experimental data closely with a normalized RMS error of 11.5%. Figure 7.3 shows the validation results. To ensure that any arbitrary network would not produce the same reaction forces, we also simulated a latex network slightly altered from the one used for the experiments in our tendon network simulator. We then compared the reaction forces predicted for the altered network with the previous experimentally measured values. The errors in this case were much larger.

7.4.2 Results of sensitivity analysis

We observed that the sensitivity of the fingertip force output to the different properties of the extensor mechanism varied largely with finger posture (Fig. 7.4). This was not very surprising because it has been shown in early cadaver studies that the tension distribution within the bands of the extensor mechanism changes with finger posture (Sarrafian et al. 1970, Micks & Reswick 1981) with more force being transmitted to the terminal slip in extended postures and to the central slip in flexed postures. The sensitivity of the fingertip force is also different for the different properties of the extensor mechanism.

Based on the local sensitivity analysis performed here, we observe that the fingertip output is most sensitive to the resting lengths of the bands of the extensor mechanism. $\pm 25\%$ perturbation of the resting length can lead to more than 40 degrees of change in fingertip output and more than 200% change in force magnitude. Topology of the
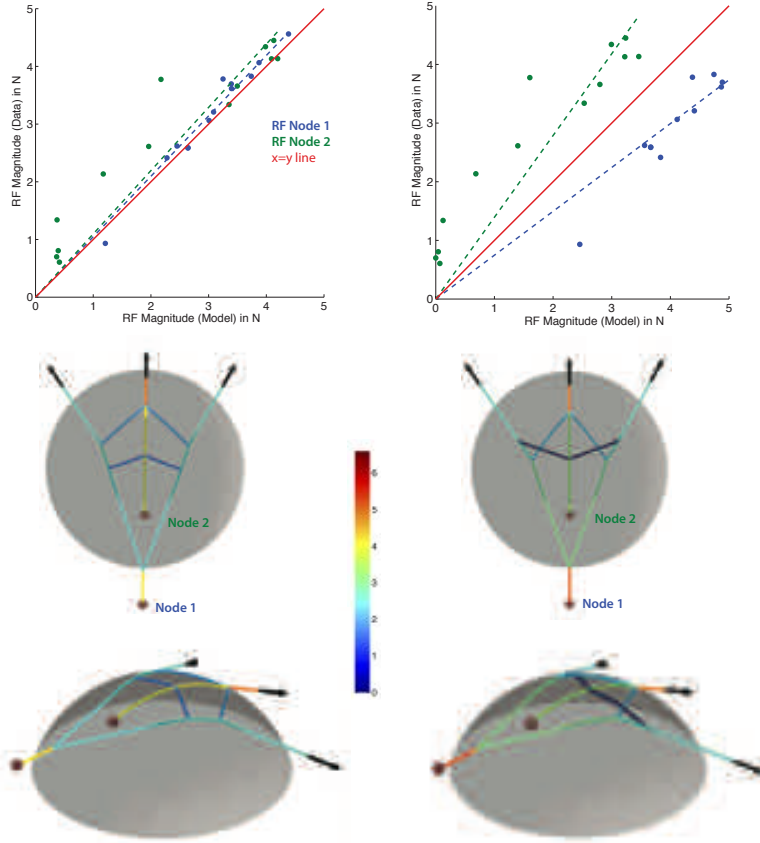
Figure 7.3: Comparison of experimental and simulated data for latex network draped on hemisphere. The figure shows a comparison of force magnitudes at the two fixed nodes of the latex network recorded experimentally vs. calculated in simulation using the tendon network simulator. The left column shows results when the same network topology and parameters were generated in simulation as those used for the experiment. The force magnitudes in the experimental and simulated cases matched closely seen by their proximity to the x=y line. The right column shows comparison of the same experimental data with simulated data from a network with a modified topology than the one used for the experiment. The experimental and simulated force magnitudes do not align closely to the x-y line unlike before. This demonstrated that the tendon network simulator accurately represented the physical latex network and the matching up of the experimental and simulated data was not mere coincidence.

network is also critical and the removal or addition of specific bands of the network can also lead to a change in direction of up to 40 degrees and magnitude up to 180 %. Node positions and cross-sectional areas play a less significant role in changing fingertip force output. While altering node positions could change the output by up to 50% in force magnitude and 10 degrees in direction the changes upon altering cross-sectional area are very small. But, one should remember that this is a local sensitivity analysis performed by perturbing one set of parameters at a time from the base model, keeping the others fixed. In reality, these parameters interact nonlinearly to produce fingertip output.
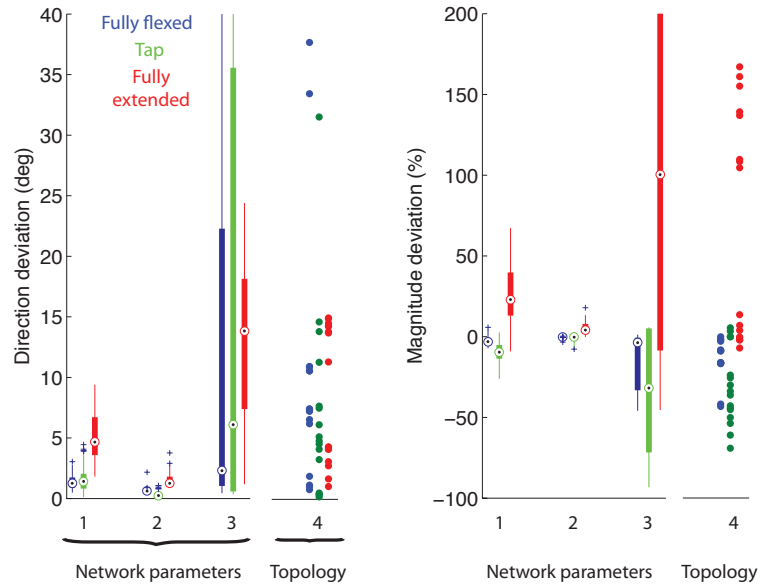
Figure 7.4: Box plots showing deviation in fingertip force direction and magnitude in the three finger postures upon varying the properties of the extensor mechanism from those in the base condition : 1. Node positions, 2. Cross sectional areas, 3. Resting lengths of the elements, 4. Topology of the network. The box plot for the first three properties shows that the fingertip force magnitude and direction are highly sensitive to resting lengths of the bands, less sensitive to node positions and least sensitive to cross sectional areas of the bands. The deviations for all the 16 topologies is shown using a scatter plot. Some topologies have larger deviation than others and the deviation in the different postures is also different.However, this is the local sensitivity of the network and does not fully capture the global landscape.

7.5 Discussion

Here we have presented a novel simulator to model the interactions of elastic tendon networks with arbitrarily shaped bones in three-dimensions. We have validated this simulator with experimental data from a latex network draped on a hemispherical dome and shown that the model prediction match closely with the data (RMS error of 13% in reaction forces). Some reasons for the slight mismatch between the model and the experimental data could be attributed to measurement errors, friction on the hemisphere, errors in calculation of force vector direction from motion capture data and also replication of the exact experimental setup in simulation (Eg. location of the network on the hemisphere, location of the fixed nodes where the reaction forces were measured, etc).

It has also been shown in cadaveric observational studies of the extensor mechanism (Garcia-Elias, An, Berglund, Linscheid, Cooney Iii & Chao 1991) that there are large changes in spatial arrangement of the components of the extensor mechanism in the different postures.We observed this in simulation too. While the actual deformation of the components itself was not very large, the components did shift and the distribution of tension in them changed substantially with finger posture. This was also seen in the sensitivity analysis where the sensitivity of the fingertip force output direction and magnitude was different in different postures.

We model the extensor mechanism as a set of elastic strings connected to each other at distinct nodes. This is an approximation of the true structure which consists of several thin elastic collagenous fibers interlaced to form a sheet of collagen. Also the base network assumed here is based on the Winslow's rhombus topology and the node positions were

chosen to approximately represent the network as seen in textbooks of anatomy, based on anatomical observation in cadaveric specimens. In Chapter 8 we will infer a more accurate topology and set of parameter values directly from experimental data collected by testing of a cadaveric index finger.

As mentioned earlier, the sensitivity analysis described here is a local sensitivity analysis where individual properties were varied independently keeping all the other properties fixed at the base level. But since these different properties interact in a nonlinear fashion, the sensitivity profile could change if different base parameter values are assumed for the properties or if multiple properties are varied simultaneously. A more rigorous sensitivity analysis based on Monte Carlo sampling methods (Santos, Bustamante & Valero-Cuevas 2009) would be more comprehensive.

The sensitivity analysis demonstrated that the fingertip force output is most sensitive to topology and resting lengths of the bands. For a stiff elastic network like the tendon networks, the deformation of the network upon loading with low forces like the ones applied here or those applied by muscles in the human fingers is very small. Hence, the largest effect of fingertip force is due to changes in connectivity of the network because force distribution largely depends on which bands are transmitting forces. Changing the resting length or changing the topology perform the same function of changing this connectivity. Hence the fingertip force output is most sensitive to these properties.

While the tendon network simulator here has been used to determine finger forces in an isometric scenario, it could be easily extended to simulate slow finger movements as a quasi-static solver. Joint torques would be calculated the exact same manner as shown

here and the joint angles of the finger are changed to reach a new equilibrium posture of the finger.

7.6   Appendix

The tendon network simulator relies on solving a nonlinear finite element problem. The tendon network is represented as a set of elastic elements connected to one another at distinct nodes. These elements have the same elastic properties as human tendons and they exert forces only in tension. Hence the network is represented as a truss network but with elements transmitting force only in tension (string or cable network). The bones are represented as tessellated solids, rotated to represent the posture being simulated. They are modeled as rigid solids and their elastic deformations are neglected. The elastic network drapes on this solid and the algorithm ensures the network does not penetrate this solid. The flow chart of the algorithm used to solve the finite element problem is shown in Fig. 7.5. It is based on an incremental-iterative Newton-Raphson method (Crisfield 1991).

The external force vector $^{tot}\mathbf{F}$ consisting of x,y,z components of the external force vectors acting on each of the nodes of the tendon network is applied to the system in parts $^{(j)}\mathbf{F}$.

$$^{(j)}\mathbf{F} = {}^{(j-1)}\mathbf{F} + \frac{^{(tot)}\mathbf{F}}{N}$$

123
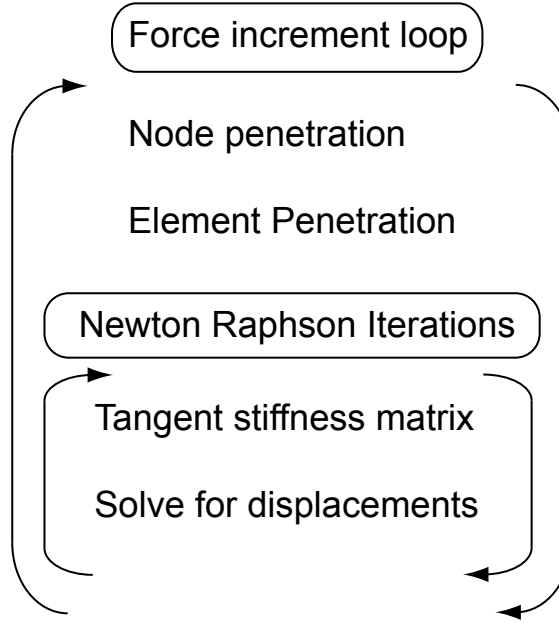
Figure 7.5: Flowchart of the algorithm used for the tendon network simulator

We would like to solve the problem $^{(j)}\mathbf{F} = \mathbf{P}(\mathbf{U})$ where P is the internal force vector arising due to the elastic deformation of the elements of the tendon network and $\mathbf{U}$ is the vector of x,y,z components of displacements of each of the nodes. Since the network has nonlinear material properties and the elements transmit forces only in tension, this forms a nonlinear system of equations and are solved numerically using the Newton-Raphson iteration technique. Hence in iteration, i,

$$\psi^i = {}^{(j)}\mathbf{F} - \mathbf{P}^i$$

$$\psi^{i+1} = \psi^i + \frac{\partial \psi^i}{\partial \mathbf{U}^i}\Delta \mathbf{U}^i$$

$$\psi^{i+1} = 0$$

$$\psi^i = -\frac{\partial \psi^i}{\partial \mathbf{U}^i}\Delta\mathbf{U}^i$$

$$\Delta\mathbf{U}^i = (-\frac{\partial \psi^i}{\partial \mathbf{U}^i})^{-1}\psi^i$$

$$\Delta\mathbf{U}^i = (\frac{\partial \mathbf{P}^i}{\partial \mathbf{U}^i})^{-1}\psi^i$$

$$\mathbf{U}^{i+1} = \mathbf{U}^i + \Delta\mathbf{U}^i$$

$\frac{\partial \mathbf{P}^i}{\partial \mathbf{U}^i}$ is called the tangent stiffness matrix (K_t^i) and is formed by assembling the tangent stiffness matrices of all elements. The $\mathbf{P}^i$ is similarly obtained by assembling the internal force vector, p^i for each element.

$$\epsilon = \frac{(l(\mathbf{U}^i) - l_0)}{l_0}$$

$$\sigma^i = \begin{cases} \frac{16}{e^{.874}-1}(e^{.874\epsilon/.02} - 1) \text{ MPa}, & \text{if } \epsilon < 2\% \\ \\ 16 + 1200(\epsilon - 0.02) \text{ MPa}, & \text{if } \epsilon \geq 2\% \end{cases}$$

$$p^i = A\sigma^i(\mathbf{U}^i)\lambda(\mathbf{U}^i)$$

$$K_t^i = \frac{\partial p^i}{\partial \mathbf{U}^i}$$

ϵ is the strain in the element, l is the current length, l_0 is the resting length, A is the area of cross section, λ is the direction cosine, and σ the stress obtained using the nonlinear stress-strain relationship for the tendon consisting of a linear and an exponential portion as described in (Zajac et al. 1989).

7.6.1   Node and element penetration tests

A node-penetration test was performed to check if any node was penetrating the solid. This was done by checking the sign of the dot product of the vector from the node to the centroid of the closest triangle and the outward normal vector to that triangle. If a node was penetrating the solid, the node was pushed out to the surface by a restoration force created by a constraint spring element from the nearest point on the surface to the penetrating node. This spring element had a negligible resting length and high stiffness, and represented the force that a solid surface applies to prevent penetration. Then an element-penetration test was performed by repeating the node penetration test at distinct points on the element. If a point on the element was penetrating the solid, a new node was created at that point and pushed to the surface in the manner described above.

Acknowledgment

Chapter 8

Inference of the topology and parameters of the tendon networks of the human fingers via sparse experimentation

8.1 Abstract

Computational models of biomechanical systems are generally developed using experimentally measured values for specific parameters of the system and fitting this to a structure that is based on anatomical observations with simplifying assumptions. However, it is not always feasible to measure all parameters in a system and there is no guarantee that the assumed anatomical structure of the model is functionally accurate. As we have demonstrated in chapters 3 and 4, models whose structure and parameter values are inferred directly from experimental data can be more accurate representations of the system whether the goal is to obtain subject-specific models or models that generalize across specimens. However, obtaining a large amount of data from biological systems can be very expensive. Here we implement a novel method to simultaneously infer the parameter values and topology/structure of a three dimensional anatomy-based model of the extensor mechanism of the index finger directly from functional input-output cadaveric

experimental data through intelligent testing that enables the inference with minimal data points. We show that the models of the extensor mechanism inferred using this technique more accurately predict fingertip force magnitude and direction in comparison to a model widely used in the literature.

8.2 Introduction

Understanding neural control of motion and force requires accurate representations of the 'plant' or the peripheral musculoskeletal system being controlled. Computational models of these musculoskeletal systems have been widely used in the literature to understand how they produce movement and force when actuated by the nervous system(Valero-Cuevas et al. 2009). These computational models are generally based on anatomical observations in cadaveric specimens. In most cases, a fixed structure and connectivity of the musculotendons to the bones and joints is assumed and the model parameters are obtained using rigorous experimental measurements (Holzbaur, Murray & Delp 2005, Brown & Loeb 2000, Murray et al. 1995) or calculated based on equilibrium conditions or solving an optimization problem (Chao & An 1978b, Lee & Rim 1990).

In some cases, it is very difficult to measure certain properties or parameter values of these musculoskeletal systems experimentally. In many cases musculoskeletal models are not one-to-one representations of the biological system. They consist of computational simplifications and hence some parameters of the model may not correspond directly to a specific properties in the system. For example, muscles with a large insertion are often represented using multiple segments (Holzbaur et al. 2005). Hence an alternative method

of inference of model parameters directly from experimental data has been used in recent years (Yeo, Tresch & Pai 2008, Gatti & Hughes 2009, Yeo, Mullens, Sandercock, Pai & Tresch 2011, Raphael et al. 2010). In these studies, model parameters are optimized such that the difference between the experimental data and the model outputs is minimum. But then, these studies still make an assumption on the *structure* of the model : the topology or the connectivity of the different components, based on the knowledge of the anatomy. But if this assumed structure itself is not correct, inferring model parameter values from experimental data and fitting them to the wrong structure would not solve the problem. Hence a new computational method was developed by Valero-Cuevas et al. (Valero-Cuevas, Anand, Saxena & Lipson 2007) to simultaneously infer model topology and parameter values of complex biomechanical systems from experimental data. Moreover this method based on the estimation exploration algorithm developed by Bongard and Lipson (Bongard & Lipson 2004*a*, Bongard & Lipson 2005*b*, Bongard & Lipson 2005*a*), demonstrates this inference through minimal experimental data points.

In this method, the concept of predator-prey coevolution is used to optimize a set of models explaining the data and a set of tests that give most information about the models. The *estimation phase* involves optimization of a set of models that best fit the available experimental data points. This is followed by the *exploration phase* that involves finding a test/tests that create most disagreement among the best models obtained so far. Only these tests are then meant to be carried out on the physical system to obtain new experimental data points. This process continues till convergence. Hence, instead of randomly picking experimental tests to perform on the system, only 'intelligent' tests chosen by this method are used. Please see (Bongard & Lipson 2005*a*) for more details on

the method and (Valero-Cuevas, Anand, Saxena & Lipson 2007) for the implementation in inference of tendon networks. It was shown here (Valero-Cuevas, Anand, Saxena & Lipson 2007) that this method of inference of structures via 'intelligent testing' performed better than using random tests in speed of convergence to good solutions as well as the accuracy of the solutions obtained. Here we apply this methodology to simultaneously infer the topology and parameter values of computational models of the finger's extensor mechanism from experimental data obtained by actuating a human cadaveric finger. Please see Chapter 7 for an overview of existing models of the index finger. We compared the inferred model of the extensor mechanism with the model proposed by Chao and An (Chao & An 1978a, An et al. 1979) most commonly adopted in the literature and which is one of the few models that actually explicitly incorporates the interactions of the components of the extensor mechanism in fingertip force prediction. But this model assumes constant force distribution through the different bands and no changes with posture which has been demonstrated in cadaveric studies to not be the case in reality (Sarrafian et al. 1970, Micks & Reswick 1981).

8.3 Methods

8.3.1 Experimental data from a cadaveric index finger

The cadaveric experimental setup used to actuate the seven tendons (FDP,FDS,EIP,LUM,FDI,FPI) of the index finger is described in Chapter 6. Using force control mode (see section 5.3), we applied a base tension of 1N on the FDP, FDS and the FDI. We applied a set of randomly generated tendon tensions (uniform distribution) lying between 1N and 11N
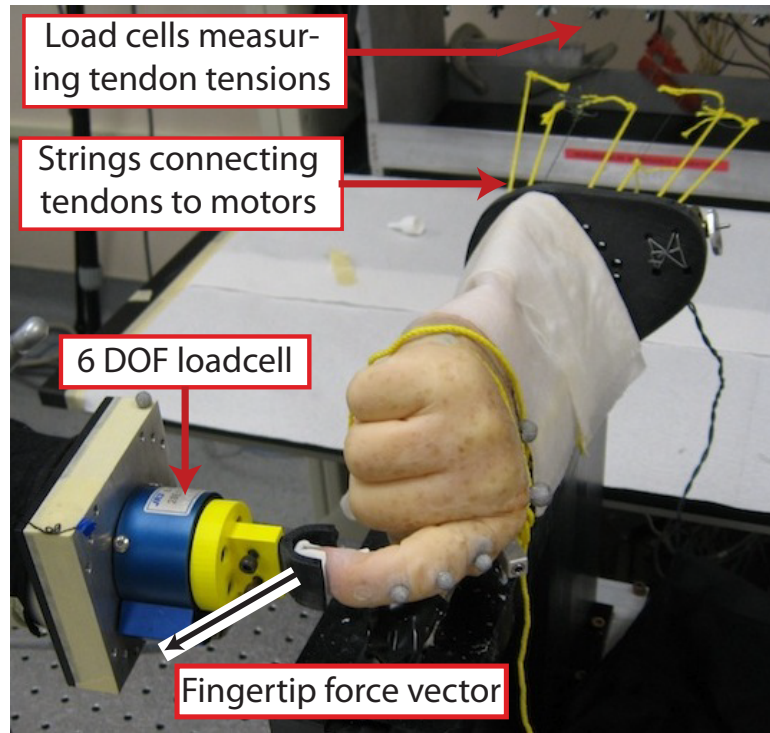
Figure 8.1: The experimental setup used to record fingertip forces from a freshly frozen cadaveric hand. We applied 24 combinations of random inputs lying in the range of 1 to 11N to the EIP, EDC, LUM and FPI tendons of the index finger and a base tension of 1N on the other three tendons (FDP, FDS and FDI). We recorded the output fingertip forces for each combination of inputs. We repeated this in three different finger postures : *fully flexed, tap* and *fully extended.*

on the EIP, EDC, LUM and FPI. Whether the FDI attaches to the extensor mechanism or not has been debated in the literature and there have been contradicting observations (Salsbury 1937, Garcia-Elias, An, Berglund, Linscheid, Cooney Iii & Chao 1991). We chose to actuate the FDI with base tension and not consider it as an input to the extensor mechanism. The fingertip was rigidly attached to a 6 DOF load cell (JR3, Woodland, CA) from which we obtained the fingertip force vector. We repeated this procedure in three different finger postures : *fully flexed, tap* and *fully extended* all in neutral ad-abduction and flexion-extension joint angles at the MCP, PIP and DIP of (26 62 35), (25 40 30), (5 30 20) degrees, respectively in the three postures. Hence the entire dataset consisted of 72 tests (24 in each of the three postures).

8.3.2   Modeling environment

The tendon network simulator used to model the interactions of the elastic tendon networks draped on the bones of the index finger is described in detail in Chapter 7. Fig. 8.2 shows the base model along with the properties of the extensor mechanism that were inferred from the experimental data : i. node positions of 6 nodes (4 variables) forming the extensor mechanism, ii. resting lengths of 13 elements (7 variables) and iii. topology of the network : 8 elements (4 variables). We chose to infer these specific properties based on the sensitivity analysis results in Chapter 7. The node positions were moved along the length of the outer segment. The resting lengths at any set of node positions were determined by first draping the network with no input tendon tension in a specific posture (neutral ad-abduction, 40,30,5 degrees flexion at the MCP, PIP and DIP, respectively) and then altering this length by the factor determined by the optimization

variable corresponding to this parameter. The topology was varied by either including or removing the specific eight bands of the extensor mechanism shown in Fig. 8.1. We assumed symmetry of the network topology and parameters about the sagittal plane of the finger for computational simplicity. The extensor mechanism model was assumed to have three inputs: the LUM, the FPI and one extensor input. The EIP and the EDC were combined as one single tendon and the tension magnitudes applied to these two tendons were summed together. Given, a set of topology-parameter values, input force magnitudes and finger posture, the fingertip force vector was determined solving the nonlinear finite element problem, calculating joint torques and using the Jacobian matrix mapping the joint angle velocities to end point velocities as described in Chapter 7.
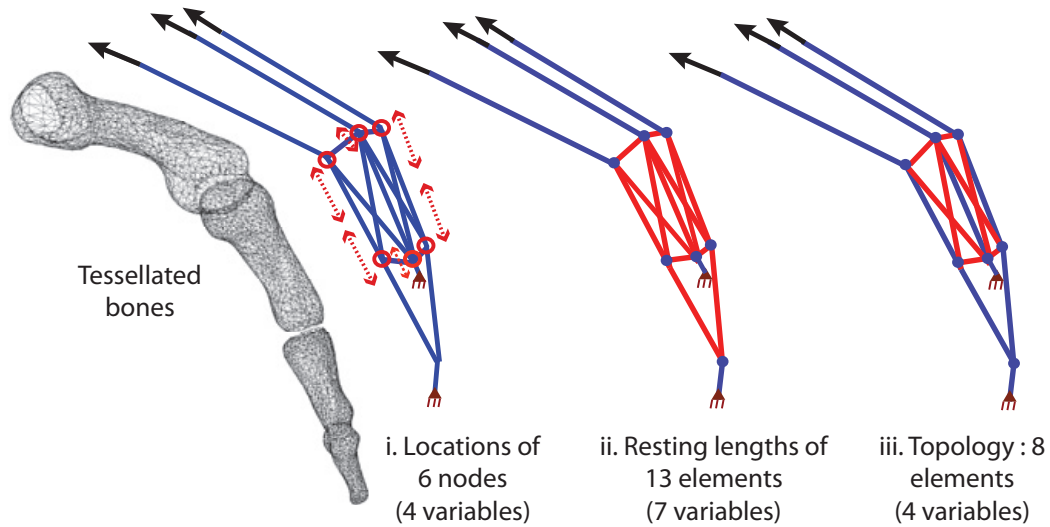
Figure 8.2: The tendon network simulator and the variables being inferred. The tendon network was modeled as a network of elastic cable elements draped on a tessellated model of the bones. Three properties of the network were varied :i. Node positions of 6 nodes (4 variables), ii. Resting lengths of 13 elements (7 variables) and iii. Topology of the network : 8 elements (4 variables).
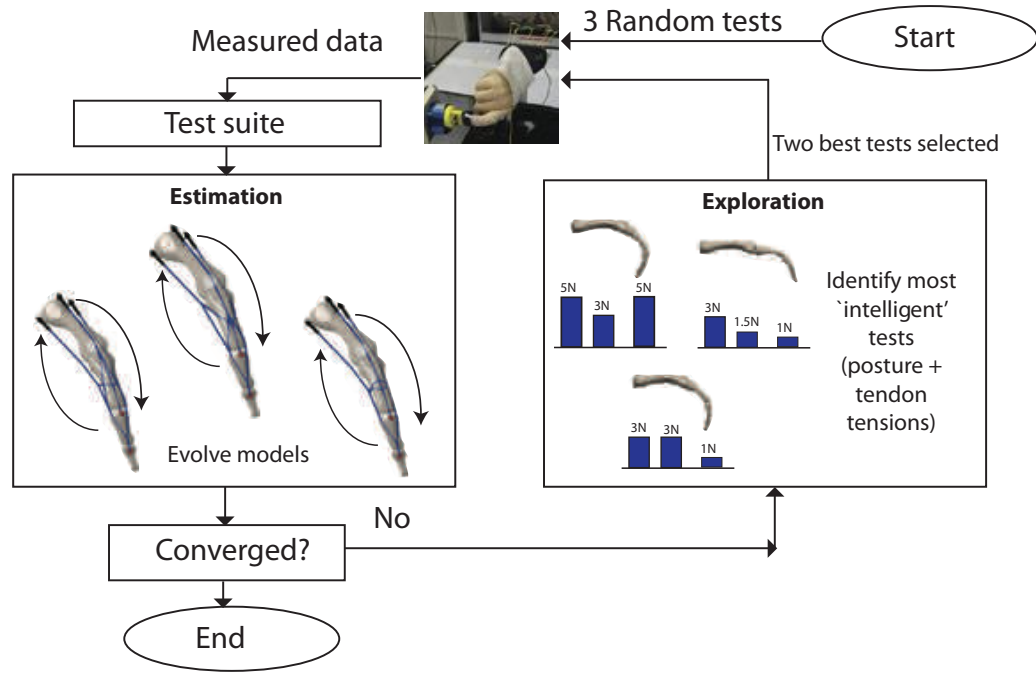
Figure 8.3: The estimation exploration algorithm. The algorithm began with three random tests consisting of input tendon tensions and experimentally recorded fingertip forces in three postures (One test in each posture). These were used to optimize individually three models of the network minimizing errors in fingertip force direction and magnitude between the experimental data and model prediction. This is the *estimation phase*. This was followed by the *exploration phase* where the two tests that cause maximum disagreement in fingertip force magnitude and direction between the optimized models from the estimation phase were picked. These data points from the experimental dataset were then added to the test suite and used for the estimation. This coevolution of models and tests was carried out for six iterations.

8.3.3 Inference algorithm

We used the estimation-exploration algorithm to infer the topology and parameter values of the extensor mechanism (Bongard & Lipson 2004a, Bongard & Lipson 2005b, Bongard & Lipson 2005a, Valero-Cuevas, Anand, Saxena & Lipson 2007). Our inference began with a *test suite* consisting of three random data points measured experimentally, *i.e* three sets of input tendon tensions and experimentally recorded fingertip forces in three postures (1 test in each posture). These were used to optimize individually three models of the network in parallel in what is called the *estimation phase* (Fig. 8.3). The optimization cost function was a weighted sum of the fingertip force magnitude error and fingertip direction error, which we shall call the *fitness error*. The fingertip force magnitude error was the root mean squared (RMS) normalized magnitude error and the force direction error was the RMS direction angle error of the fingertip force vector over all the tests in the test suite. We used a Markov-Chain Monte Carlo based optimization algorithm for the estimation. The estimation phase was followed by the *exploration phase*. Here the tests competed amongst themselves (each test consisting of posture and input tendon tensions) to create largest *disagreement* among the three optimal models obtained in the estimation phase. The disagreement produced by a test was measured by the variance in fingertip force magnitude (or fingertip force direction) when this test was applied to the three optimal models from the estimation phase, in simulation. Two tests were selected, one which when applied to the three models in simulation, resulted in the largest variance in fingertip force magnitude and the other, which resulted in largest variance in fingertip force direction. The experimental data points corresponding to these two

new tests were then added to the test suite and the estimation was repeated. This co-evolution of models that explained the available data points in the test suite and of tests that caused most disagreement among the optimal models, was repeated till we either ran out of experimental data points, the error in the estimation phase stopped improving or the error was below a certain bound which was defined by the errors in experimental measurement of joint angles and segment lengths (See below for details). This entire inference algorithm was run in a parallel computing environment using the Matlab Parallel Computing toolbox on a computer cluster at the USC High Performance Computing and Communications Facility.

We implemented the An-Chao normative model (Chao & An 1978a, An et al. 1979) of the index finger to obtain moment arm values for the tendons of interest (EIP, EDC, LUM and FPI) in the three finger postures described above. We scaled the model based on the length of the middle phalynx (An et al. 1979). We obtained fingertip force vector using the equation (Valero-Cuevas 2009), $\mathbf{F_{tip}} = J^{-T} R \mathbf{F_m}$ where $\mathbf{F_{tip}}$ is the fingertip wrench vector, J is the Jacobian matrix mapping joint angle velocities to fingertip velocities, R is the moment arm matrix, and $\mathbf{F_m}$ is the vector of tendon tensions. We only used the fingertip force components of the fingertip wrench vector for this study (not the torque produced at the fingertip).

We compared the errors of the inferred models when tested with all the data points in our dataset (72 tests, 24 in each of the three postures) against the errors for the An-Chao model (Chao & An 1978a, An et al. 1979). We compared the errors of the fingertip force direction and magnitude only in the sagittal plane of the finger. The ad-abduction force component arises from the ad-abduction torque at the MCP which is governed by

the location of the input tendons with respect to the joint center and not the properties (topology and parameters) of the extensor mechanism we were trying to infer. The RMS magnitude errors ($error_{mag}$) and RMS direction errors ($error_{dir}$) were calculated using the equations below:

$$error_{mag} = \sqrt{(\frac{1}{N} \sum_{i=1}^{N} (\frac{\|\mathbf{F}_{mod}\| - \|\mathbf{F}_{exp}\|}{\|\mathbf{F}_{exp}\|} \times 100)^2)}$$

$$error_{dir} = \sqrt{(\frac{1}{N} \sum_{i=1}^{N} (cos^{-1}(\frac{\mathbf{F}_{mod}}{\|\mathbf{F}_{mod}\|} \cdot \frac{\mathbf{F}_{exp}}{\|\mathbf{F}_{exp}\|}))^2)}$$

where $error_{mag}$ and $error_{dir}$ are the errors in fingertip force magnitude and direction, respectively, N is the total number of tests in the data set (N=72 in our case), $\mathbf{F}_{mod}$ is the fingertip force magnitude in the model, $\mathbf{F}_{exp}$ is the experimental fingertip force magnitude.

8.3.4 Experimental measurement error

Errors in measurement of joint angles and segment lengths are almost unavoidable in experiments with biological specimens like the cadaveric index finger (using current measurement techniques: ruler and goniometer/motion capture). This is because of the existence of non-engineering joints and the presence of skin and fat over the bones whose length and posture we are trying to measure. These errors in measurement lead to errors in fingertip force direction and magnitude largely because of the nonlinear Jacobian matrix mapping joint angle velocities to fingertip velocities that also is involved in the transformation of joint torques to fingertip force. Our inference algorithm will only be

able to obtain models that are as accurate as the experimental data; in other words, the experimental measurement error defines the bound/limit on the fitness error of the models being inferred. We performed a Monte Carlo analysis by perturbing the joint angles defining the posture of the finger by ± 5 degrees and segment lengths by $\pm 5\%$ and calculated the fingertip force direction and magnitude errors in simulation, keeping the network topology and parameters fixed. This determined the experimental uncertainty bound and any model with errors below this bound would be a valid solution to the problem.

8.4   Results

The results presented here are based on four separate runs of inference using the estimation-exploration algorithm. Each inference run consisted of six iterations of the estimation and exploration phases. A total of thirteen intelligent tests were introduced. Since each run inferred three independent models, we obtained 12 'optimal' models at the end of four runs. We compared the RMS errors in force magnitudes and directions of the sagittal components of the fingertip force vectors predicted using the An-Chao model as well as the twelve inferred models. We chose to only compare the sagittal components because the ad-abduction component of the force vector arises largely from the moment arms of the tendons about the MCP which are not part of the extensor mechanism and hence not varied in the inference process. Fig. 8.4 shows the comparison results. We only show the mean and std deviation of the best five models obtained from the inference. The RMS magnitude errors for the An-Chao model was about five times larger than the mean

error for the five best inferred models. The directional errors were also 1.6 to two times larger than in the An-Chao model compared to the inferred models. The direction errors for the fully flexed posture were the largest for both types of models followed next by the tap posture and then the fully extended posture with the lowest errors. The band of experimental uncertainty shown in the figure was generated by doing a Monte Carlo analysis where the joint angles were perturbed by ± 5 degrees and the segment lengths by $\pm 5\%$, keeping the network topology and parameters fixed. These experimental errors resulted in an error of up to 1.5N in fingertip force magnitude and 14.5 degrees in force direction. This forms the bound on the accuracy of the inference algorithm. Any model with errors below this bound is a valid solution to the problem.

The best five inferred models of the extensor mechanism are shown in the fully extended posture in Fig. 8.5. The color map indicates the tension in each of the bands of the extensor mechanism. The models differ in their topology and parameter values, but have a similar fingertip force direction and magnitude error. This demonstrates the issue of non-uniqueness that has been discussed in earlier work as well (Valero-Cuevas, Anand, Saxena & Lipson 2007). We discuss more details about unobservability and non-uniqueness in Chapter 9.
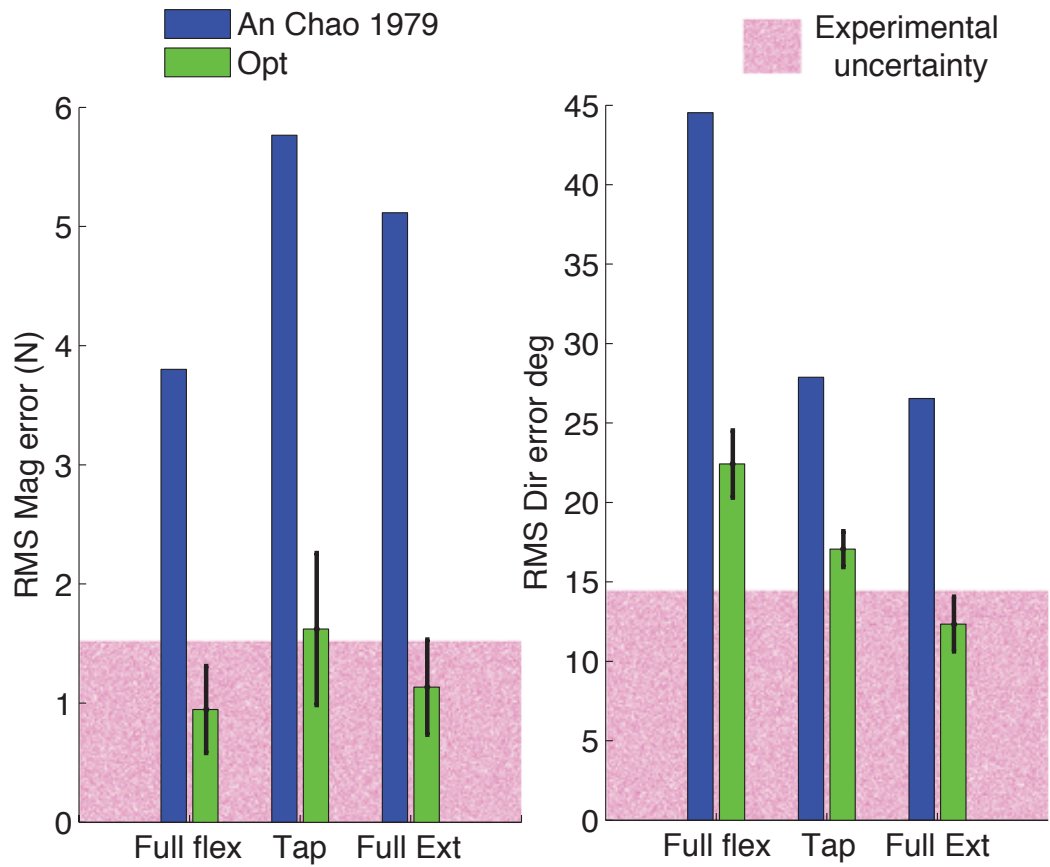
Figure 8.4: Comparison of magnitude and direction errors of the saggital plane compo-
nent of the fingertip force vector in the best five inferred models vs. An-Chao normative
model (Chao & An 1978*a*, An et al. 1979) in the three finger postures *fully flexed*, *tap*
and *fully extended*. The RMS magnitude errors as well as directional errors were much
larger for the An-Chao model compared to the inferred models in each of the three
postures.

Figure 8.5: The best five inferred models obtained using the estimation-exploration algorithm. These models have similar input-output behavior but vary in their topology and parameters, demonstrating non-unique solutions.

8.5 Discussion

Here we have demonstrated for the first time the inference of a functional 3-dimensional model of a musculoskeletal system from experimental data collected from an intact cadaveric system using intelligent testing. The inferred models capture the functional behavior of the system more accurately than the model most commonly used in the literature.

The An-Chao model as well as its modified versions (Weightman & Amis 1982) do not explicitly model the elastic properties of the tendon networks or the physics of interactions of the different components constituting these networks. Another big drawback of the An-Chao model is that it assumes a fixed distribution of tendon tensions in the different components with changes in posture. But cadaveric studies have shown that the geometry of the bands as well as the force distribution through them, change significantly with posture (Garcia-Elias, An, Berglund, Linscheid, Cooney Iii & Chao 1991, Sarrafian et al. 1970, Micks & Reswick 1981). The models inferred here give insight on how the geometry and force distribution changes in the different finger postures.

The inferred models had a fingertip direction error of 10-25 degrees (in the sagittal plane). While this may seem a like a large error, one should keep in mind that fingertip force output is very sensitive to measurement in joint angles (Goehler & Murray 2010) as has been demonstrated using the Monte Carlo analysis. Hence models with very low errors (lower than the 14.5 degree error bound) in fingertip force direction would be overfitting to these measurement errors. Uniform scaling of the entire model would lead to a reduction in the magnitude error considering that the transformation from joint torques to fingertip force is linear when the posture is fixed.

While the An-Chao model is a simple mathematical representation and very easy to implement computationally, the finite element simulator described here is more mathematically involved. Chapter 7 gives details on the implementation of this model. Also, while it is more complex than the An-Chao model, it is much simpler and faster than detailed finite element models used to describe cartilage-ligament-joint mechanics in musculoskeletal systems (Huiskes & Chao 1983).

A small error in the measurement of joint angles and segment lengths leads to a large deviation in fingertip force vector output. This is primarily caused by the nonlinear Jacobian matrix transforming joint angle velocities to fingertip velocities (Valero-Cuevas 2009). Hence, it is extremely important to be able to measure these properties accurately during experimentation. However, some error is unavoidable considering that we are modeling the biomechanical system using simple engineering joints and the joint angle and segment length measurements are made in the presence of fat and skin. These fingertip force vector errors produced by errors in posture and segment length measurements define the limit on how accurately the tendon network topology and parameters can be identified. Any network obtained using the inference algorithm with fingertip force magnitude and direction errors lower than this limit are potential solutions for the problem. This results in a problem of non-uniqueness that is different from the one discussed in (Valero-Cuevas, Anand, Saxena & Lipson 2007). We describe the different forms of non-uniqueness in more detail in Chapter 9. This experimental uncertainty bound has other implications in addition to biomechanical model inference. This raises interesting questions from a neuromuscular control perspective. Small deviations in estimates of joint angles and finger segment lengths would result in a fingertip direction error of up to 15 degrees which is

larger than the friction cone angle for many surfaces. Hence a very accurate estimate of joint angles and segment lengths would be needed by the nervous system to be able to grasp such a surface. Also, one needs to keep in mind that these sensitivities of the Jacobian are true only if we assume engineering hinge like joints for the index finger. It is possible that the deviation from engineering joints could make the system much more robust to errors in posture and segment lengths.

We observed that multiple sets of topologies and parameter values give similar fingertip force vector at the end point. In other words multiple solutions exist that do the same functional mapping from inputs to outputs. This could mean that the specific set of topology and parameters observed in the real system could be due to evolutionary reasons or for goals not related to fingertip force production (Eg. joint protection, etc.).

In this study, we used a set of experimental data points that had been obtained prior to the inference. Even in this setup the estimation-exploration algorithm has the computational advantage of using fewer data points and has been shown in an earlier study (Valero-Cuevas, Anand, Saxena & Lipson 2007), to produce more accurate solutions than using randomly generated tests. However, the ultimate goal of using this algorithm would be to run the inference in real-time and only perform those experiments on the cadaveric specimen as suggested by the exploration phase. Thus the damage to the specimen can be minimized through intelligent testing.

While most musculoskeletal models are based on a one-kind fits all approach where a generic model is developed based on cadaveric studies and the model is uniformly scaled to fit different subjects (Eg. (An et al. 1979)), the idea of subject-specific modeling where data from individual specimens is used to develop personalized musculoskeletal models

is gaining ground. This has been spearheaded by advances in magnetic resonance and ultrasound imaging (Blemker et al. 2007). In these cases it is very important to have computational methods to infer accurate subject-specific representations of the system being modeled. The method presented here based on the estimation exploration algorithm would enable the inference of accurate subject-specific models with minimum number of experimental data points.

While in this chapter, we have demonstrated the inference of functional models of the extensor mechanism of the index finger, this novel method of inference through intelligent testing can be applied to the inference of functional models of other musculoskeletal models in the body as well.

8.6   Appendix: Inference of networks in simulation

Fig. 8.6 demonstrates the inference of the topology and parameter values of an elastic tendon network draped on a hemisphere from simulated data generated using a target network. This was a test of concept to see if we can accurately infer a 3D network draped on a solid directly from input-output data. In simulation, with no noise, our optimization algorithm based on Stochastic Hill Climbing with Learning by Vectors of Normal Distributions (Rudlof & Köppen 1996) was able to uniquely identify the network directly from the input-output data with no knowledge about the physical connectivity of the network or the positions of the nodes.
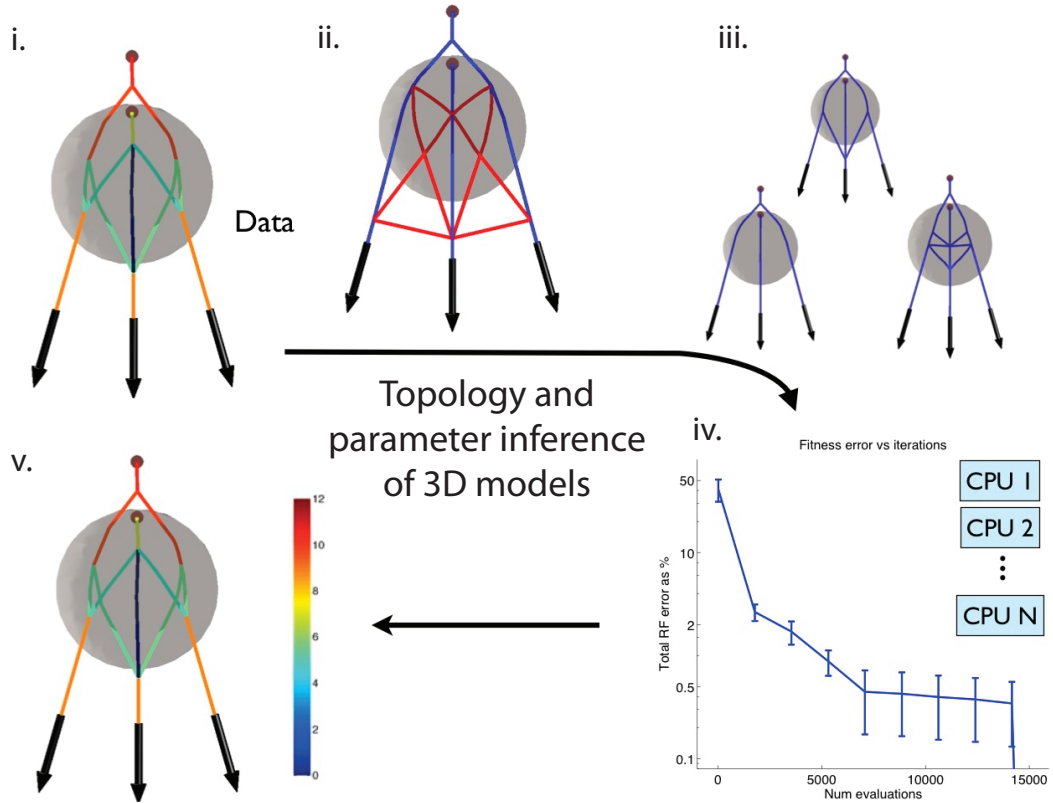
Figure 8.6: Inference of network topology and parameter values in simulation. A Markov-Chain Monte Carlo based optimization was able to successfully infer topology and parameters of an elastic tendon network draped on a hemisphere, in simulation. i. A target network is defined in simulation and an input-output dataset generated by applying different input tendon tensions and calculating the reaction forces at the fixed nodes using the tendon network simulator. ii. The inference process begins with a primordial soup from which can be generated several random instances (iii). iv. The node locations and topology are optimized in a parallel computing environment till the fitness error goes below a tolerance limit. v. The inferred network matched the target network. Hence we were able to successfully infer the network topology and parameters directly from the input-output data.

Acknowledgment

Chapter 9

Discussion: Challenges in the inference of computational models of tendon networks.

In this chapter, we will be discussing some of the challenges faced and lessons learned during the process of inference of computational models of biomechanical systems. Future work in this area would need to consider these issues.

9.1 Measurement of joint angles

Measurement of joint angles in the human finger is a challenging task considering that biological joints are not the same as the engineering joints that we use to model them, the exact locations of the joints are hard to determine, and there are skin deformations displacing the reflective markers used to determine the joint angles. In the cadaveric index finger, this was particularly true for the MCP joint and the measurement of the ad-abduction angle. While new techniques based on probabilistic inference have been suggested in the literature (Todorov 2007), we had little success in implementing them with data from the cadaveric finger. There is definitely a need to model musculoskeletal

joints more accurately and for algorithms that can be used to infer joint angles from motion-capture data.

9.2   Unobservability and non-uniqueness

There exists the problem of unobservability as well as non uniqueness when it comes to elastic networks like the tendon networks described in this dissertation. What is specifically being referred to here is the fact that it is not possible to determine all the hidden states of the system simply from the measured inputs and outputs. In the case of the tendon networks of the fingers, the inputs and outputs measured were the tendon tensions applied to the FPI, LUM and EDC/EIP and the output was the fingertip force vector. The hidden states of the system are the existence of the nodes and elements of the finite element representation of the extensor mechanism and the positions of these entities. This issue of unobservability can also be flipped around and termed as an issue of non-uniqueness; i.e. multiple topologies and parameter values, i.e. elements and node combinations exist that result in the same input-output transformation. This issue exists at multiple levels. One is inherent in the network topology and parameters itself as is demonstrated in Fig. 9.1 in 2-dimensional elastic networks (Valero-Cuevas, Anand, Saxena & Lipson 2007). The other level of unobservability/non-uniqueness exists when working with experimental data like the data from the cadaveric specimen that was described in the previous chapter. The latter arises due to the mismatch between the model and the experimental system mostly occurring due to experimental measurement uncertainties which will be discussed in more detail in section 9.3. This mismatch sets

a limit on how accurately a system can be identified. A model that is inferred from a set of experimental measurements can only have errors as large as this limit. Smaller errors simply mean that the model is over fitting to the experimental data. Hence two different networks with different topologies and parameter values could in simulation give rise to different outputs for the same inputs and would hence be uniquely identifiable. However, if the difference in the outputs of these two networks is within the limit set by the model-experimental data mismatch, then they would never be uniquely identified from experimental data.

For example, consider network A in Fig 9.2. This is the model of the true latex network that was used to collect an experimental dataset consisting of tendon tension inputs and reaction force outputs (See Chapter 7 for more details). The error between the experimental measurements and the predictions of this model is 11.5 %. This is the model-experimental data mismatch that sets the limit on how accurately a model of this network can be inferred from the experimental data. Network B in Fig 9.2 could result in different outputs for the same inputs when compared with network A in simulation. However when tested with the experimental data obtained (whose true model is network A), the error between model predictions and experimental measurements is 10.95% which is less than the limit set by the model-experimental data mismatch. Hence network A can never be uniquely inferred from experimental data. There will be network B and other networks which will all have errors within the limit and hence be equally good solutions to the inference problem.
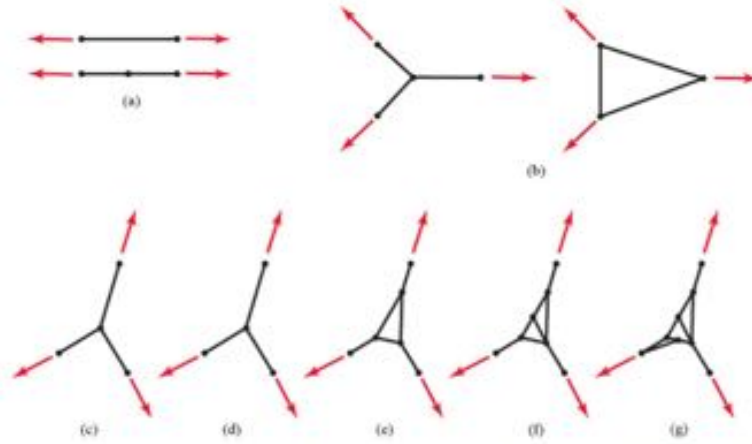
Fig. 10. Separability, observability, and uniqueness of network components and topologies. (a) The 1-D (b) 2-D substructures that can be equivalent under certain parameter settings. These two equivalencies can be used to (c) transform network into (d)–(g) a series of equivalent topologies. Reverse application of these equivalence operators can transform networks (d)–(g) into their canonical form (c).

Figure 9.1: Demonstration of the problem of unobservability/non-uniqueness in elastic tendon networks in two dimensions (Valero-Cuevas, Anand, Saxena & Lipson 2007).

i. Network A   i. Network B
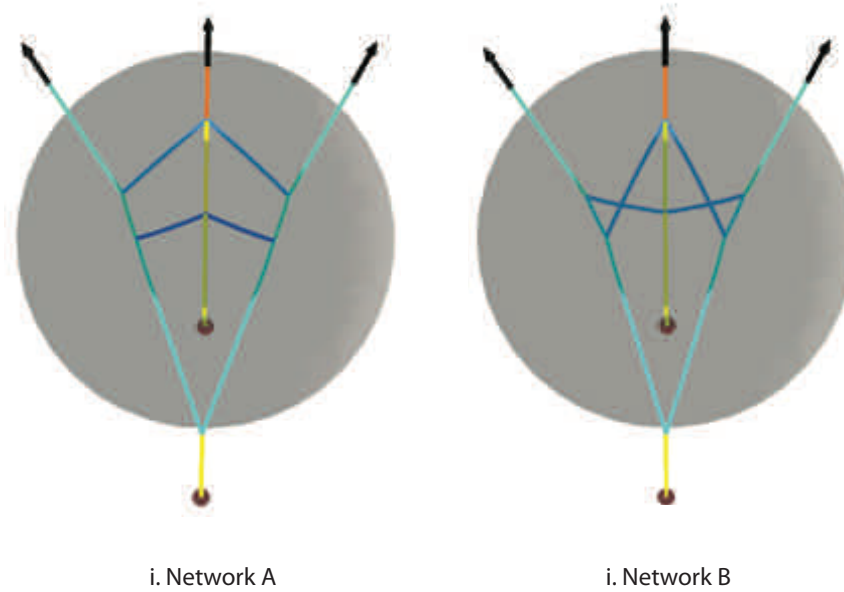
Figure 9.2: Unobservability/Non-uniqueness issue when dealing with experimental data from elastic networks draped on solids, in 3 dimensions. Networks that give rise to outputs whose errors lie within specific limits determined by model-experimental data-mismatch cannot be distinguished from each other. In this figure, network A is the true model of the latex network used in the experiment described in Chapter 7. However, network B also has similar errors as network A when tested against experimental data. Hence network A cannot be uniquely inferred from the experimental data.

9.3 Model-Experimental data mismatch due to uncertainties in experimental measurements

There are several factors that lead to mismatch between model predictions and the experimental data. One of the main sources of error is the uncertainty in experimental measurements. This is particularly significant in measurements from biological systems. Here we will discuss how the measurement of the fingertip force output used in the inference in Chapter 8 is sensitive to the measurement of joint angles and segment lengths. Deviations in measurement of the joint angles and the segment lengths results in model-experimental data mismatch in two ways: i. Transformation of forces from the sensor coordination system to the finger coordination system. ii. The model not accurately representing the system posture and segment lengths.

9.3.1 Transformation from the force sensor coordination system to the finger coordination system

The fingertip force vectors used in the inference in Chapter 8 are in the finger coordinate system that need to be transformed from the coordinate system of the force sensor used in the experiments (See Fig. 8.1). This transformation is done through four rotation matrices (one for each degree-of-freedom) that rotate the force vector from the fingertip to the base of the finger. Errors in joint posture measurement result in errors in the rotation matrix and hence the fingertip force vector. Fig. 9.3 shows the results of a simple Monte Carlo simulation to test deviations in fingertip force vector for deviations in ± 5 degrees in joint angle measurements for each of the four joint angles and $\pm 5\%$

deviation in segment lengths of the index finger. We observed that this resulted in an error of about 12 degrees in fingertip force direction. This transformation error does not affect the fingertip force magnitude because the rotation matrices only rotate the force vector without altering the force magnitude.
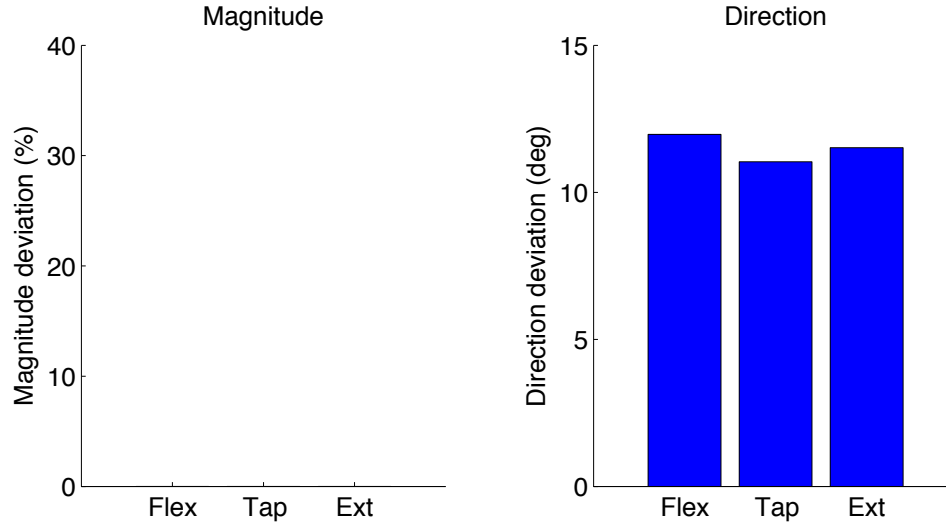
Figure 9.3: Errors in fingertip force vector arising from coordinate transformation from force sensor to finger.

9.3.2 Effect of inaccuracies in model posture and segment lengths

Since the measured joint angles and segment lengths are replicated in the tendon network simulator, any errors in joint angle and segment length measurements would imply that the model is not an accurate representation of the experimental system. A recent study by Goehler and Murray (Goehler & Murray 2010) demonstrates that small deviations in these measurements can lead to large variations in fingertip force output. We performed a Monte Carlo simulation where we perturbed the four joint angles representing the posture of the finger by ± 5 degrees and the segment lengths by $\pm 5\%$, keeping the network

topology and parameter values the same in the tendon network simulator, and observed the deviation in fingertip force vector direction and magnitude. Fig. 9.4 shows the results. The large deviations in force magnitude and direction demonstrate that the model is highly sensitive to these kinematic parameters. In addition to the issue of non-uniqueness/unobservability that was discussed in the previous section, these results have implications on neuromuscular control. Since a 15-20 degree deviation in fingertip force vector is larger that the friction cone angle for many surfaces, an inaccurate estimate of the joint angles and segment lengths by the nervous system could result in an object being dropped. But this rarely happens and hence raises the question on how the nervous system bypasses this issue. It is also possible that the engineering joints we use to represent the degrees of freedom of the finger are not accurate representations of the biological system in which case the fingertip force vector may not be as sensitive to joint angles and segment lengths as seen in the above results.

9.4   Ambiguity of the model of the MCP joint

The kinematics of the MCP joint is still not well understood. Hence there is a larger scope of error of MCP angle measurement. In addition, the orientation of the ad-abduction axis with respect to the flexion-extension axis has also been debated. See (Valero-Cuevas 1997) for a description on different models of the MCP joint. Here, we performed another Monte Carlo simulation to see how changing the angle between the MCP flexion-extension and ad-abduction joint axes affected fingertip force vector (Fig. 9.5). We perturbed this angle between 70 and 100 degrees and observed that the fingertip force vector magnitude
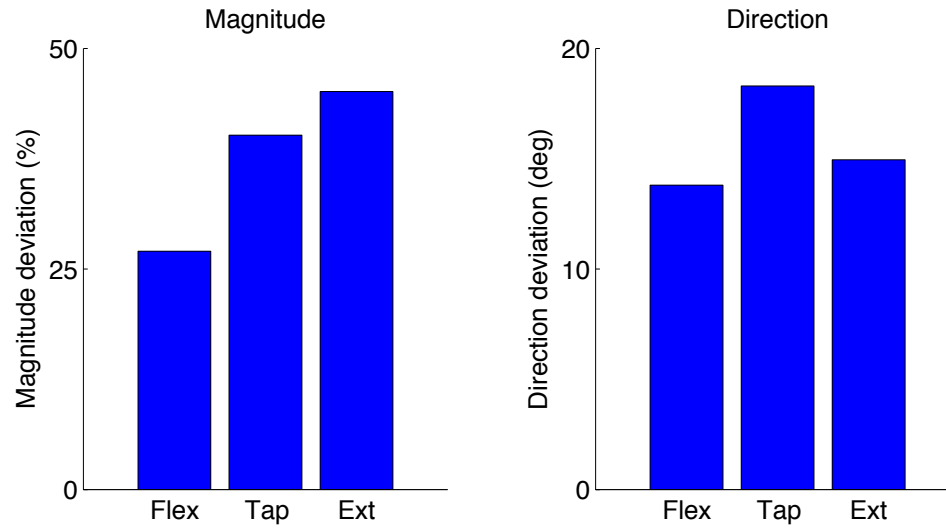
Figure 9.4: Errors in fingertip force vector arising due to model being an inaccurate representation of the experimental system. A Monte Carlo analysis shows there is an error of 25-50 % in fingertip force magnitude and around 15 degrees in force direction arising from a $\pm 5\%$ perturbation in segment lengths and ± 5 degrees in joint posture. This demonstrates how sensitive the fingertip force vector is to these kinematic parameters.

and direction are very sensitive to this parameter. Hence, there is a need to accurately characterize the kinematic nature of the MCP joint and the orientation of the MCP joint axes.

9.5 Stiffness of the tendon network

Unlike muscles, tendons have low compliance. The extensor mechanism is a network of very stiff collagenous strings that stretch very little. For all the elements of this network to transmit force upon loading, they need to be connected in a very specific manner with accurately determined lengths. Otherwise, there is a high chance that part of the network would go slack and hence not contribute to force transmission. It would also be interesting to compare the string like representation used in this dissertation to model
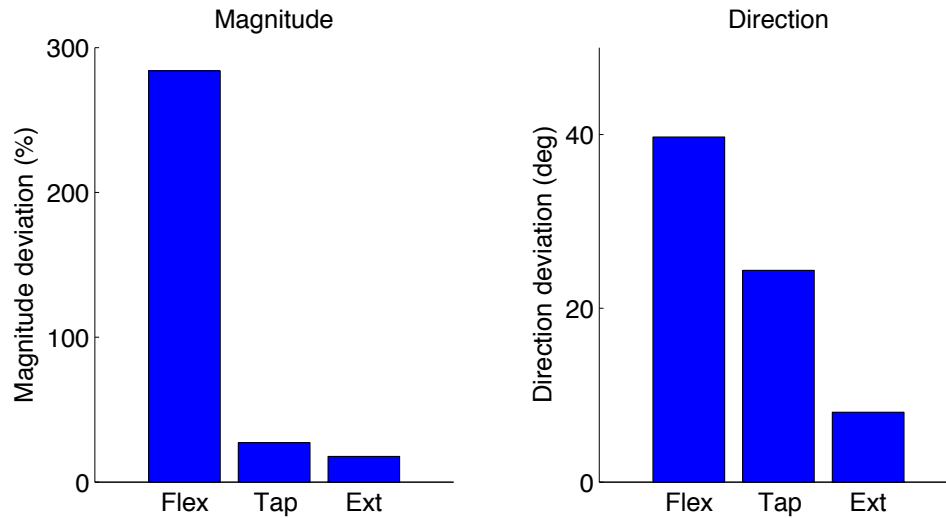
Figure 9.5: Sensitivity of fingertip force vector to changes in angle between MCP flexion-extension and ad-abduction axes. The nature of the MCP joint is not clearly understood. A Monte Carlo simulation where the angle between the MCP flexion-extension and the MCP ad-abduction axes was perturbed between 70 and 100 degrees resulted in large fingertip force output deviations thus demonstrating that the fingertip force vector is very sensitive to this angle parameter.

the collagenous network of the extensor mechanism, against a sheet like representation.

It is possible that the existence of a large number of fibers in the sheet introduces a

redundancy that allows slackening of some fibers and still allow force transmission.

9.6   Implementation in the clinic

The ultimate goal would be to apply the computational techniques described in this dissertation to infer accurate subject-specific models of tendon networks in patients with tendon injury as well as those with nerve palsies, in the clinic. The main challenge to achieve this goal is the measurement of forces exerted by the muscles on the tendon networks (or alternatively, the tendon excursions produced by muscle contraction/stretching). Currently, there is no way to infer these quantities accurately in live subjects. While electromyogram

is useful to determine when a particular muscle or group of muscles is on or off, its relation to muscle force or muscle displacement is not understood(Inman et al. 1952, Disselhorst-Klug et al. 2009). However, recent technological advances particularly in imaging show promise that we could, in the near future, be able to measure musculotendon movements in real-time in live subjects (Blemker et al. 2007). In addition to this, there have also been studies to infer muscle forces using fluctuations in endpoint force (Kutch, Kuo & Rymer 2010). Until the technology is available, we will have to settle with generalizable models that capture behavior across a population. However, it is possible that there exists a finite number of 'types' or 'classes' of tendon networks that exist in the population. This has been shown to be the case with respect to human thumb models as described in (Santos & Valero-Cuevas 2006). Such classes of tendon networks could be identified from testing of multiple cadaveric specimens using the inference methods described in this dissertation.

9.7   Acknowledgement

Chapter 10

Conclusions and Future Work

In this dissertation, we have presented novel methods for the computational modeling of musculoskeletal systems. These methods are based on the inference of accurate models of these systems from sparse experimental data. Using the complex tendon networks of the human fingers as an example, we have demonstrated the development of two kinds of computational models – analytical models consisting of functions mapping joint angles to tendon excursions, and physics-based models capturing the interactions of a network of elastic tendons with the bones of the fingers. We have implemented a novel inference technique based on symbolic regression to infer mathematical forms and parameter values of tendon routing in musculoskeletal systems. We showed that the functions inferred using this method are more accurate, require fewer training data points, have fewer parameters, are more robust to noise, and can extrapolate better than polynomial regression models, the state of the art in musculoskeletal modeling. We applied this technique to learn analytical models modeling the tendon excursions of the human index finger and showed that these functions are more accurate than Landsmeer-based models or polynomial regressions whether our goal is to obtain subject-specific models or models that

generalize across specimens. We successfully controlled a human cadaveric index finger to produce a slow tapping motion for the first time ever (to the best of our knowledge) and learned that a spring-based 'muscle-like' control was more effective in producing slow finger motions than simple force or position control. We demonstrated that the finger has neutral equilibrium in a specific range of postures when the input tendon tensions are in(or close to) the null space of the moment arm matrix of the finger in those postures. Stable equilibrium was observed in other postures. We developed a novel finite element method based tendon network simulator to simulate the interactions of elastic tendon networks with arbitrarily shaped solids and used this to study the sensitivity of fingertip force magnitude and direction to the elastic properties and topology of the extensor mechanism. We concluded that the output is most sensitive to the resting lengths of the fibers and the topology of the structure. We then implemented a novel inference algorithm to infer the three dimensional network structure of the extensor mechanism of the fingers from minimal experimental data through intelligent testing. The models of the extensor mechanism inferred more accurately matched with experimental data compared to the An-Chao normative model used extensively in the literature.

The computational methods developed in this dissertation are a combination of techniques in biomechanics, machine learning and electromechanical experimentation. They can be used for the inference of accurate models of different musculoskeletal systems in the body. Analytical models are critical for dynamical simulations especially for control. The analytical models for the index finger presented here are currently being used as a representation of the biomechanics of the 'plant' to test theories of motor control in human manipulation. More work needs to be done to see how the nervous system could

be using the neutral equilibrium in the fingers observed here and its implications on our understanding of grasp and manipulation. The tendon network environment developed here can be a useful tool for clinical research to understand how damage or injury to the network can affect fingertip force production. The inference of the three dimensional structure of the finger model demonstrated in this dissertation is a step towards the inference of subject specific models of musculoskeletal systems. Combining it with real time magnetic resonance or ultrasound imaging could in the future enable development of individualized models of these systems and to study specific changes on damage or repair.

Bibliography

Abend, W., Bizzi, E. & Morasso, P. (1982), 'Human arm trajectory formation', *Brain* **105**(Pt 2), 331–48.

An, K., Linscheid, R. & Brand, P. (1991), 'Correlation of physiological cross-sectional areas of muscle and tendon.', *Journal of hand surgery (Edinburgh, Scotland)* **16**(1), 66.

An, K. N., Chao, E. Y., Cooney, W. P. & Linscheid, R. L. (1979), 'Normative model of human hand for biomechanical analysis.', *J Biomech* **12**(10), 775–788.

An, K. N., Chao, E. Y., Cooney, W. P. & Linscheid, R. L. (1985), 'Forces in the normal and abnormal hand', *Journal of Orthopaedic Research* **3**(2).

An, K. N., Chao, E. Y. S. & Kaufman, K. R. (1991), 'Analysis of muscle and joint loads', *Basic orthopaedic biomechanics* pp. 1–50.

An, K. N., Takahashi, K., Harrigan, T. P. & Chao, E. Y. (1984), 'Determination of muscle orientations and moment arms', *Journal of biomechanical engineering* **106**, 280.

An, K. N., Ueba, Y., Chao, E. Y., Cooney, W. P. & Linscheid, R. L. (1983), 'Tendon excursion and moment arm of index finger muscles', *J Biomech* **16**(6), 419–25.

Anderson, A. E., Ellis, B. J. & Weiss, J. A. (2007), 'Verification, validation and sensitivity studies in computational biomechanics', *Computer methods in biomechanics and biomedical engineering* **10**(3), 171–184.

Anderson, F. C. & Pandy, M. G. (2001), 'Dynamic optimization of human walking', *Journal of biomechanical engineering* **123**, 381.

Andriacchi, T. P., Natarajan, R. N. & Hurwitz, D. E. (1991), 'Musculoskeletal dynamics, locomotion, and clinical applications', *Basic orthopaedic biomechanics* p. 51.

Bartel, D. L., Bicknell, V. L. & Wright, T. M. (1986), 'The effect of conformity, thickness, and material on stresses in ultra-high molecular weight components for total joint replacement', *J Bone Joint Surg Am* **68**(7), 1041–1051.

Bendz, P. (1985), 'The functional significance of the oblique retinacular ligament of landsmeer. a review and new proposals', *The Journal of Hand Surgery: Journal of the British Society for Surgery of the Hand* **10**(1), 25–29.

Berme, N., Paul, J. P. & Purves, W. K. (1977), 'A biomechanical analysis of the metacarpo-phalangeal joint', *Journal of Biomechanics* **10**(7), 409–412.

Bernstein, N. (1967), 'The co-ordination and regulation of movements'.

Blankevoort, L., Kuiper, J. H., Huiskes, R. & Grootenboer, H. J. (1991), 'Articular contact in a three-dimensional model of the knee', *Journal of Biomechanics* **24**(11), 1019.

Blemker, S. S., Asakawa, D. S., Gold, G. E. & Delp, S. L. (2007), 'Image-based musculoskeletal modeling: applications, advances, and future opportunities', *Journal of Magnetic Resonance Imaging* **25**(2), 441–451.

Blemker, S. S. & Delp, S. L. (2005), 'Three-dimensional representation of complex muscle architectures and geometries', *Annals of Biomedical Engineering* **33**(5), 661–673.

Bongard, J. C. & Lipson, H. (2004*a*), Automating genetic network inference with minimal physical experimentation using coevolution, *in* 'Genetic and Evolutionary Computation Conference (GECCO) 2004', Springer, pp. 333–345.

Bongard, J. C. & Lipson, H. (2005*a*), 'Nonlinear system identification using coevolution of models and tests', *Evolutionary Computation, IEEE Transactions on* **9**(4), 361–384.

Bongard, J. & Lipson, H. (2004*b*), Once more unto the breach: Co-evolving a robot and its simulator, *in* 'Proceedings of the Ninth International Conference on the Simulation and Synthesis of Living Systems (ALIFE9)', pp. 57–62.

Bongard, J. & Lipson, H. (2005*b*), 'Active coevolutionary learning of deterministic finite automata', *The Journal of Machine Learning Research* **6**, 1651–1678.

Brand, P. W. & Hollister, A. (1999), *Clinical mechanics of the hand*, Mosby St. Louis, MO.

Brook, N., Mizrahi, J., Shoham, M. & Dayan, J. (1995), 'A biomechanical model of index finger dynamics', *Medical Engineering and Physics* **17**(1), 54–63.

Brown, I. E. & Loeb, G. E. (2000), 'A reductionist approach to creating and using neuro-musculoskeletal models', *Biomechanics and Neural Control of Posture and Movement* pp. 148–163.

Buchanan, T. S., Lloyd, D. G., Manal, K. & Besier, T. F. (2004), 'Neuromusculoskeletal modeling: Estimation of muscle forces and joint moments and movements from measurements of neural command', *J Appl Biomech* **20**(4), 367–395.

Buchner, H. J., Hines, M. J. & Hemami, H. (1988), 'A dynamic model for finger interphalangeal coordination', *J Biomech* **21**(6), 459–68.

Buford Jr, W. L., Ivey Jr, F. M., Malone, J. D., Patterson, R. M., Pearce, G. L., Nguyen, D. K. & Stewart, A. A. (1997), 'Muscle balance at the knee-moment arms for the normal knee and the acl-minus knee', *Rehabilitation Engineering, IEEE Transactions on* **5**(4), 367–379.

Bunnell, S. (1945), 'Surgery of the hand', *Southern Medical Journal* **38**(3), 228.

Cappozzo, A., Catani, F., Leardini, A., Benedetti, M. G. & Della Croce, U. (1996), 'Position and orientation in space of bones during movement: experimental artefacts', *Clinical Biomechanics* **11**(2), 90–100.

Cerveri, P., De Momi, E., Marchente, M., Lopomo, N., Baud-Bovy, G., Barros, R. M. L. & Ferrigno, G. (2008), 'In vivo validation of a realistic kinematic model for the trapezio-metacarpal joint using an optoelectronic system', *Annals of Biomedical Engineering* **36**(7), 1268–1280.

Chao, E. (1989), *Biomechanics of the hand: a basic research study*, World Scientific Pub Co Inc.

Chao, E. Y. & An, K. N. (1978a), 'Determination of internal forces in human hand', *journal of the engineering mechanics division* **104**(1), 255–272.

Chao, E. Y. & An, K. N. (1978b), 'Graphical interpretation of the solution to the redundant problem in biomechanics', *Journal of Biomechanical Engineering* **100**, 159–67.

Cheng, E. J., Brown, I. E. & Loeb, G. E. (2000), 'Virtual muscle: a computational approach to understanding the effects of muscle properties on motor control', *Journal of neuroscience methods* **101**(2), 117–130.

Clavero, J. A., Golano, P., Farinas, O., Alomar, X., Monill, J. M. & Esplugas, M. (2003), 'Extensor mechanism of the fingers: Mr imaging-anatomic correlation 1', *Radiographics* **23**(3), 593–611.

Clewley, R. H., Guckenheimer, J. M. & Valero-Cuevas, F. J. (2008), 'Estimating effective degrees of freedom in motor systems', *IEEE Trans Biomed Eng* **55**(2 Pt 1), 430–42.

Crisfield, M. A. (1991), 'Nonlinear finite element analysis of solids and structures. volume 1: Essentials'.

Damsgaard, M., Rasmussen, J., Christensen, S. T., Surma, E. & de Zee, M. (2006), 'Analysis of musculoskeletal systems in the anybody modeling system', *Simulation Modelling Practice and Theory* **14**(8), 1100–1111.

Darling, W. G., Cole, K. J. & Miller, G. F. (1994), 'Coordination of index finger movements', *Journal of Biomechanics* **27**(4), 479–491.

Davoodi, R., Brown, I. E. & Loeb, G. E. (2003), 'Advanced modeling environment for developing and testing fes control systems', *Medical Engineering and Physics* **25**(1), 3–9.

Davoodi, R. & Loeb, G. E. (2003), A biomimetic strategy for control of fes reaching, *in* 'Engineering in Medicine and Biology Society, 2003. Proceedings of the 25th Annual International Conference of the IEEE', Vol. 2. Engineering in Medicine and Biology Society, 2003. Proceedings of the 25th Annual International Conference of the IEEE.

Davoodi, R., Urata, C., Hauschild, M., Khachani, M. & Loeb, G. E. (2007), 'Model-based development of neural prostheses for movement', *Biomedical Engineering, IEEE Transactions on* **54**(11), 1909–1918.

163

Delp, S. L., Anderson, F. C., Arnold, A. S., Loan, P., Habib, A., John, C. T., Guendelman, E. & Thelen, D. G. (2007), 'Opensim: Open-source software to create and analyze dynamic simulations of movement', *IEEE Trans Biomed Eng* **54**(11), 1940–1950.

Delp, S. L. & Loan, J. P. (1995), 'A graphics-based software system to develop and analyze models of musculoskeletal structures', *Computers in Biology and Medicine* **25**(1), 21–34.

Dennerlein, J. T., Diao, E., Mote Jr, C. D. & Rempel, D. M. (1998), 'Tensions of the flexor digitorum superficialis are higher than a current model predicts', *Journal of Biomechanics* **31**(4), 295–302.

Dennerlein, J. T., Mote Jr, C. D. & Rempel, D. M. (1998), 'Control strategies for finger movement during touch-typing the role of the extrinsic muscles during a keystroke', *Experimental Brain Research* **121**(1), 1–6.

Disselhorst-Klug, C., Schmitz-Rode, T. & Rau, G. (2009), 'Surface electromyography and muscle force: Limits in semg-force relationship and new approaches for applications', *Clinical Biomechanics* **24**(3), 225–235.

Esteki, A. & Mansour, J. (1997), 'A dynamic model of the hand with application in functional neuromuscular stimulation', *Annals of Biomedical Engineering* **25**(3), 440–451.

Esteki, A. & Mansour, J. M. (1996), 'An experimentally based nonlinear viscoelastic model of joint passive moment', *Journal of Biomechanics* **29**(4), 443–450.

Fernandez, J. W. & Pandy, M. G. (2006), 'Integrating modelling and experiments to assess dynamic musculoskeletal function in humans', *Experimental Physiology* **91**(2), 371–382.

Franko, O., Winters, T., Tirrell, T., Hentzen, E. & Lieber, R. (2011), 'Moment arms of the human digital flexors', *Journal of Biomechanics* **44**(10), 1987–1990.

Fregly, B. (2008), 'Computational assessment of combinations of gait modifications for knee osteoarthritis rehabilitation', *Biomedical Engineering, IEEE Transactions on* **55**(8), 2104–2106.

Fuglevand, A. J., Winter, D. A. & Patla, A. E. (1993), 'Models of recruitment and rate coding organization in motor-unit pools', *J Neurophysiol* **70**(6), 2470–88.

Garcia-Elias, M., An, K. N., Berglund, L. J., Linscheid, R. L., Cooney, W. P. & Chao, E. (1991), 'Extensor mechanism of the fingers. ii. tensile properties of components***', *The Journal of hand surgery* **16**(6), 1136–1140.

Garcia-Elias, M., An, K. N., Berglund, L., Linscheid, R. L., Cooney Iii, W. P. & Chao, E. (1991), 'Extensor mechanism of the fingers. i. a quantitative geometric study***', *The Journal of hand surgery* **16**(6), 1130–1136.

Garcia, M., Chatterjee, A., Ruina, A. & Coleman, M. (1998), 'The simplest walking model: Stability, complexity, and scaling', *ASME Journal of Biomechanical Engineering* **120**, 281–288.

Garner, B. A. & Pandy, M. G. (2000), 'The obstacle-set method for representing muscle paths in musculoskeletal models', *Computer methods in biomechanics and biomedical engineering* **3**(1), 1–30.

Gatti, C. & Hughes, R. (2009), 'Optimization of muscle wrapping objects using simulated annealing', *Annals of Biomedical Engineering* **37**(7), 1342–1347.

Goehler, C. & Murray, W. (2010), 'The sensitivity of endpoint forces produced by the extrinsic muscles of the thumb to posture', *Journal of biomechanics* **43**(8), 1553–1559.

Gonzalez, R. V., Hutchins, E. L., Barr, R. E. & Abraham, L. D. (1996), 'Development and evaluation of a musculoskeletal model of the elbow joint complex', *Journal of biomechanical engineering* **118**, 32.

Green, P. J. & Silverman, B. W. (1994), *Nonparametric regression and generalized linear models: a roughness penalty approach*, Vol. 58, Chapman & Hall/CRC.

Haines, R. W. (1951), 'The extensor apparatus of the finger', *Journal of Anatomy* **85**(Pt 3), 251.

Happee, R. & Van der Helm, F. C. T. (1995), 'The control of shoulder muscles during goal directed movements, an inverse dynamic analysis', *Journal of Biomechanics* **28**(10), 1179–1191.

Harding, D. C., Brandt, K. D. & Hillberry, B. M. (1993), 'Finger joint force minimization in pianists using optimization techniques.', *J Biomech* **26**(12), 1403–1412.

Harris Jr, C. & Rutledge Jr, G. (1972), 'The functional anatomy of the extensor mechanism of the finger'.

Hatze, H. (1977), 'A myocybernetic control model of skeletal muscle', *Biological Cybernetics* **25**(2), 103–119.

Hatze, H. (1997), 'A three-dimensional multivariate model of passive human joint torques and articular boundaries', *Clinical Biomechanics* **12**(2), 128–135.

Hatze, H. (2002), 'The fundamental problem of myoskeletal inverse dynamics and its implications', *Journal of Biomechanics* **35**(1), 109–115.

Hatze, H. (2005), 'Towards a comprehensive large-scale computer model of the human neuromusculoskeletal system', *Theoretical Issues in Ergonomics Science* **6**(3), 239–250.

Herrmann, A. & Delp, S. (1999), 'Moment arm and force-generating capacity of the extensor carpi ulnaris after transfer to the extensor carpi radialis brevis', *The Journal of hand surgery* **24**(5), 1083–1090.

Herzog, W. & Read, L. J. (1993), 'Lines of action and moment arms of the major force-carrying structures crossing the human knee joint', *Journal of Anatomy* **182**(Pt 2), 213.

Holden, J. P., Orsini, J. A., Siegel, K. L., Kepple, T. M., Gerber, L. H. & Stanhope, S. J. (1997), 'Surface movement errors in shank kinematics and knee kinetics during gait', *Gait & Posture* **5**(3), 217–227.

Hollister, A., Buford, W. L., Myers, L. M., Giurintano, D. J. & Novick, A. (1992), 'The axes of rotation of the thumb carpometacarpal joint', *Journal of Orthopaedic Research* **10**(3), 454–460.

Holzbaur, K. R. S., Murray, W. M. & Delp, S. L. (2005), 'A model of the upper extremity for simulating musculoskeletal surgery and analyzing neuromuscular control', *Annals of Biomedical Engineering* **33**(6), 829–840.

Hoy, M. G., Zajac, F. E. & Gordon, M. E. (1990), 'A musculoskeletal model of the human lower extremity: the effect of muscle, tendon, and moment arm on the moment-angle relationship of musculotendon actuators at the hip, knee, and ankle', *Journal of Biomechanics* **23**(2), 157–169.

Huiskes, R. & Chao, E. Y. (1983), 'A survey of finite element analysis in orthopedic biomechanics: the first decade', *Journal of Biomechanics* **16**(6), 385.

Hull, M. L. & Jorge, M. (1985), 'A method for biomechanical analysis of bicycle pedaling', *Journal of Biomechanics* **18**(9), 631–644.

Inman, V., Ralston, H., De CM Saunders, J., Bertram Feinstein, M. & Wright Jr, E. (1952), 'Relation of human electromyogram to muscular tension', *Electroencephalography and clinical Neurophysiology* **4**(2), 187–194.

Inman, V. T. (1944), 'Observations on the function of the shoulder joint', *The Journal of Bone and Joint Surgery* **26**(1), 1.

Jinha, A., Ait-Haddou, R., Binding, P. & Herzog, W. (2006), 'Antagonistic activity of one-joint muscles in three-dimensions using non-linear optimisation', *Mathematical biosciences* **202**(1), 57–70.

Kamper, D. G., George Hornby, T. & Rymer, W. Z. (2002), 'Extrinsic flexor muscles generate concurrent flexion of all three finger joints', *Journal of Biomechanics* **35**(12), 1581–1590.

Karniel, A. & Inbar, G. F. (1997), 'A model for learning human reaching movements', *Biological Cybernetics* **77**(3), 173–183.

Kaufman, K. R., An, K. A., Litchy, W. J. & Chao, E. Y. S. (1991), 'Physiological prediction of muscle forces. ii, application to isokinetic exercise', *Neuroscience* **40**(3), 793–804.

Khang, G. & Zajac, F. E. (1989), 'Paraplegic standing controlled by functional neuromuscular stimulation: Part i–computer model and control-system design.', *IEEE Trans Biomed Eng* **36**(9), 873–884.

Koza, J. R. (1992), *Genetic programming: On the programming of computers by means of natural selection*, The MIT press, Cambridge, Massachusetts.

Kuo, A. D. (2002), 'Energetics of actively powered locomotion using the simplest walking model', *Journal of biomechanical engineering* **124**, 113.

Kuo, A. D. & Maxwell Donelan, J. (2009), 'Comment on "contributions of the individual ankle plantar flexors to support, forward progression and swing initiation during walking" ((neptune et al., 2001) and "muscle mechanical work requirements during normal walking: the energetic cost of raising the body's center-of-mass is significant" (neptune et al., 2004)', *J Biomech* **42**(11), 1783–5; author reply 1786–9.

Kuo, P. L., Lee, D. L., Jindrich, D. L. & Dennerlein, J. T. (2006), 'Finger joint coordination during tapping', *Journal of Biomechanics* **39**(16), 2934–2942.

Kurse, M., Lipson, H. & Valero-Cuevas, F. J. (2012), 'Extrapolatable analytical functions for tendon excursions and moment arms from sparse datasets', *IEEE Transactions on Biomedical Engineering* **59**(6), 1572–1582.

Kutch, J., Kuo, A. & Rymer, W. (2010), 'Extraction of individual muscle mechanical action from endpoint force', *Journal of neurophysiology* **103**(6), 3535–3546.

Kutch, J. & Valero-Cuevas, F. (2011), 'Muscle redundancy does not imply robustness to muscle dysfunction', *Journal of Biomechanics* **44**(7), 1264–1270.

Landsmeer, J. M. (1961), 'Studies in the anatomy of articulation. i. the equilibrium of the" intercalated" bone', *Acta morphologica Neerlando-Scandinavica* **3**, 287.

Landsmeer, J. M. F. (1949), 'The anatomy of the dorsal aponeurosis of the human finger and its functional significance', *The Anatomical Record* **104**(1).

Landsmeer, J. M. F. (1963), 'The coordination of finger-joint motions', *The Journal of Bone and Joint Surgery* **45**(8), 1654.

Lee, J. W. & Rim, K. (1990), 'Maximum finger force prediction using a planar simulation of the middle finger', *ARCHIVE: Proceedings of the Institution of Mechanical Engineers, Part H: Journal of Engineering in Medicine 1989-1996 (vols 203-210)* **204**(38), 169–178.

Lee, S. W., Chen, H., Towles, J. D. & Kamper, D. G. (2008), 'Estimation of the effective static moment arms of the tendons in the index finger extensor mechanism', *Journal of Biomechanics* **41**(7), 1567–1573.

Leijnse, J. (1996), 'A graphic analysis of the biomechanics of the massless bi-articular chain. application to the proximal bi-articular chain of the human finger', *Journal of Biomechanics* **29**(3), 355–366.

Leijnse, J., Bonte, J. E., Landsmeer, J. M. F., Kalker, J. J., Van der Meulen, J. C. & Snijders, C. J. (1992), 'Biomechanics of the finger with anatomical restrictions–the significance for the exercising hand of the musician', *Journal of Biomechanics* **25**(11), 1253–1264.

Li, Z. M., Zatsiorsky, V. M. & Latash, M. L. (2001), 'The effect of finger extensor mechanism on the flexor force during isometric tasks', *Journal of Biomechanics* **34**(8), 1097–1102.

Lieber, R. L., Jacobson, M. D., Fazeli, B. M., Abrams, R. A. & Botte, M. J. (1992), 'Architecture of selected muscles of the arm and forearm: anatomy and implications for tendon transfer', *The Journal of hand surgery* **17**(5), 787.

Lipson, H. (2006), 'A relaxation method for simulating the kinematics of compound nonlinear mechanisms', *Journal of Mechanical Design* **128**, 719.

Lipson, H., Bongard, J., Zykov, V. & Malone, E. (2006), Evolutionary robotics for legged machines: from simulation to physical reality, *in* 'Intelligent Autonomous Systems', Vol. 9, p. 9.

Littler, J. W. (1967), 'The finger extensor mechanism', *The Surgical Clinics of North America* **47**(2), 415.

Liu, J., Hughes, R. E., Smutz, W. P., Niebur, G. & Nan-An, K. (1997), 'Roles of deltoid and rotator cuff muscles in shoulder elevation', *Clinical Biomechanics* **12**(1), 32–38.

Maganaris, C. N. (2004), 'Imaging-based estimates of moment arm length in intact human muscle-tendons', *European journal of applied physiology* **91**(2), 130–139.

Magermans, D., Chadwick, E., Veeger, H., Rozing, P. & Van der Helm, F. (2004), 'Effectiveness of tendon transfers for massive rotator cuff tears: a simulation study', *Clinical Biomechanics* **19**(2), 116–122.

McLean, S., Su, A. & van den Bogert, A. (2003), 'Development and validation of a 3-d model to predict knee joint loading during dynamic movement', *Journal of biomechanical engineering* **125**, 864.

Menegaldo, L. L., de Toledo Fleury, A. & Weber, H. I. (2004), 'Moment arms and musculotendon lengths estimation for a three-dimensional lower-limb model', *Journal of Biomechanics* **37**(9), 1447–1453.

Micks, J. E. & Reswick, J. B. (1981), 'Confirmation of differential loading of lateral and central fibers of the extensor tendon', *The Journal of hand surgery* **6**(5), 462.

Murray, R., Li, Z. & Sastry, S. (1994), *A mathematical introduction to robotic manipulation*, CRC.

Murray, W. M., Delp, S. L. & Buchanan, T. S. (1995), 'Variation of muscle moment arms with elbow and forearm position', *Journal of Biomechanics* **28**(5), 513–525.

Mussa-Ivaldi, F. A., Hogan, N. & Bizzi, E. (1985), 'Neural, mechanical, and geometric factors subserving arm posture in humans', *Journal of Neuroscience* **5**(10), 2732–2743.

Neptune, R. (2000), 'Computer modeling and simulation of human movement', *Scientific Principles of Sports Rehabilitation* **11**(2), 417–434.

Neptune, R. R., Kautz, S. A. & Zajac, F. E. (2001), 'Contributions of the individual ankle plantar flexors to support, forward progression and swing initiation during walking', *Journal of Biomechanics* **34**(11), 1387–1398.

Neptune, R. R., McGowan, C. P. & Kautz, S. A. (2009), 'Forward dynamics simulations provide insight into muscle mechanical work during human locomotion', *Exercise and sport sciences reviews* **37**(4), 203.

Neptune, R. R., Zajac, F. E. & Kautz, S. A. (2004), 'Muscle mechanical work requirements during normal walking: the energetic cost of raising the body's center-of-mass is significant', *Journal of Biomechanics* **37**(6), 817–825.

Olney, S. J., Griffin, M. P., Monga, T. N. & McBride, I. D. (1991), 'Work and powe in gait of stroke patients', *Archives of physical medicine and rehabilitation* **72**(5), 309–314.

Otis, J., Jiang, C., Wickiewicz, T., Peterson, M., Warren, R. & Santner, T. (1994), 'Changes in the moment arms of the rotator cuff and deltoid muscles with abduction and rotation', *The Journal of Bone and Joint Surgery* **76**(5), 667–676.

Pandy, M. G. (2001), 'Computer modeling and simulation of human movement', *Annual review of biomedical engineering* **3**(1), 245–273.

Pandy, M. G. & Sasaki, K. (1998), 'A three-dimensional musculoskeletal model of the human knee joint. part 2: analysis of ligament function', *Computer methods in biomechanics and biomedical engineering* **1**(4), 265–283.

Pandy, M. G., Sasaki, K. & Kim, S. (1997), 'A three-dimensional musculoskeletal model of the human knee joint. part 1: theoretical construction', *Computer methods in biomechanics and biomedical engineering* **1**(2), 87–108.

Patriarco, A. G., Mann, R. W., Simon, S. R. & Mansour, J. M. (1981), 'An evaluation of the approaches of optimization models in the prediction of muscle forces during human gait', *Journal of Biomechanics* **14**(8), 513.

Piazza, S. J. (2006), 'Muscle-driven forward dynamic simulations for the study of normal and pathological gait', *Journal of NeuroEngineering and Rehabilitation* **3**(1), 5.

Piazza, S. J. & Delp, S. L. (2001), 'Three-dimensional dynamic simulation of total knee replacement motion during a step-up task', *Journal of biomechanical engineering* **123**, 599.

Pigeon, P., Yahia, L. H. & Feldman, A. G. (1996), 'Moment arms and lengths of human upper limb muscles as functions of joint angles', *Journal of Biomechanics* **29**(10), 1365–1370.

Prilutsky, B. I. & Zatsiorsky, V. M. (2002), 'Optimization-based models of muscle coordination', *Exercise and sport sciences reviews* **30**(1), 32.

Purves, W. & Berme, N. (1980), 'Resultant finger joint loads in selected activities', *Journal of Biomedical Engineering* **2**(4), 285–289.

Raphael, G., Tsianos, G. & Loeb, G. (2010), 'Spinal-like regulator facilitates control of a two-degree-of-freedom wrist', *The Journal of Neuroscience* **30**(28), 9431–9444.

Rawlinson, J. J. & Bartel, D. L. (2002), 'Flat medial-lateral conformity in total knee replacements does not minimize contact stresses.', *J Biomech* **35**(1), 27–34.

Rawlinson, J. J., Furman, B. D., Li, S., Wright, T. M. & Bartel, D. L. (2006), 'Retrieval, experimental, and computational assessment of the performance of total knee replacements.', *J Orthop Res* **24**(7), 1384–1394.

Rockwell, W. B., Butler, P. N. & Byrne, B. A. (2000), 'Extensor tendon: Anatomy, injury, and reconstruction', *Plastic and Reconstructive Surgery* **106**(7), 1592.

Rudlof, S. & Köppen, M. (1996), Stochastic hill climbing with learning by vectors of normal distributions, pp. 60–70.

Rugg, S. G., Gregor, R. J., Mandelbaum, B. R. & Chiu, L. (1990), 'In vivo moment arm calculations at the ankle using magnetic resonance imaging (mri)', *Journal of Biomechanics* **23**(5), 495–497, 499–501.

Salsbury, C. (1937), 'The interosseous muscles of the hand', *Journal of Anatomy* **71**(Pt 3), 395.

Sancho-Bru, J. L., Perez-Gonzalez, A., Vergara-Monedero, M. & Giurintano, D. (2001), 'A 3-d dynamic model of human finger for studying free movements', *Journal of Biomechanics* **34**(11), 1491–1500.

Sancho-Bru, J., Perez-Gonzalez, A., Vergara, M. & Giurintano, D. (2003), 'A 3d biomechanical model of the hand for power grip', *Journal of biomechanical engineering* **125**, 78.

Santello, M., Flanders, M. & Soechting, J. F. (2002), 'Patterns of hand motion during grasping and the influence of sensory guidance', *J Neurosci* **22**(4), 1426–35. Santello, Marco Flanders, Martha Soechting, John F NS-15018/NS/NINDS NIH HHS/United States Clinical Trial Research Support, U.S. Gov't, P.H.S. United States The Journal of neuroscience : the official journal of the Society for Neuroscience J Neurosci. 2002 Feb 15;22(4):1426-35.

Santos, V. J., Bustamante, C. D. & Valero-Cuevas, F. J. (2009), 'Improving the fitness of high-dimensional biomechanical models via data-driven stochastic exploration', *IEEE Transactions on Biomedical Engineering* **56**(3).

Santos, V. J. & Valero-Cuevas, F. J. (2006), 'Reported anatomical variability naturally leads to multimodal distributions of denavit-hartenberg parameters for the human thumb', *IEEE Trans Biomed Eng* **53**, 155–163.

Sarrafian, S. K., Kazarian, L. E., Topouzian, L. K., Sarrafian, V. K. & Siegelman, A. (1970), 'Strain variation in the components of the extensor apparatus of the finger during flexion and extension: A biomechanical study', *The Journal of Bone and Joint Surgery* **52**(5), 980.

Schieber, M. H. & Santello, M. (2004), 'Hand function: peripheral and central constraints on performance', *Journal of Applied Physiology* **96**(6), 2293.

Schmidt, M. D. & Lipson, H. (2006), 'Co-evolving fitness predictors for accelerating and reducing evaluations', *Genetic Programming Theory and Practice IV* **5**.

Schmidt, M. & Lipson, H. (2005), 'Coevolution of fitness maximizers and fitness predictors', *GECCO Late Breaking Paper* .

Schmidt, M. & Lipson, H. (2009), 'Distilling free-form natural laws from experimental data', *science* **324**(5923), 81.

Schutte, L. M., Rodgers, M. M., Zajac, F. E., Glaser, R. M., Center, V. A. M. & Alto, P. (1993), 'Improving the efficacy of electrical stimulation-induced leg cycleergometry: an analysis based on a dynamic musculoskeletal model', *IEEE Transactions on Rehabilitation Engineering* **1**(2), 109–125.

Scott, S. H. (2004), 'Optimal feedback control and the neural basis of volitional motor control', *Nature Reviews Neuroscience* **5**(7), 532–546.

Scovil, C. & Ronsky, J. (2006), 'Sensitivity of a hill-based muscle model to perturbations in model parameters', *Journal of Biomechanics* **39**(11), 2055–2063.

Shadmehr, R. & Mussa-Ivaldi, F. A. (1994), 'Adaptive representation of dynamics during learning of a motor task', *Journal of Neuroscience* **14**(5), 3208–3224.

Smith, R. J. (1974), 'Balance and kinetics of the fingers under normal and pathological conditions', *Clinical orthopaedics and related research* **104**, 92.

Soechting, J. F. & Flanders, M. (1997), 'Evaluating an integrated musculoskeletal model of the human arm', *Journal of biomechanical engineering* **119**, 93.

Spoor, C. W. (1983), 'Balancing a force on the fingertip of a two-dimensional finger model without intrinsic muscles', *Journal of Biomechanics* **16**(7), 497–504.

Spoor, C. W. & Landsmeer, J. M. F. (1976), 'Analysis of the zigzag movement of the human finger under influence of the extensor digitorum tendon and the deep flexor tendon', *Journal of Biomechanics* **9**(9), 561–566.

Spoor, C. W., Van Leeuwen, J. L., Meskers, C. G. M., Titulaer, A. F. & Huson, A. (1990), 'Estimation of instantaneous moment arms of lower-leg muscles', *Journal of Biomechanics* **23**(12), 1247–1259.

Stark, H. H., Boyes, J. H. & Wilson, J. N. (1962), 'Mallet finger', *The Journal of Bone and Joint Surgery* **44**(6), 1061.

Stern Jr, J. T. (1971), 'Investigations concerning the theory of 'spurt' and 'shunt' muscles', *Journal of Biomechanics* **4**(5), 437–453.

Sueda, S., Kaufman, A. & Pai, D. K. (2008), 'Musculotendon simulation for hand animation', *ACM Transactions on Graphics* **27**(3).

Thelen, D. G., Anderson, F. C. & Delp, S. L. (2003), 'Generating dynamic simulations of movement using computed muscle control', *Journal of Biomechanics* **36**(3), 321–328.

Theodorou, E., Todorov, E. & Valero-Cuevas, F. J. (2011), Neuromuscular stochastic optimal control of a tendon driven index finger model, *in* 'American Control Conference (ACC), 2011', pp. 348–355.

Todorov, E. (2007), 'Probabilistic Inference of Multijoint Movements, Skeletal Parameters and Marker Attachments From Diverse Motion Capture Data', *IEEE Trans Biomed Eng* **54**(11), 1927–1939.

Valero-Cuevas, F. (1997), Muscle coordination of the human index finger, PhD thesis, Doctoral Dissertation, Stanford University, Stanford, CA.

Valero-Cuevas, F. (2000*a*), Applying principles of robotics to understand the biomechanics, neuromuscular control and clinical rehabilitation of human digits, *in* 'Robotics and Automation, 2000. Proceedings. ICRA'00. IEEE International Conference on', Vol. 1, IEEE, pp. 270–275.

Valero-Cuevas, F. & Hentz, V. (2002), 'Releasing the a3 pulley and leaving flexor superficialis intact increases pinch force following the zancolli lasso procedures to prevent claw deformity in the intrinsic palsied finger', *Journal of orthopaedic research* **20**(5), 902–909.

Valero-Cuevas, F., Hoffmann, H., Kurse, M., Kutch, J. & Theodorou, E. (2009), 'Computational models for neuromuscular function', *IEEE Reviews in Biomedical Engineering* **2**, 110.

Valero-Cuevas, F. J. (2000*b*), 'Predictive modulation of muscle coordination pattern magnitude scales fingertip force magnitude over the voluntary range', *J Neurophysiol* **83**(3), 1469–79.

Valero-Cuevas, F. J. (2005), 'An integrative approach to the biomechanical function and neuromuscular control of the fingers', *J Biomech* **38**(4), 673–84.

Valero-Cuevas, F. J. (2009), 'A mathematical approach to the mechanical capabilities of limbs and fingers', *Adv. Exp. Med. Biol.* **629**, 619–633.

Valero-Cuevas, F. J., Anand, V. V., Saxena, A. & Lipson, H. (2007), 'Beyond parameter estimation: extending biomechanical modeling by the explicit exploration of model topology', *IEEE Trans Biomed Eng* **54**(11), 1951–64.

Valero-Cuevas, F. J., Johanson, M. E. & Towles, J. D. (2003), 'Towards a realistic biomechanical model of the thumb: the choice of kinematic description may be more critical than the solution method or the variability/uncertainty of musculoskeletal parameters', *J Biomech* **36**, 1019–1030.

Valero-Cuevas, F. J. & Lipson, H. (2004), A computational environment to simulate complex tendinous topologies, *in* 'Conf Proc IEEE Eng Med Biol Soc', Vol. 6, pp. 4653–6.

Valero-Cuevas, F. J., Towles, J. D. & Hentz, V. R. (2000), 'Quantification of fingertip force reduction in the forefinger following simulated paralysis of extensor and intrinsic muscles', *J Biomech* **33**(12), 1601–9.

Valero-Cuevas, F. J., Yi, J. W., Brown, D., McNamara, R. V., r., Paul, C. & Lipson, H. (2007), 'The tendon network of the fingers performs anatomical computation at a macroscopic scale', *IEEE Trans Biomed Eng* **54**(6 Pt 2), 1161–6.

Valero-Cuevas, F. J., Zajac, F. E. & Burgar, C. G. (1998), 'Large index-fingertip forces are produced by subject-independent patterns of muscle excitation', *J Biomech* **31**(8), 693–703.

Van der Helm, F. C. T. (1994), 'A finite element musculoskeletal model of the shoulder mechanism', *Journal of Biomechanics* **27**(5), 551–559.

Van Langelaan, E. J. (1983), 'A kinematical analysis of the tarsal joints. an x-ray photogrammetric study', *Acta orthopaedica Scandinavica. Supplementum* **204**, 1.

Van Zuylen, E. J., Van Velzen, A. & van der Gon, J. J. (1988), 'A biomechanical model for flexion torques of human arm muscles as a function of elbow angle', *Journal of Biomechanics* **21**(3), 183–190.

Venkadesan, M. & Valero-Cuevas, F. J. (2008), 'Neural control of motion-to-force transitions with the fingertip', *J Neurosci* **28**(6), 1366–73.

Vigouroux, L., Quaine, F., Labarre-Vila, A. & Moutet, F. (2006), 'Estimation of finger muscle tendon tensions and pulley forces during specific sport-climbing grip techniques', *Journal of Biomechanics* **39**(14), 2583–2592.

Visser, J. J., Hoogkamer, J. E., Bobbert, M. F. & Huijing, P. A. (1990), 'Length and moment arm of human leg muscles as a function of knee and hip-joint angles', *European journal of applied physiology and occupational physiology* **61**(5), 453–460.

Weightman, B. & Amis, A. A. (1982), 'Finger joint force predictions related to design of joint replacements', *Journal of Biomedical Engineering* **4**(3), 197–205.

Winter, D. A. (1990), *Biomechanics and motor control of human movement*, Wiley-Interscience.

Winters, J. M. (2000), 'Terminology and foundations of movement science', *Biomechanics and Neural Control of Posture and Movement* p. 3.

Wismans, J., Veldpaus, F., Janssen, J., Huson, A. & Struben, P. (1980), 'A three-dimensional mathematical model of the knee-joint', *Journal of Biomechanics* **13**(8), 677.

Woltring, H. J., Huiskes, R. & de Lange, A. (1983), Measurement error influence on helical axis accuracy in the description of 3d finite joint movement in biomechanics, *in* 'Proceedings of the American Society of Mechanical Engineers Biomechanics Symposium', Proceedings of the American Society of Mechanical Engineers Biomechanics Symposium, Houston, Texas, June, pp. 19–22.

Yamaguchi, G. T. (2005), *Dynamic modeling of musculoskeletal motion: a vectorized approach for biomechanical analysis in three dimensions*, Springer Verlag.

Yeo, S., Mullens, C., Sandercock, T., Pai, D. & Tresch, M. (2011), 'Estimation of musculoskeletal models from in situ measurements of muscle action in the rat hindlimb', *Journal of Experimental Biology* **214**(5), 735–746.

Yeo, S., Tresch, M. & Pai, D. (2008), Optimal design of musculoskeletal models using force field data, *in* 'Engineering in Medicine and Biology Society, 2008. EMBS 2008. 30th Annual International Conference of the IEEE', IEEE, pp. 3710–3714.

Yoon, Y. S. & Mansour, J. M. (1982), 'The passive elastic moment at the hip', *Journal of Biomechanics* **15**(12), 905.

Yoshikawa, T. (1990), *Foundations of robotics: analysis and control*, The MIT Press.

Youm, Y., Gillespie, T., Flatt, A. & Sprague, B. (1978), 'Kinematic investigation of normal mcp joint', *Journal of Biomechanics* **11**(3), 109–118.

Zahalak, G. I. & Ma, S. P. (1990), 'Muscle activation and contraction: constitutive relations based directly on cross-bridge kinetics', *Journal of biomechanical engineering* **112**, 52.

Zajac, F. E. (1992), 'How musculotendon architecture and joint geometry affect the capacity of muscles to move and exert force on objects: a review with application to arm and forearm tendon transfer design.', *J Hand Surg Am* **17**(5), 799–804.

Zajac, F. E. (2002), 'Understanding muscle coordination of the human leg with dynamical simulations', *Journal of Biomechanics* **35**(8), 1011–1018.

Zajac, F. E., Biosci, J., Physiol, J. C., Biol, J. E., Physiol, Z. V., Lond, J. Z., Physiol, Z. J., Soc, J. G. E., Acta, B. B. & Biochem, A. (1989), 'Muscle and tendon: properties, models, scaling, and application to biomechanics and motor control', *Crit Rev Biomed Eng* **17**, 359–411.

Zajac, F. E., Neptune, R. R. & Kautz, S. A. (2002), 'Biomechanics and muscle coordination of human walking part i: introduction to concepts, power transfer, dynamics and simulations', *Gait and Posture* **16**(3), 215–232.

Zancolli, E. (1979), *Structural and dynamic bases of hand surgery*, 2nd edn, Lippincott, Philadelphia.

Zdravkovic, V., Jacob, H. & Sennwald, G. (1995), 'Physical equilibrium of the normal wrist and its relation to clinically defined', *The Journal of Hand Surgery: Journal of the British Society for Surgery of the Hand* **20**(2), 159–164.